Dealing with fuel contaminants in biogas-fed solid oxide fuel cell (SOFC) and molten carbonate fuel cell (MCFC) plants: Degradation of catalytic and electro-catalytic active

Dealing with fuel contaminants in biogas-fed solid oxide fuel cell plants: degradation of catalytic and electro-catalytic active surfaces and related gas purification methods

Andrea Lanzini[a*], Hossein Madi[b], Vitaliano Chiodo[c], Davide Papurello[a], Susanna Maisano[c], Massimo Santarelli[a,d], Jan Van herle[b]

[a] *Energy Department, Politecnico di Torino, Corso Duca degli Abruzzi 24 –10129, Torino, Italy*

[b] *FuelMat Group, Faculty of Engineering Sciences (STI), Ecole Polytechnique Fédérale de Lausanne (EPFL), CH-1951 Sion, Switzerland*

[c] *Institute CNR-ITAE "Nicola Giordano", Via S. Lucia sopra Contesse, 5 – 98126, Messina, Italy*

[d] *Energiteknik, KTH, Brinellvägen 68 S-100 44 Stockholm, Sweden*

** Corresponding author: andrea.lanzini@polito.it*

Abstract

Fuel cell and hydrogen technologies are re-gaining momentum in a number of sectors including industrial, tertiary and residential ones. Integrated biogas fuel cell plants in wastewater treatment plants and other bioenergy recovery plants are nowadays on the verge of becoming a clear opportunity for the market entry of high-temperature fuel cells in distributed generation (power production from a few kW to the MW scale).

High-temperature fuel cell technologies like molten carbonate fuel cells (MCFCs) and solid oxide fuel cells (SOFCs) are especially fit to operate with carbon fuels due to their (direct or indirect) internal reforming capability. Especially, systems based on SOFC technology show the highest conversion efficiency of gaseous carbon fuels (e.g., natural gas, digester gas, and biomass-derived syngas) into electricity when compared to engines or gas turbines. Also, lower CO_2 emissions and ultra-low emissions of atmospheric contaminants (SO_X, CO, VOC, especially NO_X) are generated per unit of electricity output. Nonetheless, stringent requirements apply regarding fuel purity. The presence of contaminants within the anode fuel stream, even at trace levels (sometimes ppb levels) can reduce the lifetime of key components like the fuel cell stack and reformer. In this work, we review the complex matrix (typology and amount) of different contaminants that is found in different biogas types (anaerobic digestion gas and landfill gas). We analyze the impact of contaminants on the fuel reformer and the SOFC stack to identify the threshold limits of the fuel cell system towards specific contaminants. Finally, technological solutions and related adsorbent materials to remove contaminants in a dedicated clean-up unit upstream of the fuel cell plant are also reviewed.

Keywords: biogas, fuel contaminants, SOFC, Ni-anode, reformer, siloxanes.

Index

List of Acronyms

AD	Anaerobic Digestion
ADG	Anaerobic Digestion Gas
BoP	Balance-of-Plant
CHP	Combined Heat and Power
FAO	Food and Agriculture Organization of the United Nations
FC	Fuel Cell
GHSV	Gas Hourly Space Velocity
LFG	Landfill Gas
LHV	Lower Heating Value
LLU	Large Livestock Unit (cow = 1 LLU)
MCFC	Molten Carbonate Fuel Cell
MSW	Municipal Solid Waste
PEM	Proton Exchange Membrane
SOFC	Solid Oxide Fuel Cell
VOC	Volatile Organic Compounds
VS	Volatile Solid
WWTP	Waste Water Treatment Plants

Overview of this work

Scope and Motivation

Integrated biogas fuel cell systems in wastewater treatment plants and other bioenergy recovery plants are now on the verge of becoming a clear opportunity for the entry of high-temperature fuel cells in the stationary market. In this work, the focus is restricted to SOFC technology. MCFC technology shares much of the same auxiliary infrastructures (regarding the Balance-of-Plant) and protocols of operation with the SOFC; hence, degradation issues are similar to those of the SOFC when it comes to anode contamination from fuel impurities. Also, threshold limits for contaminants in fuel cell quality feeds and clean-up design recommendations reported in this work are equally useful and extendable to natural gas, and syngas from biomass gasification.

One of the barriers for the deployment of CHP fuel cell systems comes from the degradation of the fuel cell stack. This technical barrier has direct economic consequences. Higher degradation rates translate in the lower lifetime of the stack, which is a large cost item of the whole plant installation. Fuel cell performance degradation from fuel contaminants is detrimental for the whole plant availability, as altered stack performance limits the operability of the system.

This paper attempts to summarize, analyze and discuss in detail recent findings and advances in the field of SOFCs running on gaseous bio-fuels. Especially, the focus is on an SOFC fed by anaerobic digestion or landfill biogas. There is a great potential to further increase biogas energy recovery, and SOFC technology seems a perfect match to maximize the efficiency of this use. Dealing with biogas fuel, on the other hand, might add complexity and further degradation to the SOFC and related BoP components (e.g., the fuel reformer). Therefore, in this study, we analyze the pathway from raw biogas to the use of clean biogas in the SOFC to understand the risks due to the contaminants, and how to manage and eventually minimize them.

Structure of this work

Briefly, the work is articulated into five main sections:

- the first one provides an overview of current trends and issues for biogas use in advanced fuel cell systems as well as the biogas production potential from different organic substrates;
- the second one deals with the origin, type and amount of contaminants expected in typical biogases;
- the third section investigates the impact of fuel contaminants on the Ni-based reformer catalyst;
- the fourth reports on the impact of fuel contaminants on the SOFC Ni-anode;
- the last section describes biogas purification techniques; methods and materials for the removal of harmful contaminants down to ppb-levels, as sometimes required by the fuel cell, are discussed in detail.

In more detail, the paper is organized as follows. First, we provide an overview of the biogas use and potential in Europe. The focus is limited to Europe since several installations are located in this macro-region and several data were freely available especially for this area. In fact, most of the biogas potential is roughly

proportional to the number of inhabitants living in a given area. Therefore, results obtained from Europe could be extrapolated to some extent to different geographic regions that share similar features in terms of economic development, diet patterns, and waste management.

The detrimental impact of biogas contaminants on the end-user device, i.e., the fuel cell, then follows in the paper. Some fuel contaminants can lead to a fast and irreversible degradation of catalytic and electro-catalytic active surfaces. The effect of biogas contaminants on the fuel cell Ni-based reformer and Ni-anode are thus assessed.

The study is limited to the Ni-based reformer and the Ni-anode SOFC as they represent state-of-the-art materials of pre-commercial systems and are expected to remain the dominant design solution for the coming years. The focus is mostly on the impact of H_2S and siloxanes for both the reformer catalyst and the fuel cell anode since they are known to be the most dangerous compounds, as will be corroborated in this study. The effect of heavier hydrocarbons is also reviewed since enhanced carbon formation rates are observed when co-feeding methane with other hydrocarbons (C2, C3 compounds). The fuel cell anode is also tested against HCl (which is not present in high concentration in biogases, expect for landfill biogas; however, HCl, along with H_2S, is abundant in coal syngas [1,2] and we deemed useful to extend the study to this chemical species as well).

Finally, we provide an in-depth overview of both scientific and some engineering aspects connected to the removal of biogas contaminants. Given the harmful effects of most of the biogas contaminants on the reformer and fuel cell performance, biogas purification is required. After reviewing various techniques for the contaminants removal, the focus is on solid sorbents since they can provide a deep clean-up of the incoming fuel that complies with SOFC fuel quality requirements. We will show how impregnated activated carbons are effective for the removal of H_2S and siloxanes.

Chapter 1 – Biogas potential and its use in Solid Oxide Fuel Cells (SOFCs)

Biogas potential

The global biogas potential is estimated to lie around 36,000 PJ [3], 6.5% of the world total primary energy supply in 2012. Energy crops would cover more than one-third of the overall potential thus taking the largest share. The second largest contributor would be manure collected from animal farming – covering about one fourth of the overall potential. In Table 1, different biogas sources are listed.

Table 1. Organic feedstocks for biogas production

Organic feedstocks for biogas	
Agriculture	**Waste Streams**
Livestock manure	Landfill
Energy crops, catch crops	Sewage sludge (urban and industrial
Landscape management	Municipal solid waste
Grass	Food waste, dairy industry waste
Other agricultural residues/by-products	Other waste

In 2007, the European production of biogas was 248 PJ [4], with the following provenance: 49% from landfill, 15% from sewage and 36% from other biogases (including among others manure, agricultural residues, and food waste digesters). Seven years later, with an annual growth of 15%, the biogas primary energy production increased to 560 PJ [4], more than doubling the 2007 value. In 2013, the overall production was achieved with 13,800 digesters and around 7.4 GW of electricity generating capacity [5].

In 2013, the scene remained unchanged in absolute numbers concerning landfill biogas production[*], while sewage biogas production from industrial and urban sludge increased by 40% (see Table 2). A much higher increase occurred for biogas from other sources (including decentralized agricultural plants, municipal solid waste methanization plants, and centralized co-digestion plants), the overall contribution of which rose from 2.1 Mtoe (89 PJ) in 2007 to 9.2 Mtoe (388 PJ) in 2013. This increase was the result of heavily subsidized biogas production especially in countries like Germany and Italy, which favored the conditions for the widespread diffusion of anaerobic digesters treating manure, agricultural residues, dedicated crops, and the organic fraction of municipal solid waste [4,5].

In Table 3, a full account of biogas production in the European zone is given for the period 2006-2013 for the three main sources mentioned above (landfill, sewage, and other biogas). The comparison between data taken from the Eur'Observer database and Eurostat database is also reported regarding overall biogas

[*] According to EU legislation (see Directive 1999/31/EC) landfilling is the least preferable option and should be limited to the necessary minimum.

production (in fact, Eurostat data only gives overall biogas production). Significant discrepancies are observed only for the years 2009 and 2010.

The trend of biogas production in Europe is also depicted in Figure 1. Landfill production remained almost unchanged during the past years, while sewage biogas production slightly increased. Biogas from the other sources (agricultural residues, MSW and co-digestion plants where food waste is also processed) was instead responsible for almost all of the increase in biogas production. Unfortunately, available statistics do not report a further level of disaggregation for the item 'other biogas'.

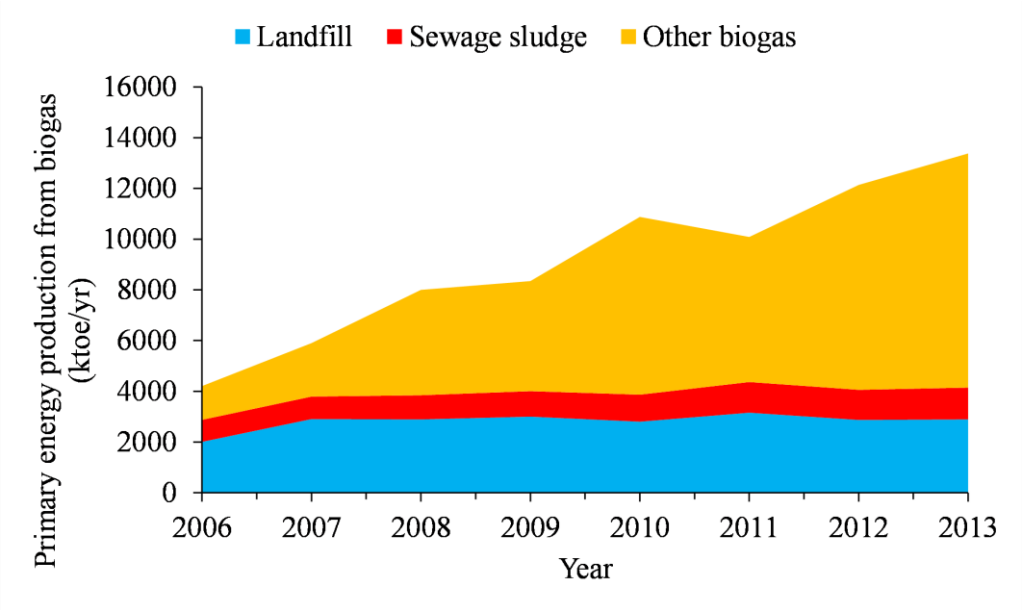

Figure 1. Primary energy production from biogas in Europe during the period 2006-2013 with disaggregated data for main biogas sources (source: Eur'ObservER).

Table 2. Biogas production in Europe in 2007 and 2013

	Biogas production (ktoe)			
Area; year	**Landfill gas**	**Sewage sludge gas**	**Other biogas**	**Total**
EU-25; 2007	2 905	887	2 108	5 900
EU-28; 2013	2 892	1 254	9 233	13 379

Table 3. Biogas production in Europe from 2006 to 2013. Data taken from Eur'Observer database are compared to Eurostat data.

Data in PJ

Year	Landfill	Sewage sludge	Other biogas	Total (Eur'ObservER)	Total (Eurostat)
2006	84	36	56	177	184
2007	122	37	89	248	242
2008	121	40	175	336	277
2009	126	42	182	351	310
2010	118	45	294	457	356
2011	133	51	240	424	434
2012	121	50	339	510	505
2013	121	53	388	562	566

Finally, we have also analyzed historical trends of biogas production starting from 1990. Notably, there was a more than twenty-fold increase in biogas production over the last 25 years (see Figure 2).

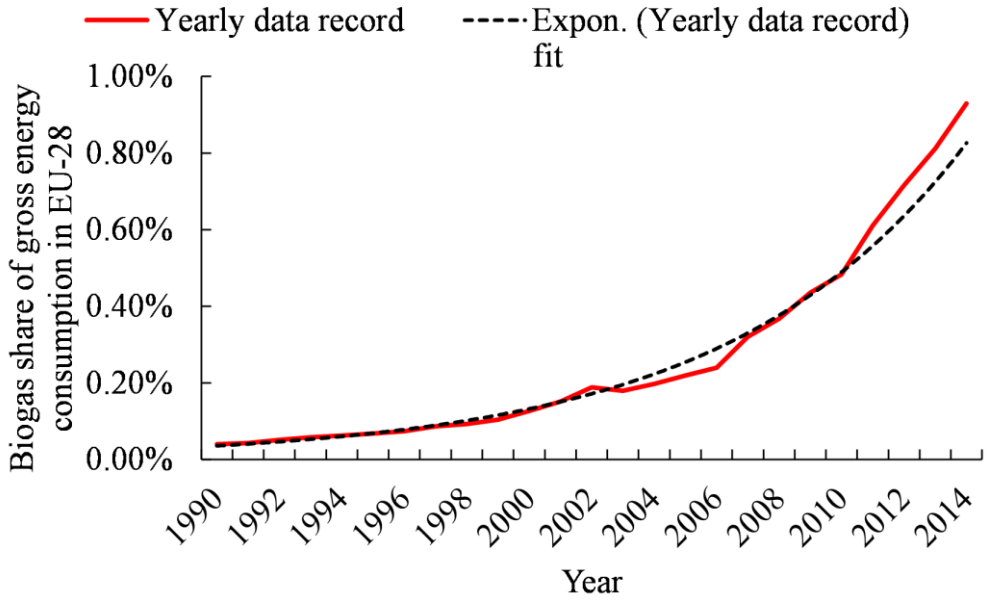

Figure 2. Primary energy production in Europe during the period 1990-2014 (Source: Eurostat database [6]*).*

Biogas could account for nearly 7% of the overall renewable primary energy production in Europe, but most of the potential remains unexploited. According to the European Biomass Association (AEBIOM), the biogas potential in Europe for 2020 is about 40 Mtoe (~1700 PJ) [7]. However, it is worth mentioning that much of this potential comes from energy crops, which accounts for 80% of the total (the assumption is that 5% of arable land is dedicated to energy crops). Many anaerobic digesters have a mixed diet of organic waste (e.g., manure) and forage (e.g., maize or sweet sorghum silage) so that it is difficult to have detailed statistics on the current organic substrates used for biogas production.

One way to grasp the intrinsic potential of biogas resources is to look at per head (humans or animals) biogas potential. For instance, the average citizen in developed countries uses almost 300 liters/day of water that end up in the sewer [8]. With the total suspended solid in sewage water of 220 mg/l, roughly 60 g/person/day of putrescible organic matter (or sludge) are thus collected in the wastewater plant connected to the sewage system. A realistic methane yield from sludge is about 200 L of CH_4 per kg of dry sludge, resulting in about 12 L CH_4/person/day, or 20 L/person/day of biogas when assuming that 60 vol% of biogas is CH_4. This biogas production corresponds to an LHV power of 5 W/person. A municipality of 100'000 inhabitants with an equivalent sewage plant would thus entail a biogas production rate of 500 kW. A 50% electrical efficient SOFC plant that consumes this available sewage biogas would then produce 250 kW of continuous electric power.

A similar calculus can be applied to animal farms. Manure is indeed a good substrate for anaerobic digestion. The typical biogas yields from different animal waste sources are summarized in Table 4. The specific biogas potential is much higher compared to sewage sludge as farming animals have often higher living weight (this is the case of cattle, for instance) and higher metabolic rates. Values in Table 4 are only approximate estimates. For instance, the exact methane (or biogas) yield from manure depends on many factors, e.g., the barn type (and related systems for manure and other slurry effluents management), on the country, on the age of the cow, and on the digester (e.g., mesophilic, thermophilic). For slurry-type waste in farms, a sensible range for biogas production rate is 0.56-1.5 m^3/LLU/day (average value is 1.11, in Germany), for manure it is 1.5-2.9 m^3/LLU/day (average value is 2.0 in Germany) [9]. Both average values are thus higher than the value given by Smil [10]. For chicken farms, the typical range is 3.5-4 m^3/LLU/day (the average value is 3.75 in Germany) [9]. Since one chicken corresponds to 0.003 LLU, the resulting CH_4 production rate is 0.010-0.012 m^3/chicken/day, which is a value very close to that reported by Smil. For pigs, for slurry waste, the range is 0.6-1.25 m^3/LLU/day (the average value is 0.88 in Germany) [9]. Since one pig corresponds to 0.33 LLU, the resulting CH_4 production rate is 0.2-0.41 m^3/pig/day, which is again a value quite consistent with the typical value given by Smil.

Table 4. Typical biogas yields from animal manure (adapted from Smil[10]*)*

Domestic animal	Total dry solid waste (kg solid/head/day)	Biogas production rate (m^3 biogas/day/head)	Power rate (W/head)
Buffaloe	2.74	0.73	54
Camel	4.11	1.37	244
Cattle	3.15	0.84	158
Chicken	0.03	0.01	2
Goat	0.27	0.09	19
Horse	4.11	1.37	244
Mule	4.11	1.37	244
Pig	0.68	0.35	75
Sheep	0.41	0.14	26

The biogas yield of different organic waste is given by the amount of methane (or biogas) produced from 1 kg of volatile matter. It is useful to refer to the volatile matter (VS) content since organic waste is mostly wet and not all the solid or suspended organic content is convertible to a gas.

In Table 5 the methane yields of manure and food waste are given. Interestingly, co-digestion of the two feedstock results in a higher overall yield [11]. According to the authors, compared with the digestion of food waste alone, co-digestion of manure and food waste might reduce the accumulation of intermediates during the initial period of digestion. The biogas yield of several organic solid substrates is also reviewed in the work of Raposo et al. [12].

Table 5. Biogas yields from animal manure and food waste[11]

Organic substrate	Volatile Solid (g/kg, wet basis)	Biogas yield (L/kgVS)	Methane yield (L/kgVS)	CH_4 content of biogas (%)	CH_4 production rate (L/kg, wet basis)
Unscreened manure	110	331	218	66%	24
Food waste	241	520	255	49%	61
Mixed (48% of food waste + 52% manure)	172.9	504	292	58%	51

As we did for mixed urban and industrial wastewater and animal waste, it is possible to calculate an intrinsic biogas potential production rate for food waste. On average, the US inhabitant generates about 2 kg of municipal solid waste (MSW) per day, which corresponds to more than 700 kg/yr [13]. Of this amount, roughly 15% is food waste. (In Europe, food waste is comparable – even if slightly lower – to that in North America; FAO estimates give for these regions a per capita waste by consumers between 95-115 kg a year [14].) Using the biogas yield given in Table 5, the resulting per capita methane production rate is about 18 L CH_4/person/day, which corresponds to a (chemical) power rate of 7.4 W (LHV basis). This value is quite comparable to the sewage biogas potential.

Table 6. Biogas potential from food waste

Per capita MSW generation (kg/person/day)	2.0
Share of food waste	14.6%
Per capita food waste generation (kg/person/day)	0.292
Methane production rate (L/person/day)	17.9
Methane production rate (W/person)	7.4

Biogas final use

Biogas is renewable energy that can be used for different services, most commonly electricity and heat through cogeneration. Biogas is also burnt in boilers to recover thermal energy only.

In 2013, the EU-28 biogas electricity output stood at about 52.3 TWh, which corresponds to almost 4.5 Mtoe. Of this amount, about two-thirds were produced in CHP mode. Heat provided to district heating networks or industrial units accounted for less than 0.5 Mtoe. Self-use of thermal energy (for the digester and other thermal needs of the plant) accounted for another 2.0 Mtoe [5]. By diving the overall electricity production by the overall biogas production in 2013 (13.38 Mtoe, see Table 2), we calculate an average electric conversion efficiency of around 33.6%.

A great impetus is now being given to biogas upgrading to methane fuel (also called 'biomethane'). Different technologies can be applied to remove CO_2 and other minor impurities/gases from the biogas stream (e.g., water or solvent scrubbing, membrane technology, PSA) in order to obtain a purified stream containing a high concentration of CH_4 (i.e., >95 vol.), which is compatible with the gas grid or for gas vehicles. Hence, biomethane can be either injected into the grid or used as local transportation fuel [15].

Overview on the status of fuel cell technology in various sectors

Fuel cell technology is approaching maturity status in the mobility sector with first commercial deployments having started in 2015-2016 [16]. Due to the fast dynamics operation required in this sector, low-temperature technology like proton exchange membrane (PEM) fuel cells dominate the scene.

The residential sector with combined heat and power (CHP) devices installed in single houses or multi-family buildings is less developed compared to the mobility sector. Field trials have been successfully completed or are ongoing. Both PEM and SOFC technologies are currently deployed in this sector. In the framework of the ENE-FARM program, in Japan, about 120,000 fuel cell micro-CHP units had been already installed by 2015 [17]. In Europe, through the Callux program first – launched across Germany– and then with the Ene.field program across several EU countries [18], the overall number of micro-CHP devices installed will exceed 1,000 units by 2016.

The use of fuel cells as stationary CHP generators is one of the most important long-term objectives for the deployment of high-temperature fuel cells. Both MCFC and SOFC technologies have the potential to compete with engines and micro-turbines in the range spanning from kW to a few MW, offering both higher energy efficiency and environmental benefits. The intrinsic modularity and excellent part-load performance make fuel cells particularly competitive on this scale with variable fuel input supply. Variable fuel supply is the situation often found when the FC is combined with anaerobic digestion biogas or other bio-syngas fuels (e.g., from the gasification of residual lingo-cellulosic biomass fuel). In the multi-MW range, fuel cell hybrid concepts can be applied to compete with engines and turbines, with also here the potential for higher electrical efficiency and lower pollutant emissions [19–22].

High-efficiency electricity production from biogas

Biogas is conventionally exploited in Internal Combustion Engines (ICEs). The electrical efficiency of ICEs can exceed 40% for units with an installed capacity of several hundreds of kW (> 500 kW_{el}) installations and is maximally about 43% for MW installations up to few MW (< 4 MW). However, the efficiency is lower for plants with a capacity below roughly 200 kW electric [23]. The electrical efficiency of the SOFC lies in the range 50-60%. The building block is a 50-100 kW unit that can be replicated several times to reach even multi-MW plants [24]. The efficiency of ICE's is size-dependent, as already mentioned. Figure 3 compares the SOFC with data from commercially available ICEs manufactured and/or commercialized by General Electric [25] and AB Group [26]. It is worth noting how the SOFC takes the highest advantage at small-scale (below 200 kW) in terms of conversion efficiency of biogas into electricity. Regarding emissions, the SOFC is always outperforming ICEs since virtually no NOx, SOx and particulate matter are emitted.

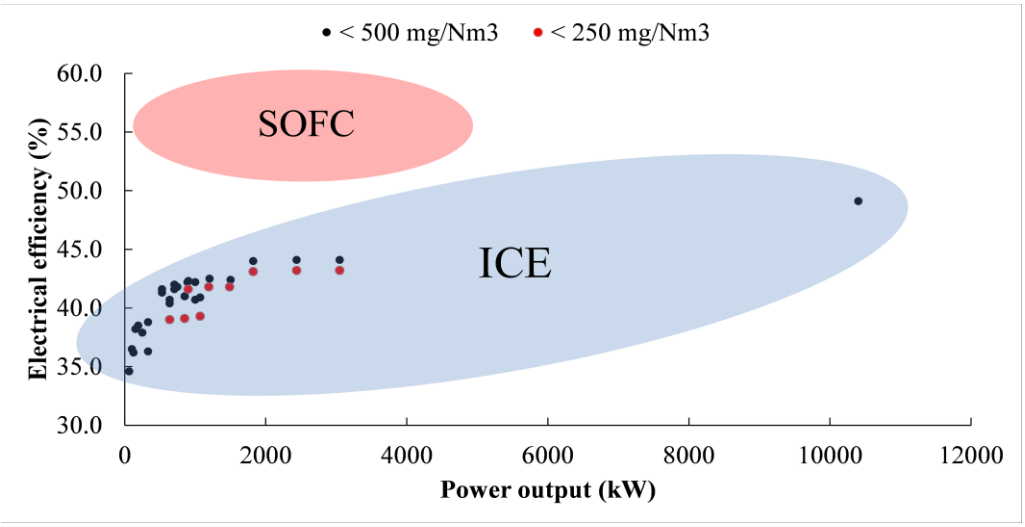

Figure 3. Performance comparison between ICE and SOFC for different plant capacities (ICE: black dot markers and red dot markers indicate machines with NOx emissions below 500 and 250 mg/Nm^3, respectively).

The electrical efficiency of ICEs is surpassed by high-temperature fuel cell generators like molten carbonate fuel cells (MCFC) and solid oxide fuel cells (SOFC), in particular in the lower power scale (< 50 kWe). Especially, the SOFC technology is the most promising one because the highest electrical efficiency can be realized [27].

The exploitation of biogas fuel in SOFC generators has been studied since several years [28–33]. Practical and operational experience has been gained through pilot plants. Industrial installations are also gaining momentum. In California, a capital support is offered to fuel cell installations with an additional bonus in case of biogas feeding. The capital bonus is provided under the Self-Generation Incentive Program (SGIP) [34] and the overall support is 2,800 US$/kW installed (1,490 $/kW for fuel cell generation, plus an adder of 1,310 for biogas fuel use; 100% of the support is awarded only to installations below 1 MW electric).

Several plant configurations are potentially available for the high-efficiency electrical generation in biogas-fed SOFC systems. Large integrated biogas SOFC plants with either atmospheric or pressurized SOFC operation, SOFC-GT hybrid power generation with a gas turbine as bottoming cycle and carbon capture via anode-exhaust oxycombustion, were analyzed recently [35]. The overall electrical efficiency of the analyzed plant configurations ranged in the interval between 50-70%. Hybridization of the SOFC with a gas turbine bottoming cycle effectively boosts the electrical efficiency to 70% when fuel utilization (FU) is 90%.

There are additional advantages related to the use of biogas in SOFC (or MCFC). We envision future energy plants with an enhanced exhaust recovery [36,37] (e.g., hydrogen recovery) and carbon management (i.e., CO_2 recovery and possibly further re-use). In the framework of the EU-funded project SOFCOM [38], a 2 kWe SOFC stack was operated with sewage biogas (Figure 4). The integrated biogas SOFC plant consisted of an innovative treatment of the anode exhaust gas via oxy-combustion and subsequent water vapor condensation that allowed for the recovery of a high-purity CO_2 exit stream [39]. The CO_2 was recycled to a photobioreactor in which micro-algae biomass is harvested. In this way, a closed carbon cycle was obtained in which organic carbon from sewage sludge is eventually recycled into another fuel (algae biomass). In the photobioreactor, micronutrients (nitrates and phosphates) are taken from wastewater that is circulated in a semi-closed loop. Hence, a further biological water treatment process is achieved while growing biomass.

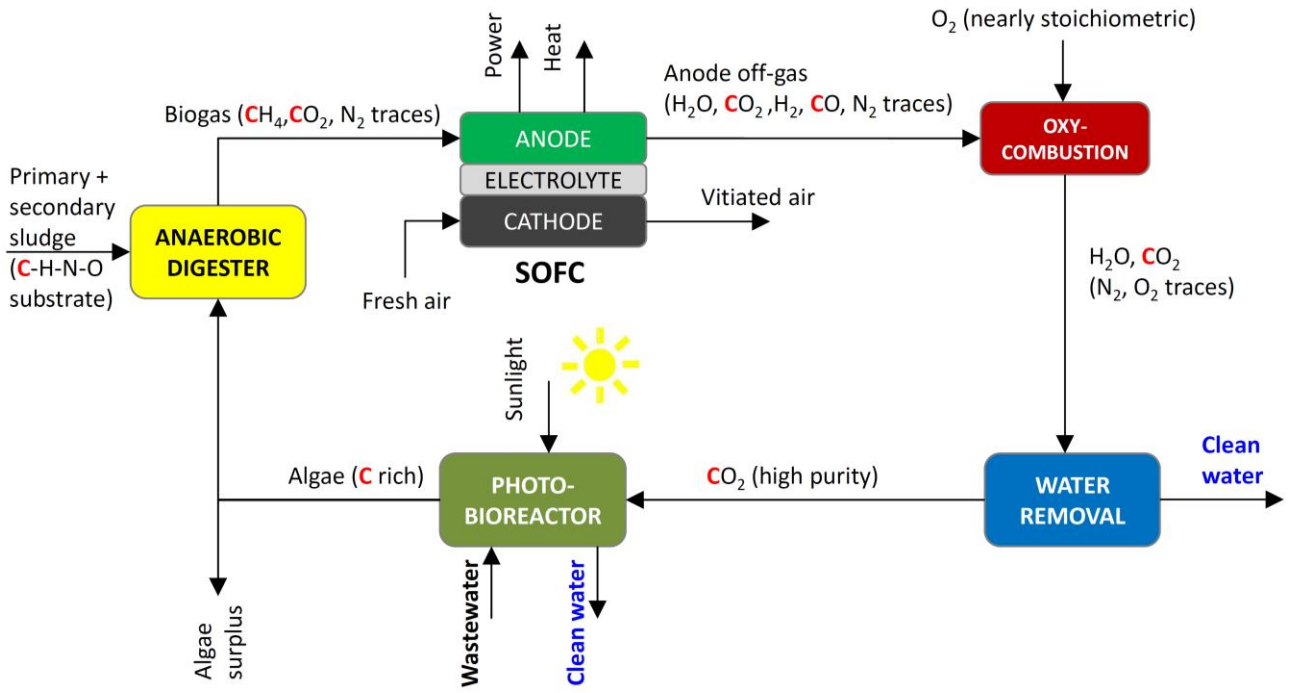

Figure 4. The 'carbon re-cycle' concept in the SOFCOM plant [40].

The issue of contaminants

Biogas fuel contains on average 50-65% vol. CH_4 and 35-50% vol. CO_2. A range of concentrations of the main biogas constituents is provided in Table 7. Only landfill biogas might result in a composition that goes beyond ranges indicated in Table 7. Landfill biogas (LGF) is produced from municipal solid waste that is stored in anaerobic underground or undercover waste cells. The biogas quality varies significantly during the landfill lifetime. On average, a peak production is reached 5 to 7 years after the waste has been dumped in the landfill, after which a decreasing trend over time is observed for the CH_4 content in the extracted gas. Thus, the CH_4 volume fraction in landfill biogas can decrease below 50%. In landfills, almost all gas is generally produced within a 20-year time frame; however, small quantities of gas may continue to be produced for 50 or more years. Therefore low-methane yield, low-CH_4 content scenarios are also possible [41].

In anaerobic digesters, fluctuations in biogas production are directly linked to the amount of organic matter treated. Especially, there are daily and seasonal fluctuations in biogas production in digesters using sludge from wastewater treatment plants (WWTPs) or livestock manure.

Nonetheless, apart from CH_4 content and production variations – that are quite predictable and substrate dependent – the main issue with biogas is dealing with contaminants. The amount and type of contaminants are widely varying depending not only on the organic substrate that undergoes anaerobic digestion (AD) but also on the digester operating conditions (temperature, hydraulic retention time) and effluent pre-treatments prior to AD.

Table 7. Main biogas constituents

Compounds	**vol. %**
Methane, CH_4	50 - 70
Carbon dioxide, CO_2	30 - 50
Water vapor, H_2O	1 - 2
Carbon monoxide, CO	0 - 0.3
Hydrogen, H_2	0 - 1
Nitrogen, N_2	1 - 5
Oxygen, O_2	From traces up to 2-3%
Hydrogen sulfide, H_2S	From tens to hundreds of ppm

Specific contaminants present in AD biogas are hydrogen sulfide (H_2S), organic sulfur compounds such as mercaptans, COS, CS_2, halides (e.g., HCl), siloxanes, aromatic compounds (e.g., toluene) and terpenes (e.g., limonene) [42]. In LFG halocarbon compounds are also quite abundant [43]. When biogas is used as a fuel for electricity generation, trace compounds may damage the combustion engines, necessitating additional maintenance costs for repairs and reducing availability due to service interruptions. During the combustion process, hydrogen sulfide is transformed to sulfur oxides – SOx (e.g., SO_2) – that have adverse impacts on both human health (with an increase of respiratory diseases) and the environment (acid rain). SOx can also form acid gas like sulfuric acid (H_2SO_4) which can damage the engine's components. Other corrosive acids like HCl and HF are also formed to a lesser extent. Siloxanes are particularly detrimental since they are thermally decomposed into silicates and micro-crystalline quartz, which contribute to abrasion of the inner surfaces of the combustion engine [44].

Economic feasibility of integrated biogas fuel cell plants

High-temperature fuel cell systems based either on molten carbonate fuel cell (MCFC) or solid oxide fuel cell (SOFC) technology are being deployed in stationary applications for the generation of electricity and heat. MCFC systems can achieve an electrical efficiency up to 47% (LHV, NG or biogas fuel) [45]. SOFC systems can easily exceed values above 50%, with the aim to reach net AC system efficiency up to 60%.

The uninstalled system cost of MCFC is in the range 2,500 – 4,500 US$/kW (ref. year 2012) [46]. The mentioned range refers to systems from the few MW scale to the sub-MW scale with an already established market of approx. 70 MW installed in 2014 [47]. SOFC modules are currently more expensive than MCFC with a unit price cost above 10,000 US$/kW for a 50 kW electric module[24]. However, a market price equal to that of MCFC is expected to be feasible as manufacturing capacity increases [48].

The clean-up capital cost is currently estimated to 500 – 1,000 $/kW (installed cost, ref. year 2015) [49]. A capital cost <500 US$/kW is considered a near-term target, while the long-term target sets the clean-up cost below 200 US$/kW [49].

Chapter 2 – The origin of contaminants in anaerobic digestion biogas: type and amounts of contaminants depending on the organic substrate and in-situ abatement measures

Biogas contains a large variety of trace impurities. Besides the main gas constituents (CH_4, CO_2, and N_2), different types and amounts of contaminants are found in biogas depending on the organic substrate and possible in-situ abatement measures (these are mostly employed for H_2S removal).

Several factors affect the concentration of these impurities, e.g., temperature, pressure, type/origin of waste, the age of waste (LFG). Table 8 shows typical untreated biogas impurities concentrations for landfill and anaerobic digestion gas. It is worth noting that halogens are very low in concentration in ADG (often below 1 ppm), while higher amounts are found in LFG.

Table 8. Typical untreated biogas contaminants concentrations (ppm) for ADG and LFG.

Biogas type	**Sulfur compounds**		**Siloxanes**	**Halogens**		**Halocarbons**	**Hydrocarbons**	**Ref.**
	H_2S	Other S-compounds	D5, D4, etc.	HCl	HF, HBr, and others		Benzene, Toluene, etc.	
ADG	121	0.5	0.24 - 2.3	0.2 - 1.4	1	0.16	1.6	[50]
ADG	24 - 63	n.a.	0.1- 0.7	0.2 - 0.8	n.a.	n.a.	0.7 - 3	[51]
ADG	1.8 - 104	0.15 - 0.66	0.6 - 1	n.a	n.a	< 0.1	0.4 - 1.7	[52]
ADG	80 - 130	n.a.	Up to 2.9	n.a.	n.a.	~1	n.a.	[53]
LFG	77 - 3400	n.a.	~ 2	n.d.	n.a.	6 - 14	100 - 300	[54]
LFG	63 - 5400	7.5 - 19	Up to 0.7	n.a.	n.a.	~7	n.a.	[53]
LFG	150 - 280	n.a.	0.5 - 0.7	11- 20		~10	86 - 150	[55]

ADG: Anaerobic digester gas, LFG: Landfill gas, n.a. = not available, n.d. = not detected.

In Table 9, the measured amount of halogens concentration in the biogas from different landfill and WWTP sites is given [56]. Once again, very low levels are observed in WWTP derived biogas compared to landfill gas.

Table 9. Halogens in landfill and WWTP biogas [56].

Plant Type	**Halogens (F, Cl, Br, I) (mg/Nm^3)**
Landfill A	79.5
Landfill B	12.2
Landfill C	36.6
Landfill D	11.2
WWTP A	0.9
WWTP B	1
WWTP C	0.9
WWTP D	0.9

Halogens are contained within waste in the form of kitchen salts and polymers (polytetrafluoroethylene: PTFE, polyvinylchloride: PVC). As such, these compounds are mostly found in biogas stemming from landfills [57,58]. Figure 5 compares organic chlorine compounds (halocarbons) measured in landfill gas and biogas produced from anaerobic digestion of sewage sludge. It is visible that average concentrations in landfill gas are higher than maximum values detected in gas stemming from sewage sludge. In fact, the halogen content in biogas from WWTPs lies in the same range as that in biogas produced on farms, and values are very low (< 1 ppm, on average).

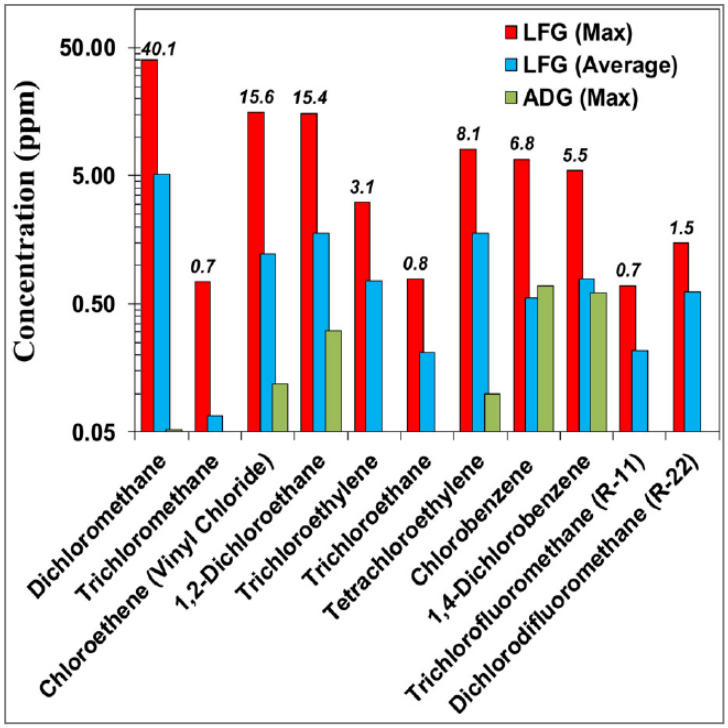

Figure 5. Organic chlorine compounds (halocarbons) in landfill gas and biogas of sewage sludge (reprinted with permission from Papadias et al. [46]*)*

H_2S is generally the most abundant contaminant and is largely found in digester gas coming from manure (hundreds or thousands of ppm) and dairy streams, where it can range from 300 to 6,000 ppm [59]. The Gas Technology Institute (GTI) reported an average H_2S content of about 3,000 ppm in raw biogas from diary streams. Definitely lower amounts of other sulfur compounds are also present (SO_2 7.73 ppm , COS 4.09 ppm, CS_2 0.17 ppm, methyl mercaptans 6.12 ppm) [60]. Biogas from organic substrates derived from animal waste products is also characterized by small amounts of siloxanes (below 0.5 ppm) and halocarbons. Hydrocarbons are instead found at the single digit ppm(v) range.

Sewage biogas also contains H_2S, but often to a lesser extent (e.g., below 100 ppm) because of the use of iron salts in the water line. Iron salts are used in WWTPs to precipitate phosphorus (P) – whose concentration in treated water must not exceed limits regulated by law in order to avoid eutrophication on land and aquatic vegetation –, but they are also able to precipitate sulfur thus reducing the overall H_2S content in the as-produced

AD biogas from sludge. Fe^{2+} removes sulfide by precipitating it as ferrous sulfide (FeS), while Fe^{3+} oxidizes sulfide chemically to elemental sulfur, with itself being reduced to Fe^{2+}, which subsequently precipitates sulfide forming FeS [61].

Volatile organic silicon compounds (VOSiC), also known as volatile methyl siloxanes (VMS) or simply siloxanes, are recognized as the most undesirable compounds in the AD biogas and LFG. Siloxanes originate from silicone based compounds which are often found in consumer products thus ending up in sewers (e.g., cosmetics, personal care products, adhesives and coatings, sealants, etc.) [62,63]. Siloxanes are indeed the building blocks of silicones. According to literature, the most frequent compounds in sewage biogas are cyclic volatile polydimethylsiloxanes (D4, D5), with D5 concentration being several times higher than D4. Especially, D4 and D5 often make up 90% of the overall silicon content of biogas. Biogas from municipal sludge digestion usually has a higher siloxane concentration than landfill gas. Landfill gas may contain significant quantities of other siloxanes, such as D3 and D6, as well as L2–L5 (see Table 10 for the nomenclature). The amount of siloxanes in old and closed landfills is generally lower than in new ones, where silicon-containing waste is continuously disposed of [58].

The main difference between landfill and AD gas in the amount and type of siloxanes contained in it depends on the water solubility of the organic silicon compounds. Water-soluble siloxanes will tend to remain in the water phase, thus being discharged back into the water system together with purified water, whereas insoluble siloxanes will adsorb into the activated sludge and be partly transferred to the gas phase within the digester [58]. Due to their high hydrophobicity and volatility, cyclic volatile methylsiloxanes (cVMS) largely tend to adsorb on activated sludge flocks in aeration tanks within the WWTP [64]. Within the anaerobic digester, where the sludge can reach a temperature around and above 40 °C, siloxanes can significantly volatilize and end up in the biogas. Among the various contaminants, siloxanes are certainly the most detrimental for end-use devices for biogas valorisation into electricity. In the combustion chamber of internal combustion engines, siloxanes are oxidized to silicates (e.g., SiO_2) [42]. The accumulation of abrasive microcrystalline silica (SiO_2) and silicates deposits on an engine's mechanical parts (pistons, cylinder heads, and valves) and leads to an early failure of the engine, requiring earlier repairing and maintenance services[65]. Recently it has been shown that siloxanes in digester biogas are highly detrimental also for solid oxide fuel cells, even when present at the ppb(v) levels in the anode feed, causing a rapid and irreversible degradation of the fuel cell performance [66].

Biogas produced from manure digestion does not contain siloxanes, although the H_2S and organic sulfur concentration are generally much higher than for WWTP biogas or LFG. Additionally, siloxanes are not found in biogas from pure food waste and dairy streams.

The average siloxanes concentration in German WWTPs (308 plants were reviewed) is 14.9 mg/m³ (with values ranging in the interval 0–317 mg/m³) [58]. The silicon concentration in German landfill gas varies between 1 and 8 mg/m³, which corresponds to approximately 3 and 25 mg/m³ total siloxane [58].

Table 10 and Table 11 provide an overview of the type and amount of siloxanes found in WWTPs. The amount of total siloxanes (or total Si) is quite scattered among the various plants. Expect for a few cases, the total Si concentration is consistently around or below 6 mg Si / m^3 for WWTPs located in Europe.

In Table 12, an overview of the type and amount of siloxanes measured in landfill sites is also provided. As for WWTPs, the situation is also quite scattered. However, on average, a lower silicon content is found in LFG compared to sewage biogas.

Finally, it is worth noting how, compared to the H_2S concentration, the siloxanes concentrations are strongly fluctuating even on a daily basis (Figure 6). Often, the non-continuous sludge feeding to the digester is responsible for the observed fluctuations.

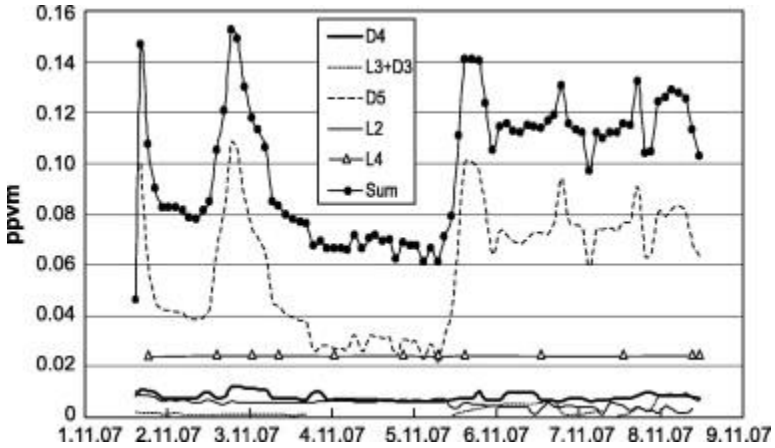

Figure 6. Daily fluctuation of siloxanes concentration in biogas produced from the digestion of sewage sludge and bio-waste. A drop in the siloxane concentration was noticed during the weekend (4–5.11) during which no sludge was fed to the reactor (reprinted with permission from Arnold and Kajolinna [67]*)*

Table 10. Siloxanes amount in different WWTPs (the location of each plant is also provided together with Reference for original source data) – Part I (to be continued on the next page)

Compound	**Chemical formula**	**M.W. (g/mol)**		Finland [67]	Finland [67] (note 1)	Finland [67] (note 2)	Germany [68]	Germany [68]	US [69] (note 3)	Italy (note 4)	Italy (note 4)	Italy (note 4)
Total siloxanes			[mg/m^3]	29.6	2.4	5.5	16.5	6.0	107.4	14.4	10.8	6.2
(D6) Dodecamethylcyclohexasiloxane	**$C_{12}H_{36}O_6Si_6$**	444.92	[mg/m^3]	n.a.	n.a.	n.a.	n.a.	n.d.	6.99	0.7	n.d.	n.d.
(D5) Decamethylcyclopentasiloxane	**$C_{10}H_{30}O_5Si_5$**	370.77	[mg/m^3]	27.05	0.90	4.46	9.31	2.78	56.61	11.0	5.50	3.63
(D4) Octamethylcyclotetrasiloxane	**$C_8H_{24}O_4Si_4$**	296.62	[mg/m^3]	1.21	0.10	0.13	6.69	2.95	32.50	2.5	1.29	0.87
(D3) Hexamethylcyclotrisiloxane	**$C_6H_{18}O_3Si_3$**	222.46	[mg/m^3]	0.00	0.03	0.06	0.17	0.19	3.27	0.0	0.26	0.36
(L4) Decamethyltetrasiloxane	**$C_{10}H_{30}O_3Si_4$**	310.69	[mg/m^3]	1.29	1.29	0.51	0.14	0.02	n.a.	n.d.	3.36	1.34
(L3) Octamethyltrisiloxane	**$C_8H_{24}O_2Si_3$**	236.53	[mg/m^3]	0.03	n.d.	0.2	0.03	0.02	1.93	0.2	0.33	n.d.
(L2) Hexamethyldisiloxane	**$C_6H_{18}OSi_2$**	162.38	[mg/m^3]	0	0.04	0.09	0.05	0.01	6.14	n.d.	0.07	0.02
(TMS) Trimethylsilanol	**$C_3H_{10}OSi$**	90.20	[mg/m^3]	n.d.	n.d.	n.d.	0.14	0.07	n.d.	n.d.	n.d.	n.d.
Si tot (*calculated*)	**-**	**-**	[mg Si /m^3]	**11.0**	**0.8**	**2.0**	**6.2**	**2.3**	**40.3**	**5.4**	**3.7**	**2.2**

n.d. = not detected / under detectability limit.

n.a. = not available / not measured.

Note 1: Sewage sludge + municipal and industrial bio-waste 70–30%.

Note 2: Sewage sludge + food waste/industrial sludge 70–30%.

Note 3: an average of 50 different municipal anaerobic digesters was analyzed.

Note 4: unpublished data from field measurements on two different WWTPs in the area of Torino, IT.

Table 11. Siloxanes amount in different WWTPs (the location of each plant is also provided together with Reference for original source data) – Part II

Compound	**Chemical formula**	**M.W. (g/mol)**		Spain [52]	Spain [57]	Austria [70]	Finland [70] (note 5)	Spain [56]	Spain [56]	Spain [56]	Spain [56]
Total siloxanes			[mg/m^3]	13.4	132.7	7.0	2.5	7.5	361.6	15.8	52.0
(D6) Dodecamethylcyclohexasiloxane	**$C_{12}H_{36}O_6Si_6$**	444.92	[mg/m^3]	n.a.	n.d.	n.a.	n.a.	0.1	8.7	0.2	2.5
(D5) Decamethylcyclopentasiloxane	**$C_{10}H_{30}O_5Si_5$**	370.77	[mg/m^3]	7.75	87.01	6.03	1.28	5.3	340.7	11.9	48.4
(D4) Octamethylcyclotetrasiloxane	**$C_8H_{24}O_4Si_4$**	296.62	[mg/m^3]	5.25	43.80	0.93	0.87	0.5	8.1	0.9	1
(D3) Hexamethylcyclotrisiloxane	**$C_6H_{18}O_3Si_3$**	222.46	[mg/m^3]	0.4	0.26	0.04	0.04	1.6	n.d.	2.8	0.1
(L4) Decamethyltetrasiloxane	**$C_{10}H_{30}O_3Si_4$**	310.69	[mg/m^3]	n.d.	0.69	n.d.	0.04	n.d.	0.7	n.d.	n.d.
(L3) Octamethyltrisiloxane	**$C_8H_{24}O_2Si_3$**	236.53	[mg/m^3]	n.d.	0.53	0.02	0.2	n.d.		n.d.	n.d.
(L2) Hexamethyldisiloxane	**$C_6H_{18}OSi_2$**	162.38	[mg/m^3]	n.d.	0.36	0.02	0.08	n.d.	3.4	n.d.	n.d.
(TMS) Trimethylsilanol	**$C_3H_{10}OSi$**	90.20	[mg/m^3]	n.d.	n.d.	n.d.	n.d.	n.d.	n.d.	n.d.	n.d.
Si tot (*calculated*)	**-**	**-**	[mg Si /m^3]	**5.1**	**50.0**	**2.7**	**0.9**	**2.8**	**136.4**	**6.0**	**19.6**

n.d. = not detected / under detectability limit.

n.a. = not available / not measured.

Note 5: max. value of each range was taken (average of 4 WWTPs in Finland).

Table 12. Siloxanes amount in different landfill sites

Compound	Chemical formula	M.W. (g/mol)		Spain [56]	Spain [56]	Spain [56]	Spain [56]	Finland [70]	Finland [67]	Finland [67]	Finland [67]	Germany [68]	US [69]
Total siloxanes			[mg/m^3]	84.3	20.7	25.6	20.5	2.3	9.8	6.7	1.4	17.5	13.5
(D6) Dodecamethylcyclohexasiloxane	$C_{12}H_{36}O_6Si_6$	444.92	[mg/m^3]	1.5	0.4	0.5	n.d.	n.a.	n.a.	n.a.	n.a.	n.d.	n.d.
(D5) Decamethylcyclopentasiloxane	$C_{10}H_{30}O_5Si_5$	370.77	[mg/m^3]	11.8	6.4	6	0.9	0.3	0.60	1.31	0.13	0.80	0.47
(D4) Octamethylcyclotetrasiloxane	$C_8H_{24}O_4Si_4$	296.62	[mg/m^3]	29.1	3.6	11.8	5	0.67	4.30	0.93	0.21	8.41	9.27
(D3) Hexamethylcyclotrisiloxane	$C_6H_{18}O_3Si_3$	222.46	[mg/m^3]	2.8	0.1	0.5	0.4	0.10	0.60	2.29	0.85	0.01	0.38
(L4) Decamethyltetrasiloxane	$C_{10}H_{30}O_3Si_4$	310.69	[mg/m^3]	n.d.	n.d.	n.d.	n.d.	n.d.	2.30	1.29	n.d.	n.d.	n.d.
(L3) Octamethyltrisiloxane	$C_8H_{24}O_2Si_3$	236.53	[mg/m^3]	n.d.	n.d.	n.d.	n.d.	0.01	n.d.	0.05	n.d.	0.04	0.04
(L2) Hexamethyldisiloxane	$C_6H_{18}OSi_2$	162.38	[mg/m^3]	3.4	0.1	0.1	1.5	0.63	n.d.	0.22	0.19	1.18	0.58
(TMS) Trimethylsilanol	$C_3H_{10}OSi$	90.20	[mg/m^3]	35.7	10.1	6.7	12.7	0.56	2	0.60	0.01	7.03	2.81
Si tot (*calculated*)	**-**	**-**	[mg Si /m^3]	**29.32**	**7.13**	**9.21**	**6.84**	**0.80**	**3.32**	**2.34**	**0.52**	**6.08**	**4.90**

Chapter 3 – Impact of biogas contaminants on Ni reforming catalyst

Introduction

Biogas essentially consists of a mixture of methane, carbon dioxide, nitrogen (to a lesser extent) and a wide range of trace compounds (mostly H_2S, siloxanes, hydrocarbons and other volatile organic compounds), which might be tricky to remove below ppm levels unless a deep clean-up stage is carried out [71]. In this context, the utilization of a biogas fuel-processing unit instead of a direct biogas feeding to the SOFC stack, is often the adopted design to protect the fuel cell stack from the risk of carbon deposition and/or sintering at the SOFC anode [72–74]. Janardhanan et al. [75] have shown how the direct internal reforming of methane can significantly reduce the gas temperature at the anode inlet section (see Figure 7), which is due to the high catalytic activity of the Ni-anode towards reforming reactions. The sudden anode gas cooling might be detrimental in terms of both a higher risk of carbon deposition and an enhanced thermal gradient across the SOFC cell.

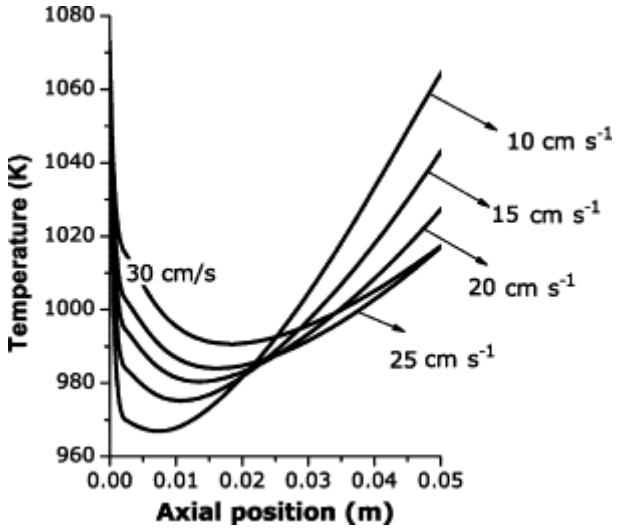

Figure 7. Gas cooling effect at different inlet gas velocities due to the internal reforming of methane inside the Ni-SOFC electrode (reprinted with permission from Janardhanan et al. [75]*)*

In principle, biogas could be converted into a hydrogen-rich synthesis gas simply by dry reforming reaction in presence of a suitable catalyst. However, since the inlet molar ratio CH_4/CO_2 is about 1.5, dry reforming alone can lead to significant carbon deposition within the reactor [76–78]. Therefore, it is desirable to add another oxidant species to the biogas feed such as steam. The addition of steam to the inlet gas stream promotes the methane steam reforming reaction.

Dry and steam-reforming reactions are summarized below:

$$CH_4 + CO_2 \rightleftharpoons 2\ H_2 + 2CO \text{ (dry reforming : } \Delta H_{298} = 59 \text{ kcal/mol)} \quad (1)$$

$CH_4 + H_2O \rightleftharpoons 3\ H_2 + CO$ (steam methane reforming : ΔH_{298}= 49 kcal/mol) (2)

In addition to reactions (1) and (2), other relevant reactions are:

$CO + H_2O \rightleftharpoons H_2 + CO_2$ (water gas shift : ΔH_{298}= - 10 kcal/mol) (3)

$CH_4 \rightleftharpoons 2\ H_2 + C$ (methane pyrolysis : ΔH_{298}= 18 kcal/mol) (4)

$2\ CO \rightleftharpoons CO_2 + C$ (Boudouard reaction : ΔH_{298}= - 41 kcal/mol) (5)

From a thermodynamic point of view, both dry and steam methane reforming reactions are highly endothermic and thus external heat must be provided to maintain a good activity on the catalyst. Instead, the water gas shift reaction is mildly exothermic and heat addition promotes the selectivity towards CO and steam. High temperature (> 600°C) reforming with a steam-to-carbon ratio equal or higher than 2 is required to provide a good feed conversion without coke formation [78–80]. Nickel-based catalysts have been already investigated for biogas steam reforming [81–83]. Nickel is widely used for reforming applications because it is less costly compared to noble metal-based catalysts [84,85]. Ahmed et al. [85] tested the performance of a rhodium-based catalyst for the steam-reforming of biogas, while varying the inlet feed gas concentrations, the gas hourly space velocity, the reactor temperature and the steam-to-carbon ratio.

It is worthwhile mentioning how the majority of the available literature on biogas reforming deals with catalytic experiments that have been carried out with clean gas. The impact of fuel impurities other than H_2S has been overlooked. In fact – in the most of the experimental setups – a synthetic biogas stream is obtained by mixing pure CH_4 and CO_2 gases that are supplied in pressurized gas cylinders. Nonetheless, the presence of fuel contaminants cannot be excluded in real applications. More importantly, the effect of fuel contamination can be substantial on both the performance and the long-term durability of the fuel processor.

The issue of carbon deposition on Ni-based catalysts is instead quite covered and will also be reviewed in this work. Light hydrocarbons (C_nH_m such as ethylene, ethane, propane etc.) can significantly affect the formation of carbon species and thus the effectiveness of the catalyst. The formation of carbon on the catalyst layer under steam reforming conditions may take place mostly through cracking of hydrocarbons as well as through the Boudouard reaction. Trimm [86,87] determined the coking tendency for steam reforming of methane in the presence of C2- and C3-hydrocarbons over a Ni catalyst. The coke formation increases with the carbon number, especially in the presence of olefin species. D'Angeli et al. [88] have also shown how coke formation increases with the molecular weight of the feed and that deactivation rates during steam reforming of ethane and propane over Ni/MgO were higher compared to methane.

Besides carbon deposition degradation issues, the most studied contaminant for deactivation of the catalytic steam reforming on Ni is sulfur, in the form of H_2S. This contaminant leads to an almost total deactivation of the catalyst. Catalyst poisoning occurs due to the strong adsorption of sulfur on active sites.

Adsorbed sulfur thus blocks or alters the adsorptivity of the other species by an electronic effect [89]. Overall, the saturation coverage of sulfur and other species (e.g., HCl) depends on the operating temperature, metal loading, and the partial pressure of reacting gases. Catalysts with lower metal loading will lose their activity at a faster rate compared to catalysts with higher metal loading [87,90]. This chapter will review the impact of different biogas poisoning species on the reforming capability of Ni catalysts, including recent findings on impurities other than H_2S.

Effect of H_2S poisoning

The presence of H_2S in the biogas adversely affects the activity of the nickel-based catalysts [91–93]. Although desulphurization technologies will reduce the amount of hydrogen sulfide present in the biogas, residual post-cleaning concentrations (few ppm, or even sub-ppm, concentrations) might be not be tolerated by the nickel-based catalyst even in the case the fuel processor is operated at higher temperatures (>700 ˚C) [83,94]. Indeed, the presence of sulfur was found to enhance nickel sintering as well as carbon deposition [95] (see Table 13).

The poisoning effect of H_2S on the catalytic surface during the reforming of hydrocarbons is even more complex due to the competition among various molecules and radicals for the active sites. For instance, the saturation coverage of H atoms on a catalytic surface is significantly affected by the partial pressure of CO in the gas mixture. The deactivation of the reforming catalyst was found to be exponential in time and deactivation times range from 5 to 20 hours [83,94]. As expected, the deactivation trend is faster as the H_2S concentration is higher. A fast drop in the activity of the Ni catalyst on exposure to H_2S (20, 50 and 100 ppm) at high temperatures (700 °C and 800 °C) has been reported by Appari et al using simulated biogas on a Ni-based catalyst [77]. Especially, for H_2S concentrations above 20 ppm in the biogas stream, an almost complete deactivation (98%) of the catalyst was observed. All the investigated H_2S concentrations led to saturation coverage at 700 °C, whereas at 800 °C the mechanisms of H_2S adsorption and recombination reactions involving sulfur lead to different saturation coverages of sulfur for different H_2S concentrations. Appari et al have also developed a detailed kinetic model for simultaneous dry and steam reforming of biogas on Ni based catalyst, which highlighted how both CH_4 and CO_2 conversion was blocked as soon as H_2S was introduced [96].

Appari et al. [77] have also investigated regeneration techniques after sulfur poisoning. Key findings were that contamination at lower temperature (700 °C) is not fully reversible upon removal of H_2S from the feed stream. However, full performance recovery is achieved at higher temperature (800 °C).

In fact, CO_2 was found to participate to the reforming reactions at 750 °C only for S/C ratios below 2.5 mol/mol [96]. However, along the length of the reactor, the poisoning is not uniform. At 973 K and 1073 K the poisoning occurs from the inlet towards the exit of the reactor as time proceeds. In fact as the poisoning proceeds, the location of the methane reforming reaction moves downstream through the reactor length.

Chattanathan et al. [97] investigated the effect of temperature (650 °C, 750 °C and 800 °C) and H_2S concentration (0.5 mole%, 1 mole% and 1.5 mole%) on dry biogas reforming using a commercial Ni-catalyst. Results showed how both CH_4 and CO_2 conversion decreased drastically even at the lowest H_2S concentration (0.5 mol. %). Post-mortem analysis revealed that the coking presence was mainly dominant in the absence of H_2S, while it became less pronounced with the introduction of H_2S. However, no sulfur presence was observed, as expected. The meaning of these findings is that catalyst sulfur poisoning prevails over coke formation. Chiodo et al. investigated the boundary sulfur concentration on the commercial Ni-catalyst tested under steam reforming conditions. Biogas steam reforming measurements were carried out adding different H_2S concentrations (0.4–2 ppm) in the inlet gas stream. Results showed how with 0.4 ppm of H_2S the catalyst activity remained stable for 100 h of test. However, the Ni-catalyst resulted completely deactivated when the H_2S concentration was increased to 1 and 2 ppm, respectively, even if different deactivation rates were recorded. The rapid observed deactivation clearly indicates that the amount of sulfur in the biogas had little impact on methane conversion in the first hours of the catalytic tests. This implies that the activity is affected by the cumulated amount of sulfur poisoning, rather than by the inlet sulfur concentration in the inlet gas stream. According to Chattanathan et al. [97], the amount of carbon deposition resulted unaffected by the amount of sulfur originally present in the fuel. In fact, the elementary analysis carried out on spent Ni-catalysts revealed carbon formation rates ≤ 0.1 $mgC g_{cat}^{-1} h^{-1}$, which is very close to carbon deposition rates observed on Ni-samples working with a clean biogas stream composed of solely methane and carbon dioxide.

A way to achieve sulfur-resistant Ni-catalysts for the steam reforming process is doping Ni with other elements [95]. Wang et al increased the sulfur tolerance by supporting nickel on ZSM-5 zeolite and by preparing bi-metallic Ni-Re, Ni-Co and Ni-Mo catalysts [98]. The use of a ceria ion-exchanged ZSM-5 catalyst with 5 wt. % nickel content showed high activity in steam reforming of kerosene and displayed little sensitivity to 20 ppm of sulfur. The activity of a traditional Ni-catalyst was also improved by adding second metals in the form of Re, Co and Mo, with Re displaying the most promising results with both high activity and promising sulfur tolerance.

In a series of papers, Xie et al. investigated the influence of sulfur on the steam reforming of liquid hydrocarbons on ceria-alumina Ni, Rh and Ni-Rh catalysts [99,100]. Neither of the catalysts containing nickel was stable in a sulfur-laden environment, even though the Ni-Rh catalyst was deactivated less quickly. Results also showed how carbon deposition was increased in the presence of sulfur in the gas stream, and this effect was more pronounced with respect to nickel. The deactivation by sulfur poisoning and carbon deposition on Rh-Ni supported on alumina was also investigated by Lakhapatri and Abraham [101].

Table 13. Review of selected literature studies on the H_2S poisoning of the Ni catalyst in steam reforming applications.

References	Catalyst	H_2S concentration	T (°C)	Test duration
Appari et al. [77]	Ni/γ-Al_2O_3	20-108 ppm	700-900	20 h
Chattanathan et al. [97]	Reformax 250 (SudChemie, USA)	0.5-1.0-1.5%	650, 750, 850	5 h
Chiodo et al. [102]	Ni/Al_2O_3 (15 wt% Ni, 73 wt% α-Al_2O_3, 8 wt% CaO)	0.4-1.0-1.6-2.0 ppm	800	100 h
Wang et al. [98]	Monometallic: Ni, Co, Mo, Re, Ru and Rh on ZSM-5 (5wt% Ni, Ru and Rh; 2wt% Co, Mo and Re)	20 ppm	580	300 h
Xie et al. [99]	Monometallic: Ni, Rh (10wt% Ni, 2wt% Rh) on CeO_2-Al_2O_3; Bimetallic: Ni, Rh (10wt% Ni, 2wt% Rh) on CeO_2-Al_2O_3;	350 ppm	550, 800	30- 55 h
Xie et al. [100]	Monometallic: Ni, Rh (10wt% Ni, 2wt% Rh) on CeO_2-Al_2O_3 (20wt% CeO_2);	350 ppm	800	55 h
Lakhapatri et al. [101]	Monometallic: Ni, Rh (10wt% Ni, 2.5wt% Rh) on Al_2O_3; Bimetallic: Ni, Rh (10wt% Ni, 0.5wt% Rh) and Ni, Rh (10wt% Ni, 2.5wt% Rh) on Al_2O_3;	100 ppm	800	10 h
Albertazzi et al. [103]	Ni/MgAl(O) (CATATOR AB)	10-50 ppm	800	140 h
Sehested et al. [104]	Ni/θ-Al_2O_3 (19.4wt% Ni) Ni/θ-Al_2O_3 (19.4wt% Ni; 1.48 K) Ni/$MgAl_2O_4$ (22wt% Ni) Ni/$MgAl_2O_4$ (22wt% Ni; 2.7wt% K) Ni/$MgAl_2O_4$ (22wt% Ni; 3090ppm Sulfur)	890-4000 ppm	550, 650, 750	50 h
Laosisipojana et al.[105]	CeO_2 Gd,Y,Nb,La,Sm on CeO_2 Ni/Al_2O_3 (5 wt% Ni) Rh/Al_2O_3 (5 wt% Rh)	10-100-500-1000 ppm	900	3 h

Effect of light hydrocarbons

Steam reforming of light hydrocarbons (C_nH_m) with n>1 (i.e., a carbon number higher than methane) involves irreversible reactions (Eq. 6), and a high risk of carbon formation and catalyst deactivation is expected [87]. Coke formation takes place via cracking reactions (Eqs. (7) and (8)) as well as the Boudouard reaction (5).

$$C_nH_m + n\,H_2O \rightarrow n\,CO + (n+m/2)\,H_2 \quad (-\Delta H_{298} < 0) \qquad (6)$$

$$CH_4 \rightleftharpoons C + 2H_2 \qquad (7)$$

$$C_nH_m \rightarrow nC + m/2\ H_2 \quad (8)$$

Few studies have been reported in literature about coke formation by hydrocarbons that might be found in biogas [106]. However, several experiments were carried out with a methane feed mixed with C2- and C3-compounds. Among the previous studies on the topic, it was recently shown how a high carbon formation rate (about 0.5 $mgC/g_{cat}^{-1}h^{-1}$ after only 25 h of test) is promoted on Ni supported on Al_2O_3 catalyst by co-feeding 800 ppm of a mixture of C2- and C3- compounds (i.e., both alkanes and alkenes) with a simulated biogas stream (CH_4/CO_2=55/45 % vol.) [102]. When the total inlet hydrocarbons concentration was ≤ 200 ppm, a stable methane conversion rate was observed instead, with only a little amount of carbon deposition (Figure 8).

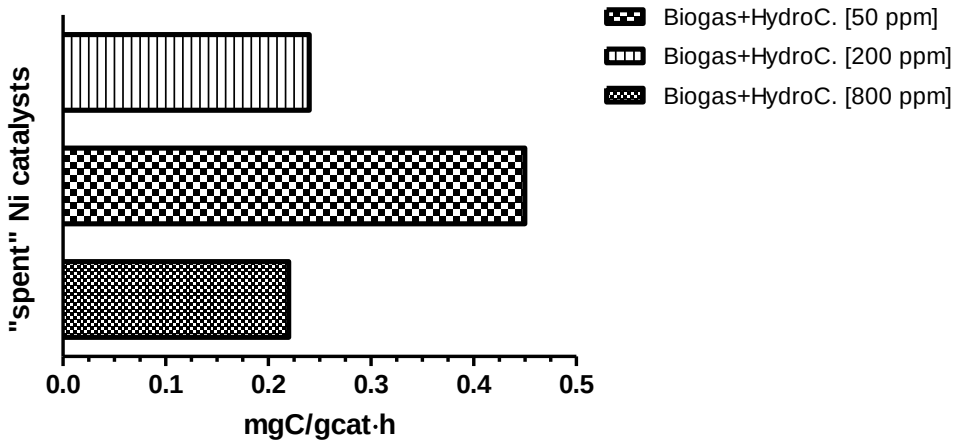

Figure 8. Carbon formation rate on spent Ni catalysts (800 °C, 1 bar, S/C=2, CH_4/CO_2=55/45 % vol.) (Adapted from Chiodo et al. [107] *with permission)*

The abovementioned findings are in agreement with results from Sperle et al. [108], who determined the coking tendency of $Ni/MgAl_2O_4$ catalyst in methane steam reforming in presence of C2 (ethane and ethene) and C3 (propane and propene). It was found that at 500 °C and S/C= 1, the tendency to coking increased having compounds with a carbon number higher than one mixed with methane. Especially, a dramatic increase was observed for alkenes (from about 1 to 150 $mgg_{cat}^{-1}h^{-1}$ for the methane only and the methane/propane/propene mixture, respectively). Hence, it is clear that the catalyst support plays an important role in terms of coke deposition and catalyst deactivation. Sidjabat and Trimm [87] elucidated the benefits of magnesia as a support for nickel catalyst. They found that coke formation increased with the molecular weight of the feed and that the deactivation rates during steam reforming of ethane and propane over Ni/MgO were higher compared to methane only. The rate of carbon formation passed through a maximum at 625 °C, with a value of 0.25 $mgg_{cat}^{-1}h^{-1}$ for Ni/MgO H_2O and 4.66 $mgg_{cat}^{-1}h^{-1}$ for Ni/Al_2O_3. These results strongly suggest that magnesia is catalyzing the gasification of carbonaceous intermediates leading to coke, thereby ensuring an active metal

surface for steam reforming. Furthermore, Didenko et al. [109] showed how Ni catalysts in presence of 2.7 mol % of ethene in methane steam reforming at 750°C highlighted that the high value of the ratio of the catalytic surface area to the free reaction volume (S/V) reduces the negative effect of ethylene in terms of carbon formation. It was supposed that the positive influence of this factor is due to an increase in the contribution of the heterogeneous component of steam reforming and the corresponding increase in the rate of interaction of coke with water vapor.

On the basis of all the above reported results, the addition of different oxides to the Ni reforming catalyst can help improving the catalytic stability with time. Especially, ceria-based oxides promote the gasification of surface carbon species [88]. Laosiripojana et al. [110] found that ceria-doped Ni/Al_2O_3 improves the coke resistance for the steam reforming of an ethane/propane mixture at 900 °C compared to Ni/Al_2O_3 (see Figure 9).

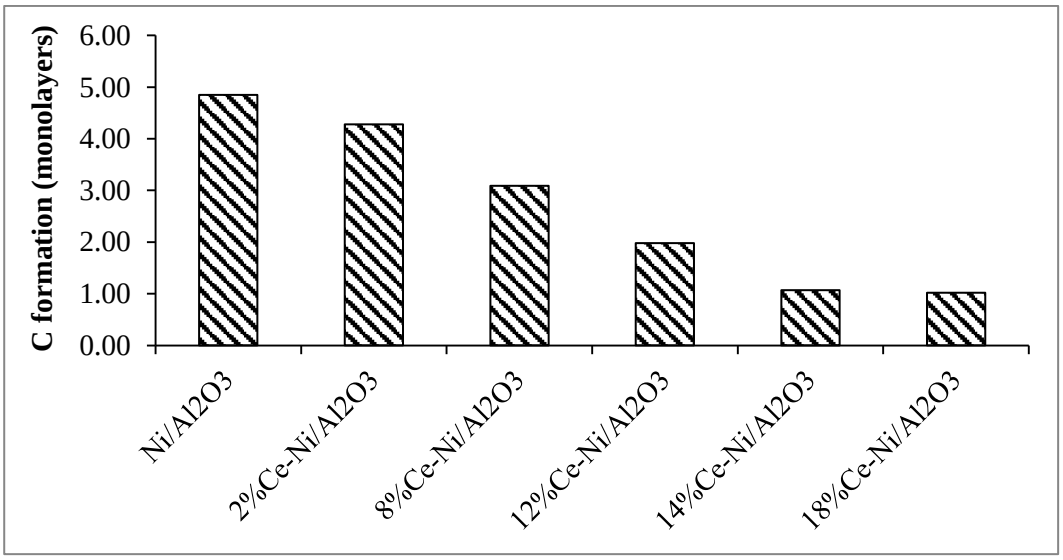

Figure 9. Carbon formation rate on Ce-doped Ni catalysts under steam reforming of an ethane/propane mixture at 900 °C, 1 bar and S/C=3) (The graph summarizes data taken from the work of Laosiripojana et al. [110]*)*

Effect of minor contaminants (siloxanes)

Catalyst deactivation might also occur due to masking or pore blockage phenomena from carbon deposition. The presence of poisonous substances in the feed other than sulfur might be also highly detrimental for the performance of Ni catalyst. The deactivation (often irreversible) might occur due to the physical deposition of foreign substances on the external surface of the catalyst. When dealing with certain biogases, the risk of deposition of foreign particles is especially high in the presence of siloxanes. Very few works are reported in literature on the poisoning of Ni surfaces from organic silicon compounds (siloxanes), and they refer on Ni electrodes of solid oxide fuel cells (see for instance the work of Madi et al., which is also further discussed later in this paper [66]).

Recently, Chiodo et al. [107] performed steam reforming experiments with simulated biogas contaminated with decamethyl-cyclopenta-siloxane (D5). Results showed that the concentration of 1 ppm of D5-siloxane promoted a fast catalytic deactivation, whereas a stable performance was observed with a concentration of D5 = 0.5 ppm (Figure 10).

Post-mortem analysis (SEM-EDX elemental mapping) on spent Ni-catalysts revealed a large amount of micro-silica (SiO_2) deposits on the Ni-surface, the amount of which was quite remarkable, i.e., 4.5 wt. % for the experiment with 1 ppm of D5 and 2.2 wt. % for the experiment with 0.5 ppm of D5. Notably, the degradation effect is cumulative. The gradual accumulation of micro-silica deposits on the catalysts surface gradually inactivates the available catalytic area.

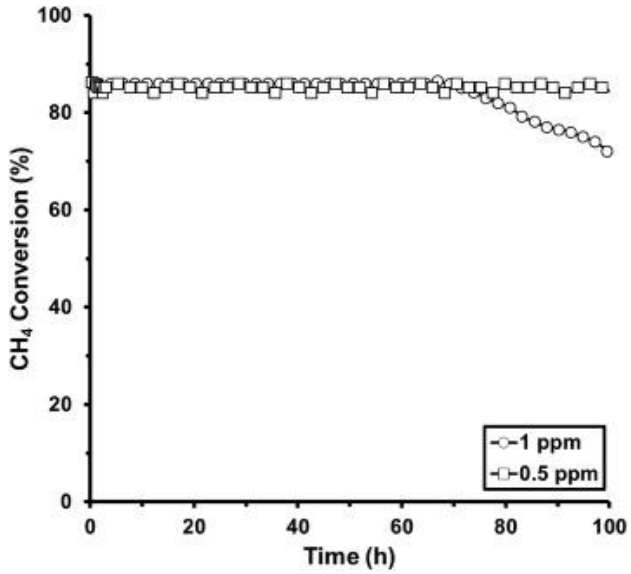

Figure 10. The impact of D5-siloxane on the conversion rate of CH4 within a biogas feed. Operating conditions: biogas steam reforming on Ni/Al_2O_3 catalyst; CH_4/CO_2 = 55/45 vol. %; H_2O/CH_4 = 2 mol/mol; D5 = 0.5 ÷ 1.0 ppm; GHSV = 50,000 h^{-1}; T = 1073 K; P = 1 bar. (Reprinted with permission from Chiodo et al. [107]*)*

Chapter 4 – SOFC Ni-anode poisoning by biogas impurities

The adsorption or deposits of contaminants at the three-phase boundary (TPB) of the SOFC anode can drastically reduce the lifetime of cells and stacks. Contaminants can also affect stack components (namely interconnects and sealant); however, the region which seems the most sensitive to contamination and related degradation is the electrode interface with the electrolyte, where the electrochemical reactions occur. Hence, the durable performance of an SOFC is strongly tied to the characteristics and evolution of electrodes' interfaces during operation [111]. Irvine et al. [112] have recently reviewed the key phenomena affecting the dynamic evolution of electrode interfaces and the three-phase, or two-phase, boundary for both air and fuel electrodes of the SOFC. The accumulation of impurities is one of the main sources of degradation, and can be reversible or irreversible.

In this section, we review the effect of sulfur, silicon and chlorine compounds on the performance of Ni-SOFC anodes. External (or exogenous) impurities as contained in the anode fuel stream are the considered sources of contamination.

There are concerns in the utilization of biogas feed in an SOFC towards carbon deposition and the effect of contaminants [113–116] that cause degradation in the cell/stack performance. Degradation can be defined as the withdrawal of a functional SOFC structure from its designed state [117]. Degradation is often expressed as an increase of area specific resistance (ASR), which are measured by I-V curves and electrochemical impedance spectroscopy (EIS). The ASR can be calculated using the following equation:

$$ASR = \frac{V_0 - V_i}{I} \quad (9)$$

where V_0 is the open circuit voltage (OCV), I is the electrical current, and V_i is the operating voltage at the given current I.

Various poisoning mechanisms have been proposed, and they depend on the nature of the impurity. Sulfur at low and high concentrations cause adsorption-type and reaction-type degradation, respectively [118]. Other chemical degradation mechanisms are sublimation-, deposition-, grain growth- and eutectic-types. In this section, we focus on the chemical durability of SOFC cells and stacks caused by exogenous species such as sulfur, chlorine, and siloxanes at operating temperature.

Sulfur poisoning

The interaction between sulfur-containing molecules and Ni-based anode materials is an important research topic in SOFCs. There are several studies concerning the loss in SOFC performance upon sulfur poisoning as a function of temperature, H_2S concentration, time, current load and anode material [116,119–124]. Ni-YSZ anode-supported SOFCs have limited tolerance towards sulfur compounds [113,125,126]. Table 14 summarizes studies on the characterization of different anode materials upon exposure to H_2S-containing fuels. The performance degradation is a result of an increase in the internal resistance of the SOFC. The

poisoning is reported as a two-step process; a rapid initial drop in the performance followed by a slower prolonged degradation. However, performance stabilization after the initial fast drop is also observed.

The initial performance drop is due to dissociative chemisorption of hydrogen sulfide on nickel active sites and blocking of the three-phase boundary for hydrogen oxidation. The reaction is the following:

$$H_2S + Ni \rightleftharpoons Ni - S + H_2(g) \qquad (10)$$

H_2S has unshared e^- pairs, which can lead to very strong chemisorption on the metal surface. The cell performance can be reversible, depending on exposure concentration and duration. Reversibility has been observed in the case of exposure to concentrations below 50 ppm(v) and short duration[123]. Zha et al. [127] evaluated the recovery of the fuel cell performance after exposure to 2 and 50 ppm H_2S at 800 °C and observed a recovery of 99% and 96% respectively, 50 h after stopping the H_2S exposure. Y. Shiratori et al. [113,114] showed that 1 ppm H_2S contamination in biogas caused about 9% voltage drop and about 40% decrease in the reaction rate of internal dry reforming (at 1000 °C, under 200 mA/cm^2, CH_4/CO_2 = 1.5): in fact, H_2S, even in small amounts (ppb-level), deactivates the steam-reforming and water gas shift reactions. This degradation was reversible and the performance stable after stopping the sulfur supply. Hagen et al. [116] observed a significant irreversible degradation in performance when the cell was poisoned with 2 ppm H_2S over 500 h under a high current load of 1 A/cm^2. At higher H_2S concentrations (>100 ppmv), sulfur will react with nickel and bulk sulfidation (NiS, Ni_3S_x) occurs, causing irreversible damage to the anode catalyst. The initial drop in voltage upon exposure to H_2S has been the focus of most studies in the literature [128–130]. Papurello et al. [121] quantified and correlated the surface coverage of sulfur on nickel-based anodes to sulfur concentration in the fuel with experiments performed both on a single cell and a stack. A Temkin-like adsorption isotherm [131] was used which describes well the time-to-coverage, and which is essential in order to determine the first degradation time. Results showed that, in anode-supported cells, sulfur contamination affects the entire available Ni surface and not just the TPB. Therefore, a wide deactivation of the Ni anode is expected also involving sites for heterogeneous catalysis (i.e., those sites involved in the chemical reactions of internal reforming and water gas shift). In Figure 11, the mechanism of S chemisorption on Ni surface is shown. Adsorbed atoms of S form a c(2x2) structure on the Ni(100) surface at high coverage (>0.7). The S/Ni atomic ratio is 0.5. The corresponding atomic density is 8×10^{14} S atoms per Ni cm^2.

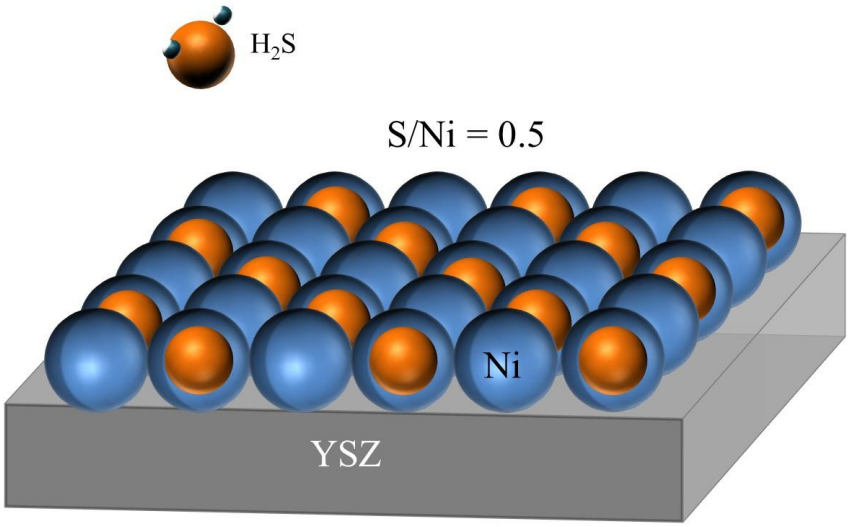

Figure 11. Sulfur coverage on Ni anode with the S monolayer having a c(2x2) structure on the Ni(1,0,0) face (own representation of the sulfur coverage mechanism).

The mechanism of H_2 oxidation and the nature of the rate-determining step remain controversial. Adsorption/desorption, surface diffusion, and charge-transfer reactions having all been suggested as plausible mechanisms[132]. In the conventional Ni-YSZ anode, the more likely mechanism is H_2 adsorption on the Ni surface. Adsorbed hydrogen ions are formed, which migrate to the site of steam formation along the Ni surface (or through bulk Ni and electrolyte). The involved reactions are:

$$H_2(g) \rightleftharpoons 2H^+ + 2e^- \quad (11)$$

$$2H^+ + O^{--} \rightleftharpoons H_2O(g) \quad (12)$$

Therefore, adsorbed S on the Ni surface thus prevents the charge transfer process causing the observed sudden increase in cell polarization.

Nonetheless, the electrolyte type should also be accounted for in the attempt to understand S-deactivation of the Ni-anode. A Ni-SSZ (scandia-stabilized zirconia) cermet resulted in higher tolerance towards sulfur poisoning compared to a conventional Ni-YSZ (yttria-stabilized zirconia)[124,133]. This evidence comes in support of the H_2 oxidation mechanism under which steam formation takes place at the stabilized zirconia surface, in proximity of the three-phase boundary, and electron transport occurs through both Ni and the electrolyte surface, summarized by the following reaction:

$$H_2(g) + O^{--} \rightleftharpoons H_2O(g) + 2e^- \quad (13)$$

Oxygen ions are transported through the electrolyte at the anode interface; here the charge transfer step is accomplished. Sasaki et al.[133], comparing the poisoning of both Ni-YSZ and Ni-ScSZ anodes, concluded that the higher ionic conductivity of SSZ, compared to YSZ, might be responsible for the different sulfur sensitivity of the two cermets. A higher ionic conductivity of electrolyte materials would lead to an extended three-phase boundary. Finally, Hagen et al.[116] have shown that the steam reforming activity (i.e., CH_4

conversion) seems not to be affected by the electrolyte type (YSZ vs. ScSZ). However, again Ni-ScSZ showed more resistance towards sulfur poisoning.

The reversible adsorption of sulfur on nickel surfaces was first reported by Perdereau and Oudar[134] in 1970, followed in 1971 by Rostrup-Nielsen[91]. Sulfur chemisorption isotherms with sulfur concentration at a level of a few ppm and elevated temperatures were measured. Results have shown how chemisorbed sulfur possesses a more negative heat of formation than the most stable bulk sulfide Ni_3S_2. According to McCarty and Wise[135], chemisorbed S is 93 kJ kmol^{-1} energetically more stable than bulk sulfide (Ni_2S_3) at 800 K. They studied the thermodynamics of sulfur chemisorption on metals, including an alumina-supported Ni catalyst. Several sulfur chemisorption isosteres were evaluated varying the temperature in the range 477 – 863 K and for different initial concentrations of H_2S, measuring for each condition the sulfur coverage (i.e., the ratio of adsorbed sulfur compared to the available Ni surface, the latter previously measured by CO adsorption experiments). Results showed how the enthalpy of reaction decreases with higher coverage fractions.

The reversible adsorption of S on Ni is well-described by the equilibrium sulfur coverage function[92], from which the coverage fraction, θ_S, can be calculated as a function of both temperature and the H_2S concentration in the gas phase. The equilibrium coverage is thus expressed by the following equation:

$$\frac{p_{H_2S}}{p_{H_2}} = e^{\left[\frac{\Delta H^0(1-a\theta_S)}{RT} - \frac{\Delta S^0}{R}\right]} \tag{14}$$

Experiments[135] have shown how the enthalpy term is affected by coverages above ~0.70, showing a decrease of the heat of adsorption as the sulfur coverage approaches saturation. By fitting experimental data, the entropy term resulted instead as independent from the coverage within the same range. The physical interpretation is that the adsorbed S film gets more instable because of repulsive forces exerted between adjacent chemisorbed sulfur atoms. The fact that the entropy term does not depend on coverage is connected to subsurface chemisorption[92]. More details on the sulfur chemisorption on nickel active sites can be found in ref[136]. Equation 14 has been used recently to correlate data on sulfur coverage on nickel surfaces in H_2 environment[131]. The following values have been determined by means of a nonlinear least-square fit on experimental data[92]: ΔH_0^0 =-289 kJ mol^{-1}, ΔS^0 =-19 J mol^{-1} K^{-1} and a = 0.69, thus resulting in Eq. 15:

$$\theta_S = 1.45 - 9.53 \cdot 10^{-5} T + 4.17 \cdot 10^{-5} T ln\left({p_{H_2S}}/{p_{H_2,eq}}\right) \tag{15}$$

Figure 12 shows the dependency of the sulfur coverage on the H_2S concentration and temperature. As the operating temperature of the SOFC is reduced, the coverage of active sites by sulfur grows, thus making the proper management (removal) of the clean-up unit more critical towards sulfur compounds.

Eventually, the performance drop of the fuel cell performance due to H_2S poisoning is linearly depending on sulfur coverage as shown in the work of Papurello et al. [121] (see Figure 13).

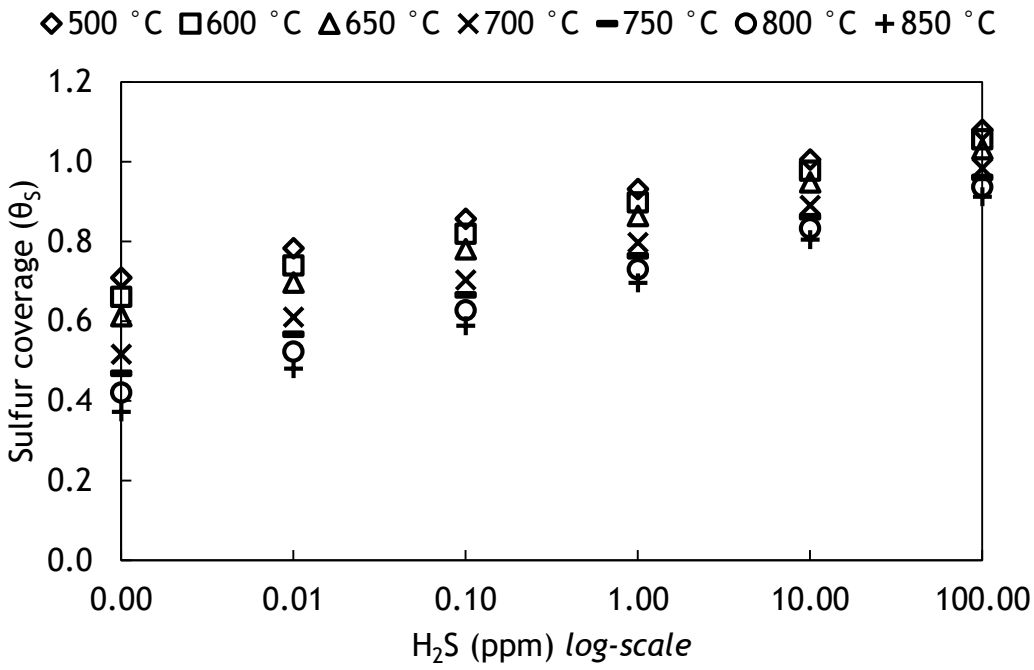

Figure 12. Sulfur coverage on Ni anode as a function of temperature and H_2S concentration (atmospheric pressure operation is assumed) (own calculation based on Eq. 15)

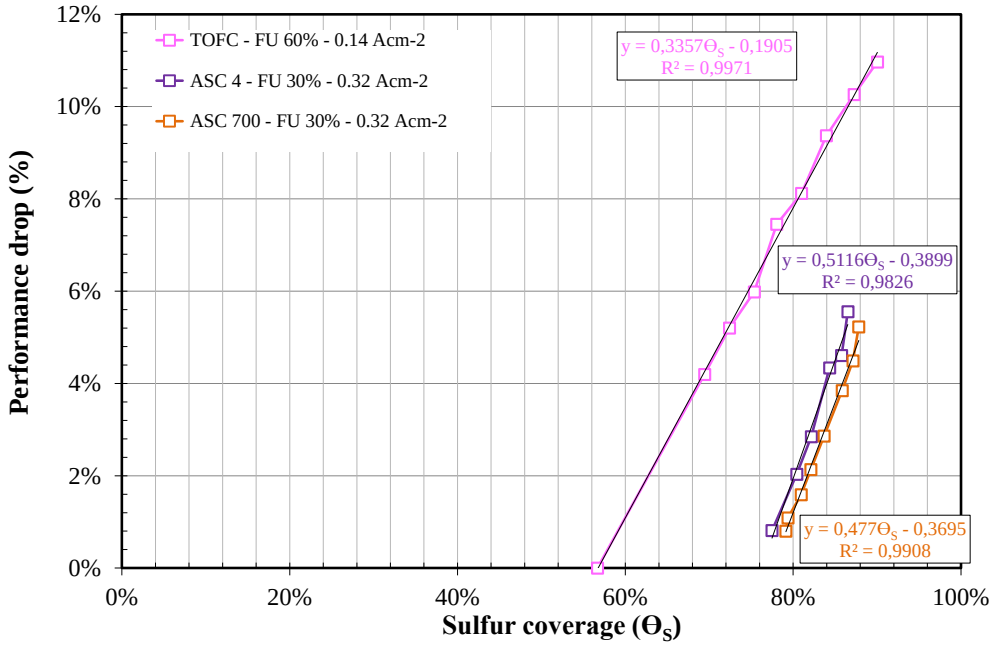

Figure 13. Performance drop vs. sulfur coverage in anode supported cell and stack environments (reprinted with permission from Papurello et al. [121]*)*

Concerning long-term degradation by sulfur poisoning, the idea is that Ni surface reconstruction might occur, enhanced by adsorbed S or S-species. Ni mobility is always present at the relevant SOFC operating temperature range, causing Ni coarsening or agglomeration [137,138]. However, different from simple agglomeration, a change in the Ni surface morphology can be observed in the case of prolonged exposure of Ni anodes to H_2S [139]. For instance, Ivey et al observed a terracing phenomenon. The extent of terracing was shown to be increasing with increasing H_2S levels and exposure time. Every change of the original as-reduced

Ni morphology can, but need not, lead to a reduction of Ni- phase connectivity and TPB. Therefore, long-term degradation connected to S-poisoning is not as easily explained as the fast degradation type linked to S-coverage of Ni sites.

Chlorine poisoning

The effect of HCl and other chlorine compounds like CH_3Cl and Cl_2 on SOFC performance has been addressed in several studies [43,126,140,141].

Table 15 summarizes these studies on the characterization of different anode materials upon exposure to Cl-containing fuels.

Li et al. [140] compared the performance degradation due to the exposure to chlorine compounds HCl, Cl_2 and CH_3Cl. No performance degradation was observed up to 8 ppm of these compounds. At higher concentrations, the degradation was more severe in the case of Cl_2 and CH_3Cl compared to HCl. Trembly et al.[1] observed an excessive degradation rate in cell performance due to exposure to HCl at 160 ppm, and believed this degradation to be due to the formation of nickel chloride. The results also implied that this chloride phase was not stable, because of the observed reversibility of the poisoning caused by HCl. Adsorption of chlorine onto Ni to reduce the triple phase boundary (TPB) was postulated as another explanation. Chemisorption of HCl on Ni and the chlorination of the Ni surface as possible mechanisms were proposed by Xu et al. [142]. They also mentioned that the formation of solid nickel chloride is energetically unfavorable.

Madi et al. [2] evaluated the poisoning effect of hydrogen chloride (HCl) on state-of-the-art Ni anode-supported SOFCs at 750 °C using either hydrogen or syngas fuel. Experiments were performed on single cells and short stacks. HCl concentration in the fuel gas was increased from 10 ppm(v) up to 500 ppm(v) at different current densities, Figure 14. Single cell experiment results showed that the poisoning is more severe when feeding with hydrogen than with syngas. Further experiments indicated higher degradation rates at higher current densities. These results are close to the findings of Xu et al. [142], who explain this behavior by chemisorption of HCl on Ni and blockage of active sites by these species. As current increases, the impact of having a reduced TPB gets more pronounced and so the HCl-poisoning effect is enhanced.

Interestingly, the stack performance was not affected by HCl up to 500 ppm in an anode feed simulating a biogas reformate[2]; actually the performance was slightly improved over the test. Even if degradation of the Ni-anode has sometimes been observed, a consistent trend of degradation when feeding HCl to the SOFC is not observed throughout the literature. Madi et al. [2] have recently reviewed and elucidated the potential Ni-anode degradation mechanism in the presence of HCl. They suggest that Ni changes are expected to take place leading to a redistribution of Ni particles that can enhance the TPB rather than reducing it. This redistribution phenomenon is confirmed by findings from other researchers [43,142].

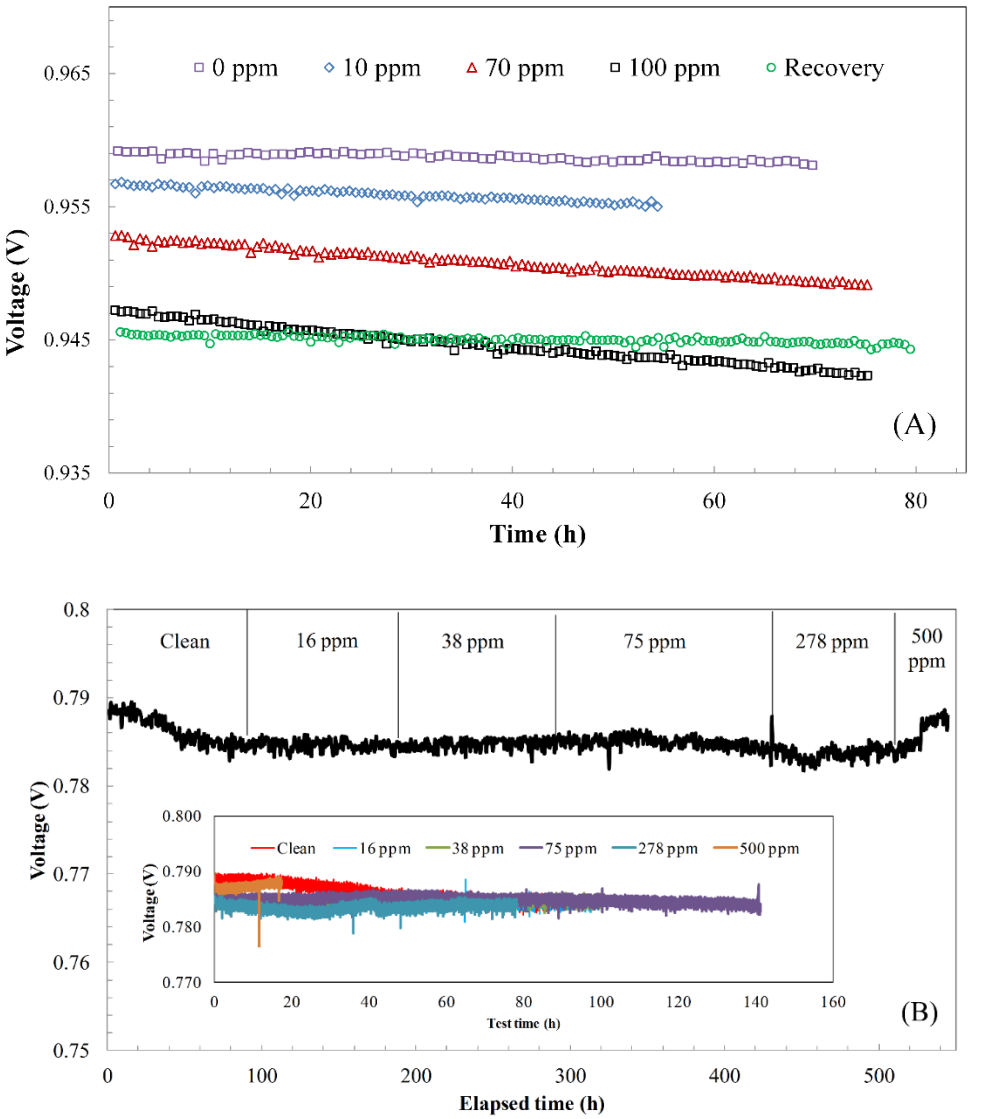

Figure 14. A) SOFC single cell operation with H_2 fuel gas at 0.25 A/cm^2, HCl contamination from 10 to 100 ppm – the recovery phase was carried out at the end of the whole test (reprinted with permission from Madi et al. [2]*). B) Short stack operation at 750 °C and 60% FU and various concentrations of HCl (reprinted with permission from Madi et al.* [2]*)*

Further, Madi et al. [2] performed SEM-EDX on the exposed samples. Traces of Cl at the edges of Ni grains were observed (Figure 15). XPS analysis of Xu et al. [142] also showed traces of Cl at the anode cross-section and the anode surface. According to Trembly et al. [1], the formation of a secondary nickel phase, $NiCl_2$(s), is not feasible. Therefore, Cl is present in the form of adsorbed species, rather than as a chlorine nickel compound.

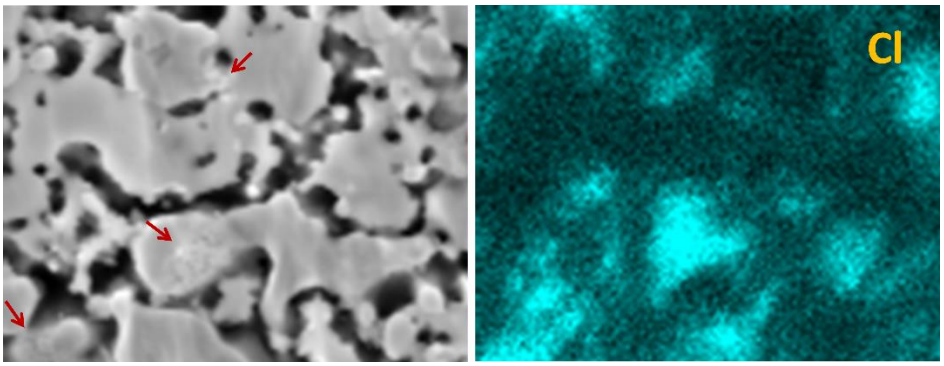

Figure 15. SEM-EDX analysis of anode cross section. Cl species are deposited on the Ni grains (reprinted with permission from Madi et al. [2]*).*

Siloxane poisoning

K. Haga et al. [143] investigated the effect of D5-siloxane at different temperatures on the cell performance and observed a marked degradation. Their *post-mortem* analysis revealed the plugging of the anode structure with SiO_2(s) deposits. They concluded that the presence of siloxane can cause deposition-type degradation, associated with the formation of SiO_2(s) according to the following reactions:

$$[(CH_3)_2SiO]_5(g) + 25H_2O \rightleftharpoons 5Si(OH)_4(g) + 10CO + 30H_2 \quad (16)$$

$$Si(OH)_4 \rightleftharpoons SiO_2(s) + 2H_2O \quad (17)$$

Madi et al. [66,144] evaluated the degradation of anode supported Ni-YSZ SOFC single cells and short stacks by siloxane D4, as a common biogas impurity, by electrochemical characterization, thermodynamic equilibrium calculations and micro-structural analysis. Experimental results showed a marked performance degradation with this impurity as shown in Figure 16 and Figure 17.

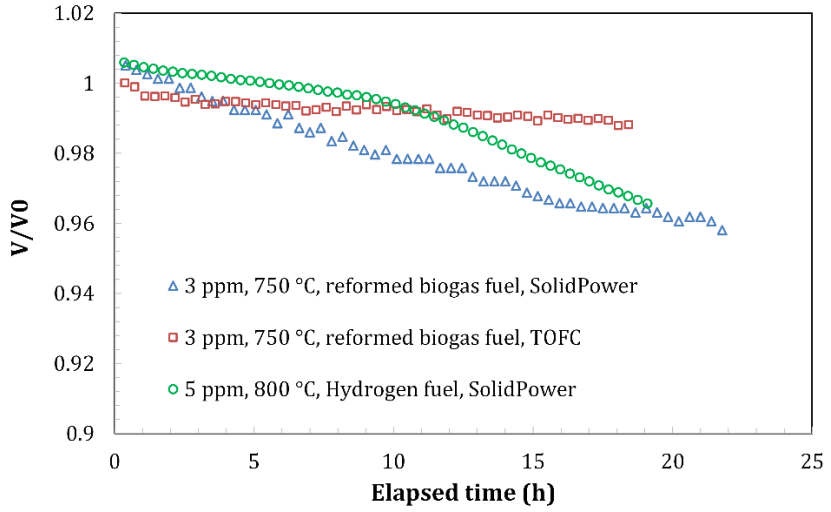

Figure 16. Degradation due to exposure to siloxane D4 (adapted from Madi et al. [66,144] *with permission). The cells were operated at 0.25 A/cm^2, 750 or 800 °C and fueled with either biogas reformate or hydrogen. Single cells were provided from SOLIDpower and TOFC companies.*

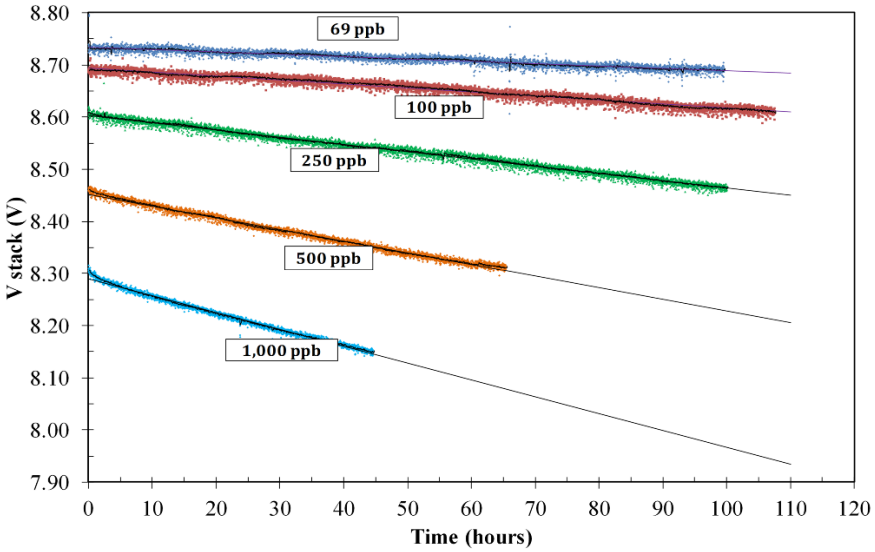

Figure 17. Durability test for TOFC SOFC stack up to 1 ppm(v) of D4 with biogas reformate fuel (reprinted with permission from Madi et al. [66]*). The FU is 60% with a current of 20 A (corresponding to a current density of ~0.22 A/cm^2). The stack temperature is around 700 °C*

EDX analysis of an exposed sample proved that Si condenses and deposits everywhere: on the current collector (Figure 18- right), the anode support (Figure 18- left), and down to the electrolyte interface at the three-phase boundary, which is responsible for the observed loss in electrochemical performance. A larger amount of Si was deposited at the anode surface with a gradient towards the electrolyte as shown in Figure 19. For the short stack experiment, a gradient in the deposition of Si between inlet and outlet fuel sections was evidenced, with more Si deposited at the fuel inlet regions both within and on the cell as well as on the interconnect plate.

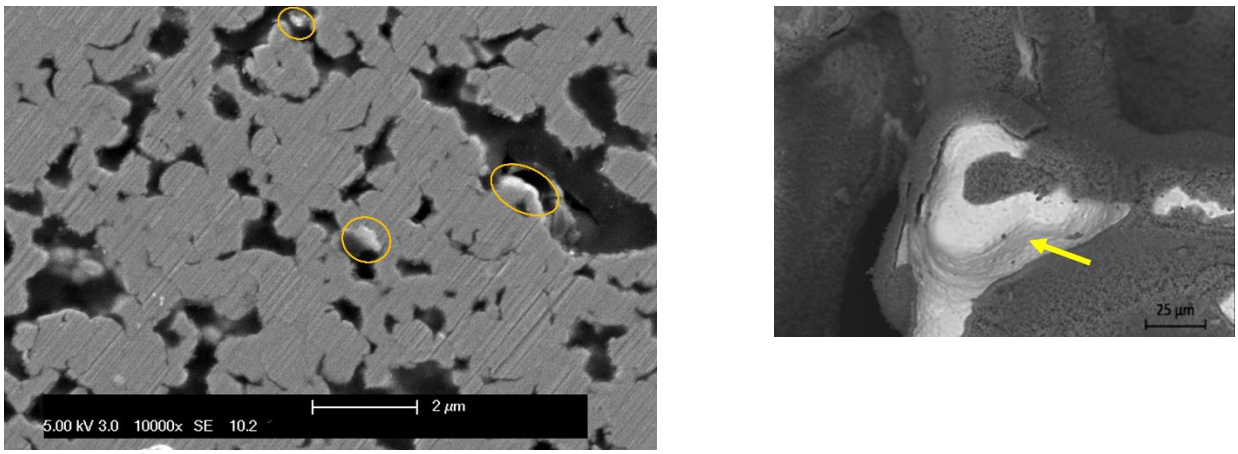

Figure 18. SEM images of the anode cross section (left, reprinted with permission from Madi et al. [144]*) and Ni-felt current collector (right, reprinted with permission from Madi et al.* [145]*).*

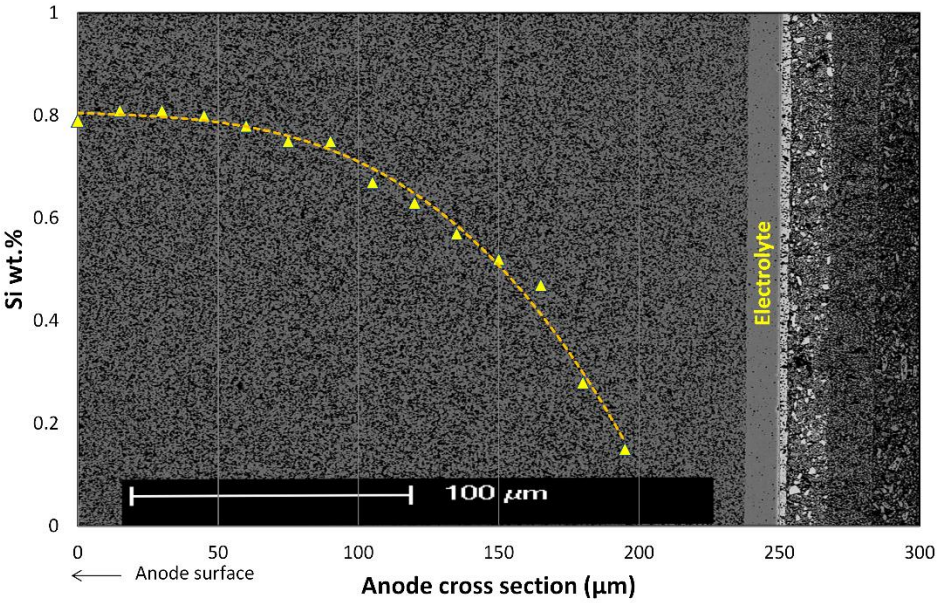

Figure 19. Si distribution through the anode cross-section: a higher amount of Si is deposited towards the anode surface than in areas close to the electrolyte (reprinted with permission from Madi et al. [144]*).*

The deposition of Si-compounds takes place due to the fast decomposition of the siloxane to SiO_2 as it reaches the fuel cell anode chamber, thus depositing silica both on the interconnect and anode current collector. Some Si also remains in the vapor phase as $Si(OH)_4$, according to Eq. 8, that further diffuses to the TPB region where it eventually precipitates too. In conclusion, siloxanes have to be removed completely from the biogas feeding the SOFC. Even trace contamination of the fuel feed at ppb level can affect the SOFC Ni anode, leading to fast degradation.

Table 14.Summary of studies involving short and long-term sulfur poisoning tests.

References	Anode	Fuel gas	T (°C)	$p(H_2S)/pH_2$ (ppm)	Test duration	Observations
A. Ishikura et al. [146]	Ni-YSZ	54% H_2, 23% H_2O, 23% N_2	900	20	800 h	The first step degradation was recovered completely, but the second-step recovered only partially due to nickel sulfide formation.
C. Grgicak et al. [147]	Ni-YSZ, Co-YSZ	H_2 and CH_4	850	100	140 h	Ni- and Co- based anodes were compared. Dense metal sulfide surrounded by YSZ formed, stable performance achieved.
I. Zhang et al. [148]	Ni-YSZ, Ni-GDC	H_2	800	5 – 700	2 h	Ni- GDC is more tolerable towards sulfur. Significant morphology change on Ni as well as GDC but not on YSZ.
E. Brightman et al. [149]	Ni-CGO	49% H_2, 49 % N_2, 2% H_2O	700, 750	0.5 – 3	5- 8 h	Full recovery of sample observed for 0.5 ppm but at higher concentration, a secondary phase formed accompanied by a change in microstructure.
Shaowu Zha et al. [127]	Ni-YSZ	50 H_2 %, 1.5% H_2O, 48.5% N_2	900	2 and 50	220 h	Higher degradation at lower temperatures. Higher cell operating temperature and larger cell current density accelerated the recovery process.
K. Sasaki et al. [126]	Ni-YSZ	50% pre-reformed CH_2	800	5	3000 h	Cell degradation rate with 5 ppm H_2S was 0.68%, slightly higher than the value without H_2S of 0.3% per 1000 h
Trembly et al. [150]	Ni-GDC	Coal syngas	750	200- 240	580 h	No major degradation for long-term test. Change in morphology was observed.

Table 15.Summary of studies involving exposure to HCl.

References	Anode	Fuel gas	T (°C)	p(HCl or Cl_2) /pH_2 (ppm)	Test duration	Observations
J.P. Trembly et al. [1]	Ni-YSZ,	Coal syngas	800, 900	20, 160 HCl	100 h	Degradation is associated with increase in charge transfer resistance. Adsorption of chlorine on Ni surface is the possible degradation mechanism.
K. Haga et al. [151]	Ni- ScSz	3% humidified H_2	800	5, 50, 1000 Cl_2	150 h	Microstructural change due to formation of Ni nanoparticles, probably via $NiCl_2$(g) sublimation.
C. Xu et al. [142]	Ni-YSZ	Coal syngas	800, 850	100 HCl	500 h	Chemisorption of HCl on Ni and chlorination of the Ni surface as possible mechanisms

Li et al. [140]	Ni-YSZ	H_2	750, 850	8 HCl, Cl_2, CH_3Cl	10 h	No performance degradation up to 8 ppm. Degradation is more severe in the case of Cl_2 and CH_3Cl.
Bao et al. [152]	Ni-YSZ	Coal syngas	750, 800	40	120 h	No significant degradation was observed during 100 h testing

Chapter 5 – Processes and materials for biogas contaminants removal

Biogas purification processes

This section is dedicated to the removal of biogas contaminants. Since both reformer and fuel cell electrode can suffer significantly by the presence of contaminants, it urges their removal.

The variety of trace contaminants depends on the used organic substrate (e.g., urban solid waste in a landfill, sludge from wastewater treatment plants, food waste, manure, etc.) [52]. Papadias and Ahmed [46] recently compiled an extensive database of contaminants found in biogas from WWTPs and landfilling; the database collects information on impurities such as sulfur compounds, organic silicon compounds (siloxanes), halogens, paraffines, cyclic hydrocarbons, and aromatics. One of the main drawbacks for SOFCs fed by biogas is indeed the impact of trace compounds on the anode electrode. The low or very low tolerance towards certain fuel impurities – mostly sulfur, chlorine and siloxane compounds – that can adversely affect the fuel cell efficiency and reduce the lifetime due to rapid degradation of the anode [121,126,153–156]. For this reason, a gas clean-up section is required to remove harmful contaminants and thus meet the SOFC gas purity requirements [46].

Biogas purification methods can be divided into two broad categories [157]:

- those involving physicochemical phenomena (adsorption and chemisorption on solid sorbents and absorption processes in either aqueous solutions or scrubbing in solvents or other liquid phases);
- those involving biological processes (e.g., bio-trickling).

Methods for the removal of H_2S and siloxanes are reviewed in detail in the following paragraphs since these compounds are often found in biogases in relatively large amounts.

The removal of tars (e.g., toluene, naphthalene) is not reviewed in this work. This is because there is a very negligible amount of tars and heavier hydrocarbons in biogases [46]. Nonetheless, the issue of tars is central for bio-syngas from biomass gasification [158]. Also, tars can be detrimental to the SOFC performance at elevated concentrations as they cannot be longer internally reformed thus leading to carbon deposition and catalyst deactivation [159]. Aravind and de Jong have extensively reviewed gas cleaning methods and processes for hot product gas from biomass gasifiers [158].

After describing methods and materials for biogas clean-up, the main equations used to model adsorption-based systems are presented in this section. Different kinetic formulations are reviewed as well as the other transport equations that are required to model full-scale adsorption vessels.

The typical experimental set-up to test solid sorbent materials, and some examples of adsorption curves on activated carbons until breakthrough of the contaminant is reached, are presented in the final part of this section. Some engineering aspects of clean-up systems are also discussed. The different reactor configurations for adsorption-based systems are briefly reviewed.

H_2S removal

In-situ abatement techniques are viable for H_2S (partial) removal either directly in the sludge or in the anaerobic digester. Having air (2-6 vol. %) in the digester headspace, or adding iron salts in the sludge feed or directly in the digester, are often employed techniques for a partial H_2S abatement.

The effect of adding iron salts was previously described in this work. Thus, we focus the discussion here on the aerobic removal of H_2S. Aerobic conditions within the digester can promote the activity of sulfide-oxidizing bacteria (SOB) which are present in the sludge and proliferate in the digester. Even the injection of a small amount of pure oxygen is efficient for H_2S removal in sewage sludge digesters. The presence of air (or oxygen) leads to chemical and biological oxidation of H_2S to S^0. Díaz et al. [160] have recently compared the techno-economic performance of micro-aerobic removal of H_2S with O_2 injection in full-scale digesters against more conventional methods of in-situ sulfur abatements, which are air injection into the digester, addition of $FeCl_3$ (iron salts) to the raw sludge and addition of an iron-sponge-bed filter inoculated with thiobacteria in the digester. According to their results, the microaerobic treatment consisting in supplying concentrated O_2 to the reactors was proved the most profitable alternative to $FeCl_3$ addition in the WWTP.

We describe next methods for H_2S removal from the biogas stream. The chemical affinity of H_2S for metallic cations drives processes employing chemical absorption. Chemical absorption of sulfur in aqueous solutions involves either the oxidation of S^{2-} to S^0 or the capture of S^{2-} through precipitation of its metallic salts [157]. For example, to the first method belongs the oxidative absorption of H_2S and O_2 by iron-chelated solutions. The H_2S is removed by means of chemical absorption in an iron-chelated solution catalyzed by Fe/EDTA, which converts H_2S into elemental sulfur (S^0) [161]. The formation of S occurs by means of sulfide oxidation by the chelated iron according to the reaction described by Eq. 18.

$$S^{2-} + 2Fe^{3+} \Leftrightarrow S^0 + 2Fe^{2+} \qquad (18)$$

A possible alternative is to use alkaline solutions (e.g., NaOH or CaO based solutions) to react with H_2S. A detailed review of the absorption methods is provided by Abatzoglou and Boivin [157].

Dry processes are based instead on the selective adsorption of trace compounds on solid adsorbents. Adsorption is the only technique which can reduce the concentration of contaminants to the extent of fuel cell specifications [157]. Often, these processes are adopted in semi-batch configuration. This is due to the gradual saturation of sorbent material and problems related to the regeneration of the same. However, continuous operation is also possible depending on the choice of the gas clean-up reactors' configuration. System layouts

with redundant reactors (in either parallel configuration or lead-and-lag configuration) allow indeed for continuous operation.

Iron oxide adsorbents are mainly adopted for sulfur removal [157]. Often, iron oxides are used for bulk sulfur removal. The best-known iron oxide adsorbent is iron sponge, which consists of an H_2S adsorption media, typically iron oxide or hydroxide, coated onto a supporting material traditionally comprised of wood chips or wood shavings [162].

The chemical reactions involved in sulfur removal are given below:

$$Fe_2O_3 + 3H_2S \rightarrow Fe_2S_3 + 3H_2O \quad \text{(sulfur removal)} \tag{19}$$

$$Fe_2S_3 + 3/2O_2 \rightarrow Fe_2O_3 + 3S \quad \text{(regeneration)} \tag{20}$$

According to the stoichiometry of the first reaction, the theoretical removal efficiency is 0.64 kg H_2S/kg Fe_2O_3.

Either operation in batch mode with regeneration or continuous operation with a small amount of air in the feed stream is possible for this type of H_2S-removal process. However, according to Abatzoglou and Boivin [157], iron-sponge activity is reduced by one-third after each regeneration cycle. Hence, regeneration can be carried out only once or twice before replacing the entire batch.

Nonetheless, the preferred operating mode is continuous regeneration by co-feeding some air (oxygen) with biogas. In this case, removal rates are as high as 2.5 kg H_2S/kg Fe_2O_3. The unit cost of iron sponge is ~0.25 $/kg [163].

Several commercial iron oxide media are also available such as SulfaTreat®, Sulfur-Rite®, and Media-G2®. As also for iron sponge, the main drawback of this type of material is the cost associated with the disposal of the spent catalyst (that can be classified as hazardous waste). Sulfatreat is currently one of the most used scavengers for H_2S removal. Sulfatreat consists of iron oxides (Fe_2O_3, Fe_3O_4) mixed with an activator oxide that are deposited on a calcined montmorillonite carrier matrix; the latter is thought to be enhancing catalytically the reactive adsorption phenomenon [164]. According to the manufacturer, the activator is made of one or more oxides of a group of metals consisting of platinum, gold, silver, copper, cadmium, nickel, palladium, lead, mercury, tin and cobalt. The amount of activator is 0.125–5%w/w of the adsorbent [164].

Sulfatreat adsorbent requires 100% water-saturated gas according to the vendor's website (Schlumberger, US); the role of water might be either that of catalyst or reactant [164]. Truong and Abatzoglou [164] derived a kinetic model from their experiments on Sulfatreat suggesting that the reaction is close to first order with respect to the H_2S concentration and zero order with respect to the media (i.e., the number of active sites per cm^3 of adsorbent). The role of water was not clearly identified.

Experiments from Truong and Abatzoglou [164] have shown that 1 g of Sulfatreat adsorbent can adsorb up to 0.11 g of H_2S (sulfur capacity of 11 wt. %). The saturation was defined experimentally as the point at which the concentrations of the inlet and outlet gas in H_2S were identical. Papadias et al. [46] developed a model of H_2S adsorption on Sulfatreat and calculated a sulfur capacity up to 6.7 wt. % with an inlet concentration of 150 ppm(v) of H_2S, and a breakthrough concentration set at 10 ppm(v).

Activated carbons (AC) are widely employed for both air purification (odor control) as well as biogas clean up. The main distinction is between impregnated AC and non-impregnated ones [165]. Impregnated AC is treated with a solid or liquid chemical in order to improve the chemical sorption of H_2S. The main impregnating compounds are sodium bicarbonate ($NaHCO_3$), sodium carbonate (Na_2CO_3), sodium hydroxide (NaOH), potassium hydroxide (KOH), potassium iodide (KI) and potassium permanganate ($KMnO_4$) [157]. Impregnated AC has a sulfur capacity as high as 30 wt. % (i.e., 300 g H_2S/kg of adsorbent) under aerobic conditions. In the absence of oxygen, the sulfur capacity is dramatically decreased to values only slightly above those of non-impregnated activated carbons [166]. The presence of water is a crucial factor enhancing hydrogen sulfide adsorption. In fact, it enables the dissociation of H_2S to HS^- ions when the pH allows [167] (a basic pH is needed to promote the formation of HS^- ions). The surface pH of the AC is also a relevant parameter. Yan et al. have demonstrated how surface pH values of the exhausted carbons show a clear trend of pH drop along the reaction extent, while a pH around 2 was observed for the bottom of the bed indicating sulfuric acid (H_2SO_4) as the predominant product [168]. Having a large micro-pore volume is also important to store the S[169] (either in the form of elemental sulfur or as sulfate, e.g., K_2SO_4 or Na_2SO_4). More details on the mechanisms of S-removal in impregnated activated carbons in the presence of oxygen can be found in the work of Bagreev and Bandosz [167]. Xiao et al. studied the breakthrough capacity of both impregnated and non-impregnated AC with and without oxygen addition to the simulated biogas feed [165,166]. The results are summarized in Table 16. The results clearly show that H_2S is removed by both adsorption and catalytic oxidation over the AC and IAC at nearly ambient temperature. Catalytic oxidation accounts for the most part of the sulfur capacity in impregnated carbon, increasing the sulfur capacity dramatically. Gutiérrez Ortiz et al. [170] have also investigated the adsorption capacity of AC (with or without impregnation) as well as in-house adsorbents for which sewage sludge was used as a precursor. The sludge was thermally treated with either N_2/air or air only, in order to activate it. Experiments were carried out at 20 °C, using a simulated biogas mixture and an inlet H_2S concentration of 2,000 ppm(v) (the breakthrough was set to an outlet concentration of 200 ppm(v) of H_2S). The adsorption capacity of fresh AC and NaOH-impregnated AC were measured as 4.4 and 12.7 mg g^{-1}, respectively. Under aerobic conditions (5% vol. O_2), the sulfur capacity of AC and IAC increased to 7.3 and 77.4, mg g^{-1} respectively. The highest adsorption capacity of sludge-derived adsorbent was measured as 8.6 mg g^{-1} under anaerobic conditions, and 17.3 mg g^{-1} under aerobic conditions. No further improvement was observed by impregnation of the sludge-derived adsorbent.

Table 16. Adsorption capacity of activated carbon with and without impregnations under either anaerobic or aerobic conditions

Adsorbent type	**AC**	**IAC**
Temperature (°C)	30	30
Equilibrium adsorption capacity under anaerobic conditions (mg g^{-1})	2.7 [165] - 6.8 [166]	9.4 [165] - 11.2 [166]
Equilibrium adsorption capacity under aerobic conditions (mg g^{-1})	140 [166]	407 [166]

Activated carbons are often adopted as the guard bed (or polisher) for the SOFC [171,172]. The main properties of activated carbon filters for the effective removal of VOCs are high porosity, high superficial area (1500 m^2 g^{-1}), high volume, pore distribution [173] and treatment with metal ions.

To summarize, impregnated activated carbons, mainly impregnated with caustic bases (NaOH, Na_2CO_3, $NaHCO_3$, KI), show typical H_2S loading capacities in the range of a few hundreds of mg per g of activated carbon. Especially, the presence of oxygen is key to achieve high sulfur capacity. The non-impregnated AC achieves H_2S removal capacities one order of magnitude lower than IAC on average. Again, the presence of oxygen is enhancing the sulfur capacity.

Digester gas typically contains from 0.1 to 2-3 vol. % of O_2, so employing IAC should be beneficial as their removal capacity can be exploited thus justifying the higher cost (typically, the adsorbent unit cost for IAC is 3-4 times higher than virgin AC). According to Seredych and Bandosz [169], the degree of humidification has an impact on the removal capacity of AC. The best performance is obtained with pre-humidified (saturated) AC then fed with moisture-free biogas. In fact, in the presence of moist gas, H_2S is first oxidized to SO_2 and then to sulfurous acid (H_2SO_3). The acid reacts with alkali or alkaline earth metals to form sulfites thus rapidly depleting active sites. With a pre-saturated bed, H_2S instead interacts with the water film formed on the carbon surface to form HS^- that are eventually converted to elemental sulfur (and/or sulfates) that is stored in the micropore volume.

Concerning the layout of the clean-up unit in order to ensure the SOFC fuel quality requirements, the recommended configuration is to have first a bulk removal stage of harmful compounds, which should be followed by one or more adsorption beds able to either simultaneously or selectively capture the remainder of the contaminants down to ppb(v) levels. Bulk sulfur removal could be accomplished by an absorption process or by an iron oxides bed, while the ultra-filtration process is most effectively carried out by using solid adsorbents, such as activated carbons.

Finally, the determination of the breakthrough time of the sorbent material is important to determine when the sorbent material must be changed, thus minimizing operating costs of the plant.

Whenever reporting sulfur (or any other contaminant) removal capacity for a given adsorbent material, it is important to state the breakthrough concentration used to calculate the integral of the adsorption curve. Especially, the threshold (breakthrough) concentration is set quite arbitrarily in scientific works reviewed in this work. The formula to calculate the breakthrough time t_s (s) is the following:

$$\frac{x}{M} = \frac{\dot{Q} M_w}{w V_m} \left(C_0 t_s - \int_0^{t_s} C(t) dt \right) \quad (21)$$

The adsorption capacity ($\frac{x}{M}$, mg of contaminant g^{-1} of AC) is thus calculated based on the inlet volumetric flow rate of biogas, $\dot{Q}$ ($Nm^3\ s^{-1}$), the adsorbent weight, w (g), the contaminant molecular weight, M_w (g mol^{-1}), the inlet concentration of contaminant in the feed stream, C_0 (ppm(v) by volume) and the (breakthrough) contaminant concentration at the reactor outlet at a given time, $C(t)$.

The breakthrough capacity thus expresses the threshold capacity above which the catalyst load must be replaced with a fresh sorbent, or regenerated. As mentioned earlier, in some works the sulfur capacity is calculated taking as breakthrough capacity the initial concentration of contaminant in the gas feed (i.e., when $C(t)$ equals C_0. Under this assumption, the calculated capacity of the sorbent is the highest. However, it is also quite common to have the breakthrough concentration set as a fraction of the inlet concentration (e.g., 10% or 1% of C_0). Lower removal adsorbent capacities are thus calculated depending on the choice made.

The (right) definition of the breakthrough capacity depends on the downstream process and the reactor configuration. In the lead-and-lag configuration, the first adsorption vessel (lead reactor) is followed by a second one (lag reactor). In this way, the lifetime of the catalyst can be extended while assuring a stringent removal. For fuel cell applications, very high fuel quality is required with sub-ppm(v) levels of H_2S. Therefore, the overall breakthrough concentration should be set as low as 1% of the inlet concentration (or even lower, depending on the minimum detection limit of the gas analyzer). Using a single reactor configuration would not be ideal as the breakthrough concentration shall be achieved relatively fast. With a lead-and-lag configuration instead (described in detail later), the breakthrough concentration in the first reactor (lead) can be exceeded, as long as the breakthrough limit is not reached after the lag reactor.

Siloxanes removal

Siloxanes can also be effectively removed by solid sorbents through adsorption. The concentration of siloxanes in biogas is such that cooling processes usually employed to remove moisture are scarcely affecting the vapor concentration of siloxanes in the gas phase as condensation is almost negligible even for the heavier organic silicon compounds (e.g., D5) [42].

Activated carbons are very effective for the removal of siloxanes. Cabrera et al.[174] have studied 12 commercial AC against D4-siloxane. The best performance was achieved by a wood-based chemically activated carbon, which achieved an adsorption capacity of 1732 ± 93 mg g^{-1} using 1000 ppm(v) (v/v) of D4 with dry N_2 as a carrier gas. The D4 adsorption capacities were strongly related to the textural features of the ACs with a positive correlation between adsorption capacity and the total pore volume. For each adsorption experiment, the adsorption column was operated until the D4 outlet concentration matched the inlet concentration (i.e., full bed saturation).

Silica gel is also quite effective in removing siloxanes, with an observed adsorption capacity exceeding 100 mg g^{-1} and possibility of regeneration (a great advantage over AC which cannot be effectively regenerated)[42].

According to experiments carried out by Matsui and Imamura [175], the adsorption capacity is 5.6-19.2 mg g^{-1} for the activated carbons, 4-77 mg g^{-1} for the molecular sieve and 104 mg g^{-1} for the silica gel. All tests were conducted using D4 as model siloxane compound and using N_2 gas as a carrier gas.

Since biogas contains a variety of harmful compounds (vapors), having concentrations spanning several orders of magnitude, competitive adsorption occurs in the solid sorbent. This is especially true for siloxanes. In fact, the presence of relatively non-volatile, organic sulfur or halogenated compounds, can greatly reduce the adsorption capacity towards siloxanes [176]. Other factors influencing the silicon capacity of activated carbon are the relative concentrations of the siloxane species to one another (e.g., L2 breaks through sooner than D5), temperature and relative humidity [177]. According to Wheless and Pierce [177], who monitored the removal of siloxane in landfill biogas, not only L2 was the quickest compound to break through, but it could be found at a higher concentration than in the inlet gas since accumulated siloxanes were then released. This phenomenon is known as ‘roll-up’ and it involves the desorption of the weaker adsorbates in downstream zones which are replaced by more strongly adsorbed compounds [52]. This phenomenon can lead to concentration peaks at the outlet of the vessel that is even larger than the inlet concentration, or it can explain the early breakthrough of the weaker compound. For instance, in the biogas clean-up plant analyzed by de Arespacochaga et al. [52], D4 was the first silicon compound to break through despite the higher amount of D5 in the inlet feed. In the same work, the measured siloxanes adsorption capacity was 5 mg g^{-1} on extruded activated carbons. The low removal capacity might be due to the low inlet concentration of siloxanes (which can strongly reduce the equilibrium adsorption capacity according to a Langmuir-type adsorption process or Freundlich adsorption isotherm) and competitive adsorption phenomena.

Ricaurte Ortega and Subrenat [178] tested different porous materials to measure their adsorption capacity toward L2 and D4 siloxanes. The materials tested were activated carbon cloths, granular activated carbon, zeolite, and silica gel. Activated carbons reached a L2 removal capacity around 300-350 mg g^{-1}, while zeolite and silica reached values around 100-150 mg g^{-1} (the lower performance of zeolite and silica is linked to their

lower surface area compared to AC). All tests were performed in air. Similar but slightly higher removal capacity holds for D4. Reducing temperature is confirmed to enhance the adsorption process according to experiments. It is worth noting the trend of the adsorption isotherm with varying inlet siloxane concentration in the experiments [178]; as the inlet concentration of siloxane in the feed gas gets lower, a much-reduced removal capacity is observed. Experimental isotherm curves were well fitted by a Freundlich isotherm model. This consideration is important because, in realistic applications, the overall siloxane concentration is often quite low (< than 50 mg/Nm^3). Therefore the adsorption capacity of the adsorbent medium reduces several times compared to values that are reached when high inlet siloxane concentrations are tested. Hence, in order to avoid an over-estimation of the adsorption capacity of a given sorbent, it is recommendable to test the siloxane removal of an adsorbent at concentrations close to those of real biogases [176].

Other VOCs removal

The most relevant volatile contaminants contained in biogenous fuels are sulfur, aromatic, carbonyl and chloro-compounds [179] and siloxanes; these groups are derived from the starting biomass loaded into the digester [179]. Studies on the effective removal of all VOCs in order to produce highly pure, fuel cell-grade biogas are rare, as the main focus is on H_2S or sulfur compound removal only [180,181]. Typically the effect that different VOCs have on each other's removal rate is overlooked. Part of the problem is related to the detection of VOCs, as a fast method with a low limit of detection has to be used. An electrochemical gas sensor is usually adopted to monitor online and real-time H_2S [182]. A GC-MS instrument is instead used to detect the other compounds [52,182], however, acquisition time is much prolonged in this case. Hence, for the monitoring of biogas trace compounds – especially for real biogases that have a rather complex matrix of contaminants –there is a need for more sensitive and robust methods for real-time online analysis. In this context, Direct Injection Mass Spectrometry (DIMS) was proven to have good performances in term of rapidity, sensitivity, and absence of pre-treatments [183]. One of the most promising DIMS techniques is the Proton Transfer Reaction-Mass Spectrometry (PTR-MS) [183]. This method is based on an efficient implementation of chemical ionization based on proton transfer from hydronium ions and allows the rapid and on-line monitoring of most volatile compounds. It has been applied in many situations ranging from breath analysis to environmental monitoring and, recently, also to issues related to waste management and odorant emission control [172,184].

As reported by Papurello et al. [171], the breakthrough time is affected, among other factors, by (in order of importance):

- the type of sulfur compounds that must be removed;
- the GHSV of the mixture gas across the adsorbent bed;
- the presence of co-vapors of organic compounds besides sulfur compounds.

It was demonstrated that even only 1 ppm(v) of aromatic, carbonyl and chloro-compounds could reduce the removal efficiency performance by 70% in case of sulfur compounds only [185]. Therefore, real-biogas experiments should follow lab-experiments to verify fully the adsorbent performance in the context of a more complex matrix of contaminants, which also contains several VOCs at either ppm or ppb levels besides the main contaminant types (e.g., H_2S and s D4-D5 siloxanes for sewage biogas).

Experimental methods for adsorption experiments

The typical experimental apparatus to test activated carbons for the removal of biogas contaminants is described in this paragraph. The set-up consists of a few centimeters long cartridge made either of Teflon tube (PTFE) or quartz (for high temperature experiments) in which the sorbent material is placed. A sterile gauze, or other inert filling body, is used to avoid dragging phenomena by the gas stream. The main factors affecting the removal efficiency of the sorbent material are the moisture in the gas feed, the operating temperature, and the gas hourly space velocity (GHSV). The sorbent materials are usually tested with inert gas or simulated biogas (CH_4 and CO_2) while varying the inlet contaminant concentration. Known concentrations of pollutants are fed using certified gas cylinders [182,185,186] or permeation tubes [187,188]. A liquid mass flow controller and a controlled evaporator mixer generally control the flow rate of demineralized water (which is then vaporized) to deliver a controlled level of moisture in the gas stream. Figure 20 shows a typical experimental set-up for testing the adsorption capacity of a solid sorbent: the red color represents the heated lines with heater strings controlled via a PID regulator. A PolyDiMethylSiloxane (20 μm) membrane filter is inserted between the filter line and the detection instrument in order to avoid obstructions from particles dragging. In order to maintain a given ratio between the particle diameter of the sorbent material and the actual reactor diameter, the sorbent materials are grounded and then with a vibratory sieve shaker sieved to a certain particle range.

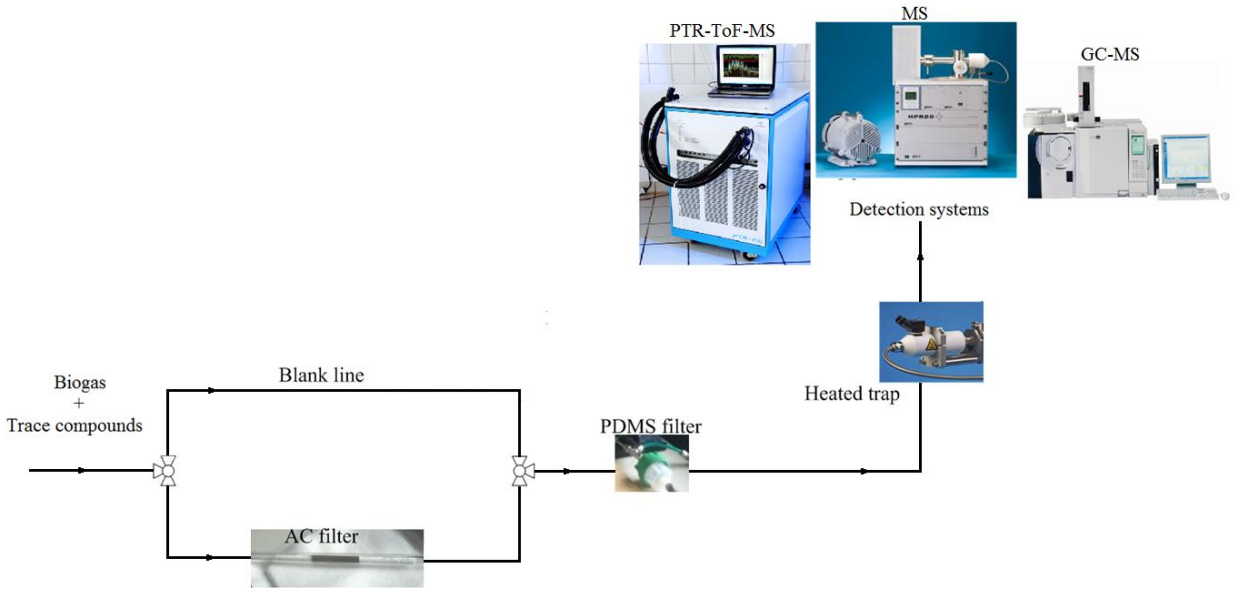

Figure 20. Typical experimental set-up for measuring the adsorption capacity of solid sorbents towards selected contaminants (Courtesy of: Hiden Analytical GmbH, Ionicon Analytik GmbH, Shimadzu GmbH; reprinted with permission from Papurello et al. [189]*).*

Equilibrium adsorption isotherms

Equilibrium adsorption isotherms describe the adsorption process of the contaminant on the solid sorbent surface. In this section, we review the main adsorption isotherm equations usually employed in the literature.

Adsorption is described through a function that connects the amount of adsorbate taken up by the adsorbent to the adsorbate concentration in the gas phase. Such a function is called isotherm under specific conditions. These conditions are isothermal and atmospheric pressure under steady state conditions. The general expression of an adsorption isotherm is the following:

$$q_{max} = f\left(C^*\right) \tag{22}$$

When the contaminants concentration typically does not exceed a few parts per billion even a linear correlation between q_{max} and C^* can be adopted [190]. q_{max} is the maximum adsorption capacity function of a given couple sorbent material - contaminant (mg g^{-1}) – when it reaches $C^*=C(x,t)$; C* (measured in ppm) is the gas concentration at the equilibrium within the pores. When the concentration is in the range of a few to hundreds (or thousands) of ppm(v), the correlation is not linear. In Table 17, the most used adsorption isotherms are reported:

Table 17. Equations of different adsorption isotherms

Isotherm type	Equation	Notes / Assumptions
Henry	$q_{max} = k_p\left(q_e\right)$ (23) [191]	Linear isotherm
Langmuir	$q_e = q_{max}\frac{k_l C^*}{1+k_l C^*}$ (24) [192]	Monolayer adsorption model
Freundlich	$q_{max} = k_f q_e^{\frac{1}{n}}$ (25) [193]	Model valid only within a limited range of concentrations
Dubinin-Radushkevich (D-R)	$q_{max} = q_e e^{-D\left[\left(RT\ln\left(\frac{p_0 MW}{q_e RT}\right)\right)^2\right]}$ (26) [194]	Semi-empirical equation
Brunauer, Emmett, and Teller (BET)	$\frac{q_{max}}{C_{ss}} = \frac{\left(\frac{p}{p_0}\right)e^{\left(\frac{\Delta H_L-\Delta H_1}{RT}\right)}}{\left(1-\frac{p}{p_0}\right)\left(1+\left(e^{\left(\frac{\Delta H_L-\Delta H_1}{RT}\right)}-1\right)\frac{p}{p_0}\right)}$ (27) [195]	Valid for multiple adsorption layers

Legend:

- C_{ss}, amount of sorbent (capacity) that is required to form a monolayer of the adsorbate,
- D, diffusion coefficient
- k_f, Freundlich isotherm constants,
- k_l, Langmuir constant (it is a function of sorbent material, contaminant, and temperature) (m^3 mg^{-1}),
- k_p, partition or distribution coefficient or Henry's constant,
- MW, molecular weight (g mol^{-1}),
- q_e, equilibrium adsorption capacity,
- ΔH_1, enthalpy of adsorption for mono layer,
- ΔH_L, enthalpy of adsorption for subsequent layers.

Monolayer molecular adsorption occurs in micropores of solids, which has pore sizes not much greater than the adsorbate molecule size. Thus, the adsorption maximum capacity of a given sorbent is governed by the accessible micropore volume.

Adsorption reactor model

The following section describes the assumptions and equations used to evaluate the adsorption of selected contaminants on an activated carbon trap (reactor). A porous particle diffusion model is used, which involves the material balance equations in both the gas-phase and the pore phase [173]. The model adopted is composed by the mass balance equation for the bulk phase in a packed bed, the mass balance equation within the particle, the isotherm equation to describe adsorption capacity of material and the ideal adsorption solution theory to consider the competitive adsorption. Several assumptions were made to build the model:

1. the adsorption process is isothermal;
2. the axial dispersion is considered only longitudinally and not radially;
3. the adsorbent particles are spherical and homogeneous in size and density;
4. the external transfer coefficient depicts the mass transfer across the boundary layer;
5. the intra-particle mass transport is characterized by the effective pore diffusion coefficient;
6. the linear velocity of the gas phase is independent by the concentration;
7. a local equilibrium condition is established between the gas concentration adsorbed and the solid particle.

The equation of the model is a partial differential equation in space and time, which was also proposed by Rosen [196] and Rasmuson [197].

$$-D_{ax}\frac{\partial^2 C\,(x,t)}{\partial x^2}+u\frac{\partial C(x,t)}{\partial x}+\frac{\partial C(x,t)}{\partial t}+\frac{1-\varepsilon_b}{\varepsilon_b}\frac{\partial q(x,t)}{\partial t}=0 \qquad (28)$$

The axial dispersion term becomes negligible under certain fluid flow conditions. In fact, the contribution of this term can be neglected when the Peclet number is below 500, which is generally attained by the gas flow across the adsorbent media. By neglecting the diffusion term from the axial dispersion, the solution of the equation is strongly simplified.

The accumulation term, $\frac{\partial q(x,t)}{\partial t}$, takes into account the mass transfer of the contaminant from bulk gas phase to solid phase. It represents the rate of adsorption, and it contains the transport kinetics of the contaminants. These conditions are related to the type of isotherm chosen and related coefficients. The necessity to know the porous media characteristics are crucial to developing a mass balance within the particle. This term can be written as follows:

$$\frac{\partial q(x,t)}{\partial t} = a(1-\varepsilon_b)k_{fk}\left(C - C^*\right) \qquad (29)$$

The boundary layer mass transfer coefficient, k_{fk}, for packed bed can be calculated using the empirical formulation by Wakao-Funazkri [198] (see also Xiao et al. [165] for a recent application of this correlation). To obtain the rate of adsorption and to complete the equation, it is also necessary to evaluate the term C^*. This term expresses the gas concentration that is obtained once the equilibrium capacity, q_{max} has been reached. The evaluation of this parameter is obtained using the Langmuir isotherm [199] or one of the other isotherm equations provided in Table 17.

Multicomponent competitive adsorption

In most practical adsorption processes, a mixture of vapors composes the adsorbed gas and therefore a multi-component adsorption phenomenon must be dealt with. As previously described, the species in the mixture having the higher adsorption capacity with regard to a specific adsorbent material may displace from the micro-pore volume the weakly adsorbed adsorbates thus modifying the breakthrough time of the system. This is the so-called *roll-up* phenomenon. Measurements of the adsorption capacities of multiple-component mixtures are therefore much more complex than for a single adsorbate, and the possibility of predicting multicomponent adsorption equilibria from pure component adsorption isotherms has been under investigation for many years in applied adsorption research. Therefore, extensions of several common single component isotherms were studied to model and approximate the entire phenomenon. Among them, the most known and used in the literature is the Extended Langmuir Isotherm Equation.

The Extended Langmuir Isotherm (ELI) was first proposed by Markham and Benton [200]. This was the first attempt to develop a multicomponent adsorption model. According to this model, the equilibrium adsorption capacity of the *i*-vapor within the multi-component mixture also depends on all the Langmuir coefficients and concentrations of the other vapor species present in the mixture.

$$q_i(C_i) = \frac{q_{m,i} k_i C_i}{1 + \sum_{j=1}^{N} k_j C_j} \tag{30}$$

where the terms $q_{m,i}$ and k_i correspond to the pure gas Langmuir isotherm constants for component *i*. It is worth mentioning that the ELI model is not thermodynamically consistent, unless the values of q_m are the same for all components in a gas mixture [201,202].

A thermodynamically consistent approach was later proposed by Myers and Prausnitz [203], who developed the Ideal Adsorbed Solution (IAS) theory to evaluate the isothermal adsorption capacity for a multi-component gas mixture. The IAS theory assumes that the Gibbs free energy definition also applies to the adsorbed phase. The IAS approach comes as an analogy of Raoult's law for vapor-liquid equilibria applied to the multi-phase 'gas-adsorbate' phase' system. The fundamental relation of the IAS model is:

$$P y_i = P_i^{\circ}(\pi) x_i \tag{31}$$

where *P* is the total pressure in the gas mixture, y_i is the gas molar fraction, $P_i^{\circ}(\pi)$ is the equilibrium gas-phase pressure at the given solution temperature corresponding to the solution spreading pressure π for the adsorption of the pure component *i* (the spreading pressure is the same concept as pressure simply transposed into a two-dimensional environment).

Recently, Simon et al. [204] developed a computer program that solves the system of non-linear equations that derives from the application of the IAS theory to a multicomponent gas mixture.

For the competitive adsorption between two vapors, the IAS equilibrium condition is given by the LeVan and Vermeulen equation [205]:

$$q_s = \frac{q_{1,m} k_{l,1} C_1 + q_{2,m} k_{l,2} C_2}{k_{l,1} C_1 + k_{l,2} C_2} \tag{32}$$

The Langmuir equation of two compounds is:

$$q_i = \frac{q_s k_{l,i} C_i}{1 + \sum_{i=1,2} k_{l,i} C_i} + \Delta_{1,2} \tag{33}$$

where i = 1,2; and $\Delta_{1,2}$ is given by the following equation:

$$\Delta_{1,2} = \left(q_{1,m} - q_{2,m}\right) \frac{k_{l,1} C_1 k_{l,2} C_2}{\left(k_{l,1} C_1 k_{l,2} C_2\right)^2} \ln\left(1 + k_{l,1} C_1 + k_{l,2} C_2\right) \tag{34}$$

Typical gas clean-up configurations

There are essentially three different gas clean-up configurations that are plausible for the gas treatment for SOFC applications: series, parallel and lead-and-lag configuration. For each configuration it is assumed that two identical columns of the same size are available.

Series configuration

For the series configuration, at least two columns are adopted. These columns increase the redundancy of the systems. The spent media is replaced simultaneously in both vessels once the effluent reaches the target breakthrough concentration. This configuration causes a plant stoppage that generates management issues.

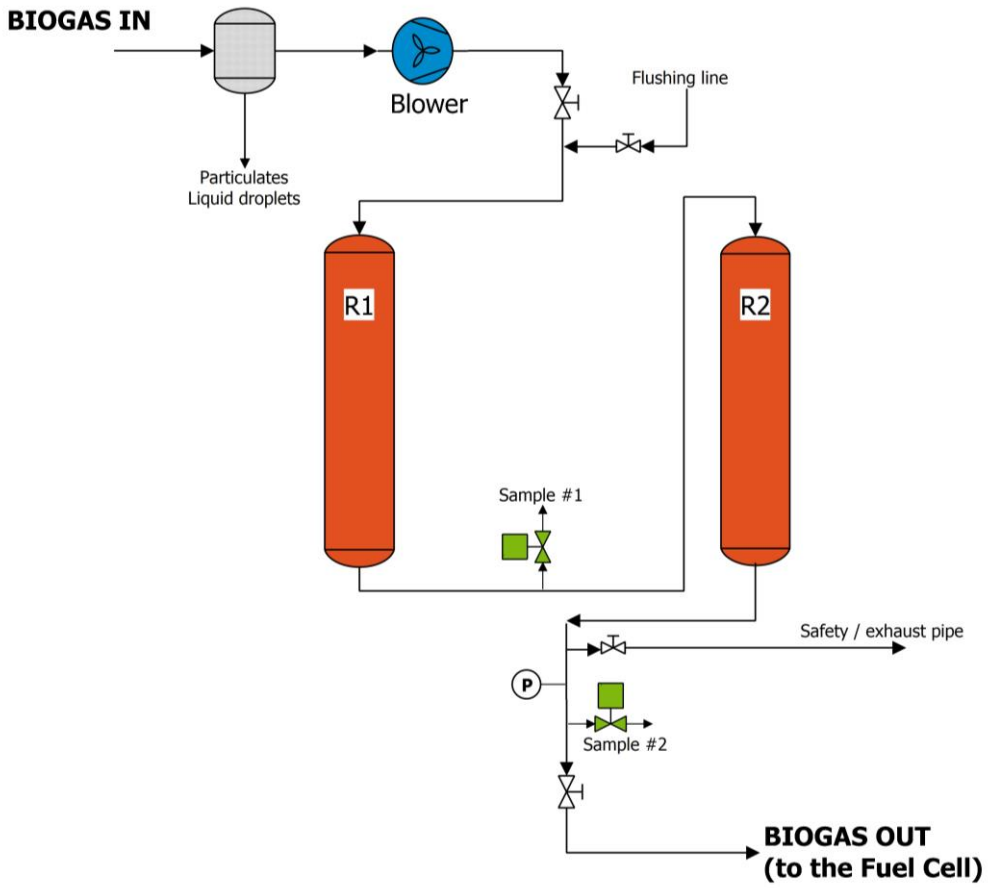

Figure 21. Biogas clean-up section: series configuration

Parallel configuration

Two columns of the same size with staggered replacement were used to represent parallel configuration. While in the "series" scheme, all columns are replaced simultaneously, for parallel arrangement the replacement is staggered to allow blending of the effluent from a newly replaced column and an old column. This approach was shown to reduce the adsorbent usage rate in many cases [206,207]. This configuration does not cause any plant stoppage, and it has no guarantee of trace compounds slipover.

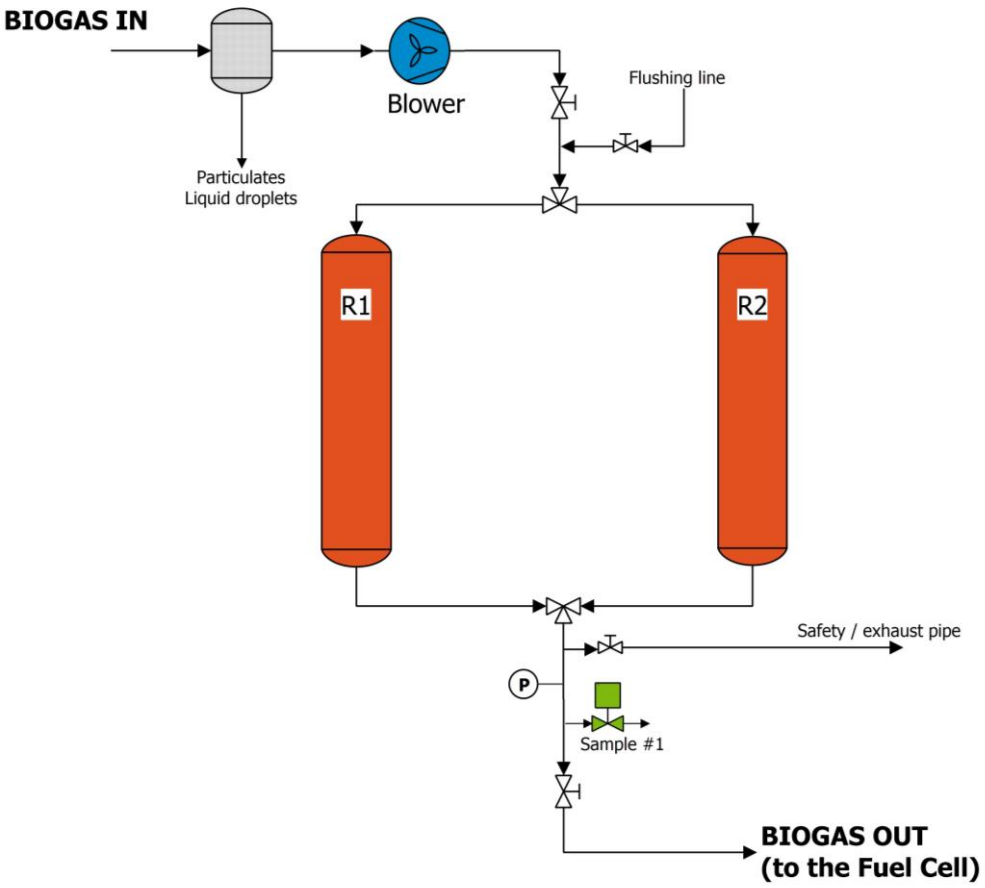

Figure 22. Biogas clean-up section: parallel configuration

Lead-and-lag configuration

For the lead-and-lag configuration, two columns of the same size are also used. One column is placed in a "lead" position, while the other one serves as a "lag" or "guard" column. A sample breakthrough curve for two columns placed in a lead-lag is shown in Figure 24. The system continues operation until the effluent from the lag column reaches the target concentration. Then, the saturated Column 1 (left) is taken out of operation, and Column 2 (right) is put online as the new "lead". The replaced, fresh Column 1 is installed in a "lag" position, providing polishing for the effluent from Column 2. The lead-and-lag configuration allows for continuous plant operation while also providing the extra adsorbent capacity to account for variations in operating conditions (such as temperature and the inlet concentration of the contaminant).

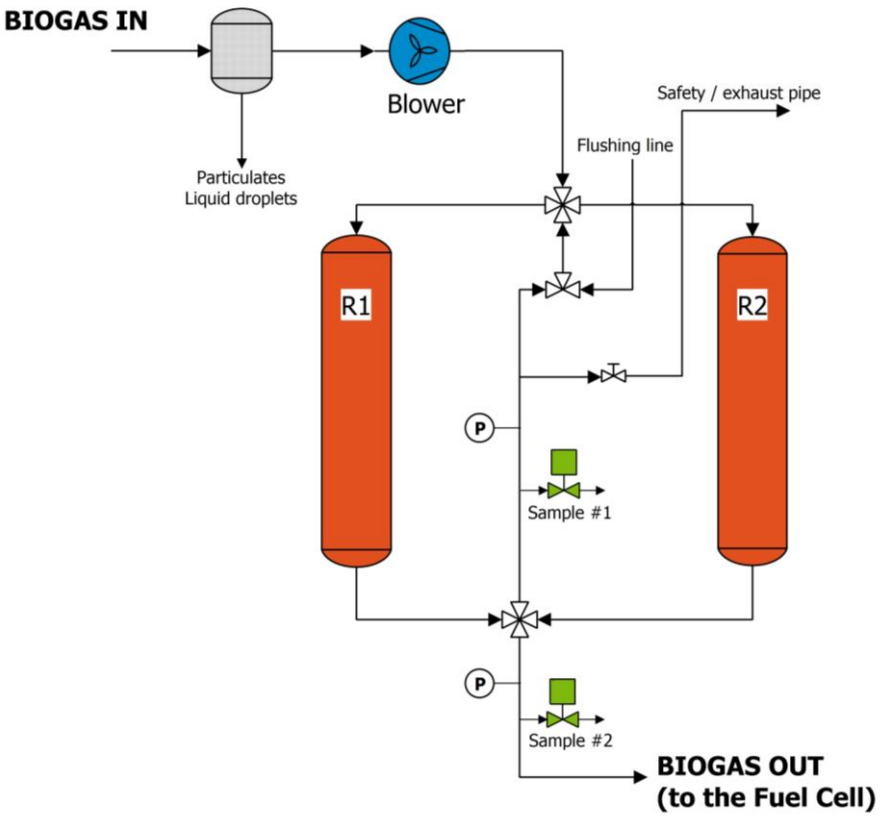

Figure 23. Biogas clean-up section: lead-and-lag configuration

Examples of adsorption curves on activated carbons

Adsorption curves for typically encountered commercial activated carbons for the removal of H_2S are reviewed in this section.

The pass through ratio (C/C_0) is generally used to describe the pollutant removal with sorbent materials, where C is the gas bulk concentration and C_0 the initial concentration, both in ppm(v). For fuel cell applications, this value was fixed at 1% and 10% in order to identify two reference concentration levels [208]. These two concentration levels were adopted to describe the nominal concentration and a maximum concentration level suitable for SOFC application, considering a biogas coming from WWTPs were generally the H_2S level ranged from 60 to 200 ppm(v). These values represent the reversible pollutant concentration for SOFC applications, as reported elsewhere [121,154,209]. In the meantime, the pass through ratio at 10% can only generate irreversible issues for SOFCs.

Papurello et al. studied the performance of the Airdep Carbox AC for fuel cell applications [210]. This material is an extruded activated carbon, activated with steam and impregnated with several metal (hydr)oxides (mainly MgO, KOH, and CaOH). A breakthrough time t_b of 107 min for C/C_0=1% was observed (Figure 24).

At the 10% level of C/C_0, the t_b was 111 min. Looking at the curve in Figure 24, we observe how the saturation level is reached soon after the initial breakthrough at C/C_0 = 1%.

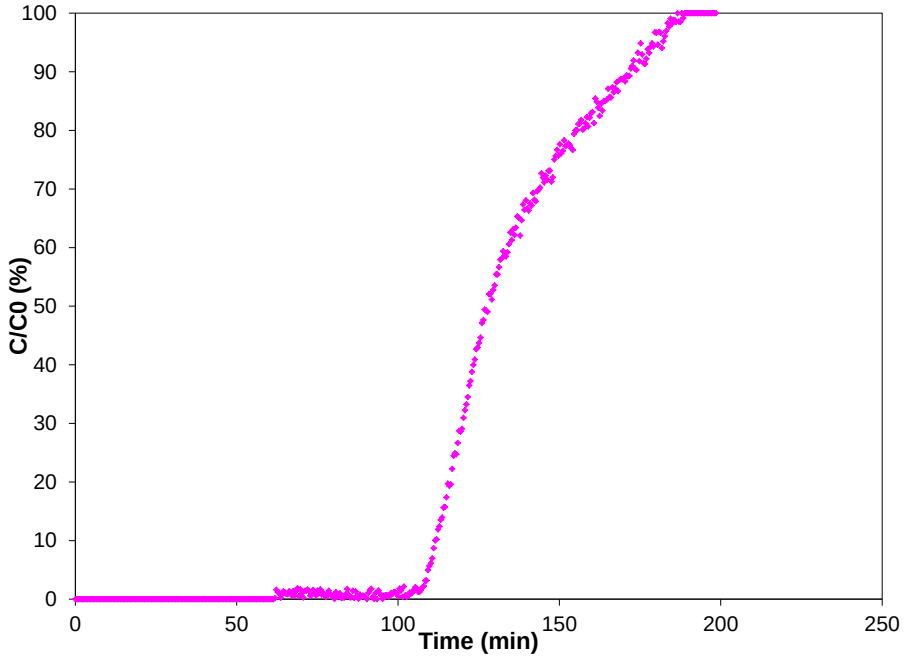

Figure 24. Single compound removal – breakthrough time

Papurello et al. [211] showed how the breakthrough time decreased when the initial concentration of the contaminant increases. By reducing the operating temperature from 45 °C to 5 °C, the removal performance of commercial carbons was improved [211]. Water vapor contained in the biogas was pre-adsorbed on the carbon that enters in competition with the organic vapor that has to be removed. This might result in a loss of adsorption capacity as well as a decreasing rate of adsorption. In fact, an RH value around 20% at 30 °C is still tolerable; here the adsorption capacity for two different commercial carbons was around 5 mg g^{-1} [211]. On the contrary, when the relative humidity value was above 50%, the adsorption capacity was close to zero [211].

Generally, sorbent materials face the contemporary presence of more than one pollutant[185]. The phenomenon that might occur during the removal of more than one trace compound is called roll-up [212,213]. Figure 25 provides an example of the roll-up phenomenon; the graph shows the breakthrough for two different pollutants, namely C1 (H_2S) and C2 (HCl) that are both present in the inlet biogas stream. The simultaneous presence of two (or more) vapors reduces the breakthrough time that each contaminant would reach if present alone in the feed. The reduced breakthrough time (t_b) is because each vapor wave front moves faster (compared to the case with only one contaminant) through the bed as the two vapors compete for the same adsorption volume. Hence, the less strongly and previously adsorbed vapor will be partially displaced by the other, which might even result in a concentration at the exit gas of the previously adsorbed contaminant higher than the inlet value. In Figure 25, we observe how C2 first eluted after 64 min of continuous gas feeding, while C1 kept occupying free sites of the carbon for a longer time. This was due to the higher adsorption capacity at saturation of C1 (391 mg g^{-1}) compared to C2 (238 mg g^{-1}) (these values were measured in single-contaminant

experiments). At 169 min, C2 reached its maximum pass-through ratio value (105%); an outlet concentration higher than the inlet is possible since C1 vapor displaces part of the previously adsorbed C2 vapor. Gradually, C1 reaches the saturation condition of the carbon filter bed (i.e., the pass-through ratio is 100%). By the time C1 reaches saturation, C2 also approaches 100% of bed saturation.

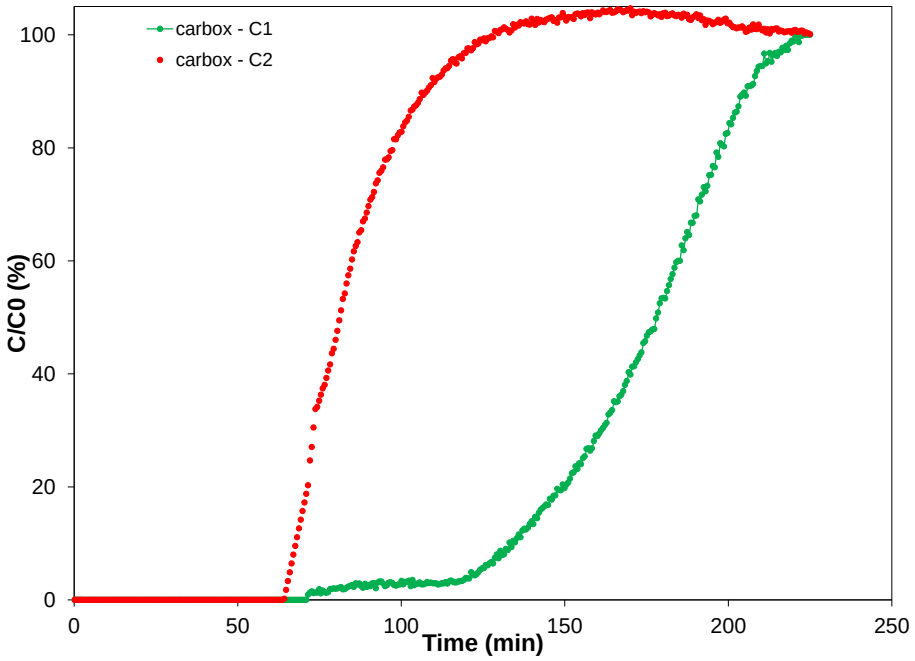

Figure 25. C1 and C2 co-removal in a Carbox activated carbon filter (reprinted with permissions from Balachia [214]*)*

Considering a more realistic case, in which the biogas from an anaerobic digester is filtered by either commercial or innovative materials, the adsorption capacities for H_2S at 1 % were measured respectively as 1.8 mg g^{-1} for activated carbons [186], 0.068 mg g^{-1} for ashes [215] and 1.05 mg g^{-1} for biochar [214].

Sisani et al.[182] studied the efficiency of H_2S removal of H_2S under simulated biogas flow conditions for different solid sorbents. They tested several commercial types of sorbents including steam activated carbons, either without impregnation, or with KOH, or Cu and Cr salts impregnation, activated alumina and zeolite. These materials are all good candidates, in principle, to reduce the sulfur level to ultra-low levels as required by the fuel cell.

Results are summarized in Table 18. It is worth noting how natural sorbents show extremely poor performances, mostly related to their almost negligible micropore volume compared to activated materials. Finally, impregnation is confirmed to be a notable boost for the removal of H_2S. This is true not only for AC, but also when alumina is used as support (see Table 18).

Table 18. The removal efficiency of different solid sorbents tested with H_2S (results adapted from the work of Sisani et al.[182]*). The adsorption capacity was expressed using a breakthrough concentration equal to 1 ppm(v) and dry nitrogen as reference carrier gas.*

Sorbent material	Micropore volume V_m (cm^3/g)	Adsorption capacity C_{ads} (mg/g)	Normalized adsorption capacity C_{ads}/V_m (mg/cm^3)
Norit RGM1 (AC impregnated with Cu and Cr salts)	0.66	27.15	41.14
Norit RB1 (non-impregnated AC)	0.44	1.71	3.89
Desotec Airpel Ultra DS (KOH-KI impregnated AC)	0.42	6.6	15.71
Norit RBAA1 (KOH impregnated AC)	0.36	20.43	56.75
Sepiolite (natural clay)	0.06	<0.1	-
Zeolite ATZ (natural zeolite)	0.04	<0.1	-
Alumina Galipur S (activated and $KMnO_4$ impregnated)	0.01	1.56	156.0

The adsorption curves for the different solid sorbents tested by Sisani et al. [182] are shown in Figure 26. It is worth noting how the curve becomes quite steep at breakthrough. In fact, as soon as the H_2S is detected in the outlet gas, its concentration increases fast over time.

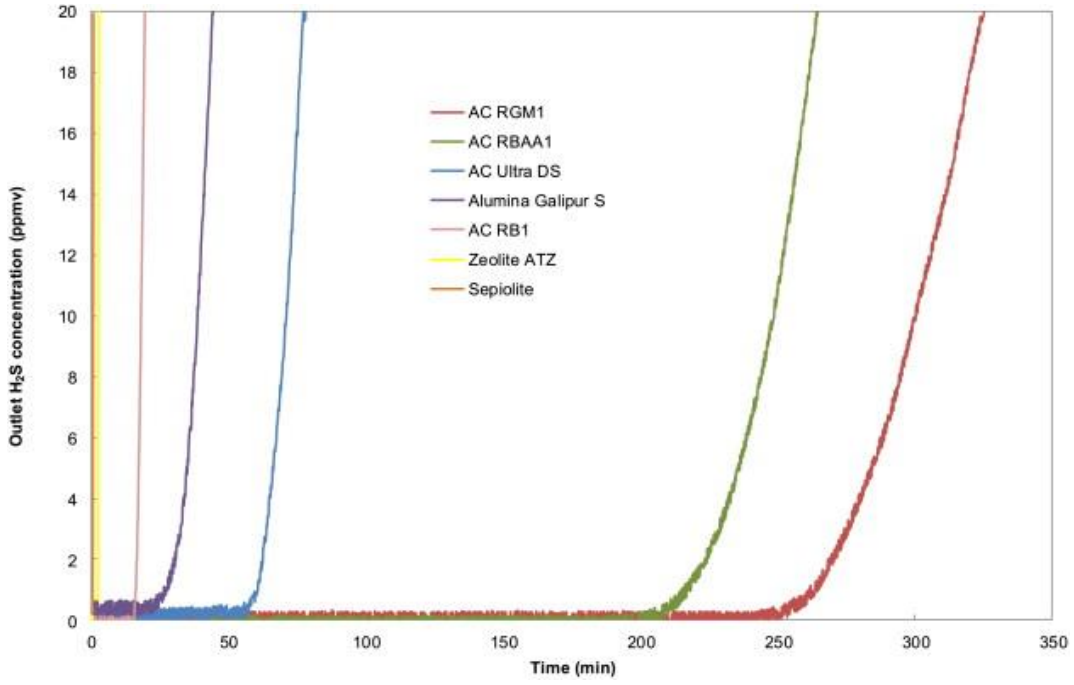

Figure 26. Breakthrough curves of H_2S on AC impregnated (Norit RGM1) with Cu and Cr salts; tests were performed using three different carrier gases (N_2, CO_2, and CH_4) and an inlet H_2S concentration of 1,000 ppm (reprinted with permission from Sisani et al. [182]*).*

Experiments on sorbent materials are often conducted in dry anaerobic conditions. However, it was previously stated how gas humidity and the presence of oxygen in the biogas stream could drastically affect the removal efficiency of the tested material. Sitthikhankaew et al. [216] studied systematically the effect of humidity, O_2, and CO_2 on the adsorption of H_2S on both AC and IAC. Results are summarized in Table 19. As expected, the presence of O_2 comes with a marked increase in the adsorption capacity of the AC. The presence of CO_2 in dry inert gas further reduces the removal capacity compared to inert gas only; this is due to the competitive adsorption of CO_2 on the active carbon sites. Finally, the gas humidity is strongly enhancing the overall adsorption capacity of the sorbent. However, looking at breakthrough curves in Figure 27, we observe how the moisturized gas is not able to remove H_2S entirely as in the case of oxygen presence. On the one hand, the overall sulfur capacity of the sorbent is augmented by the presence of moisture; on the other hand, sulfur is not completely removed. Hence, for fuel cell applications – for which ultra-low levels of H_2S must be detected at the exit gas – the presence of moisture might be detrimental since a full removal of H_2S is required. In a two- or multiple-reactor configuration and for biogas with a high H_2S concentration, the presence of moisture in the first reactor(s) might be favorable for an initial H_2S abatement. However, the following stages should foresee a dry gas for a complete sulfur removal. Finally, the simultaneous presence of humidity and oxygen provides the best performance (Figure 27). In the presence of moisture, sulfur removal is enhanced as the adsorbed H_2S dissolves in the water film forming HS^- and H^+.

Table 19. The removal efficiency of different solid sorbents tested with H_2S (results adapted from the work of Sitthikhankaew et al. [216]*). The adsorption capacity was expressed using a breakthrough concentration equal to 3,000 ppm(v), i.e., the inlet H_2S concentration).*

Sorbent material	**Micropore volume V_m (cm^3/g)**	**Adsorption capacity C_{ads} (mg/g)**			
		Dry gas	**2% O_2**	**40% CO_2**	**70% RH**
AC (commercial)	0.45	1.1	4.00	0.7	28.4
AC + steam activation	0.59	2.6	6.30	0.9	77.6
AC + KOH impregnation	0.34	4.3	8.50	0.8	47.4
AC + steam activation + KOH impregnation	0.45	3.0	21.90	0.9	90.9

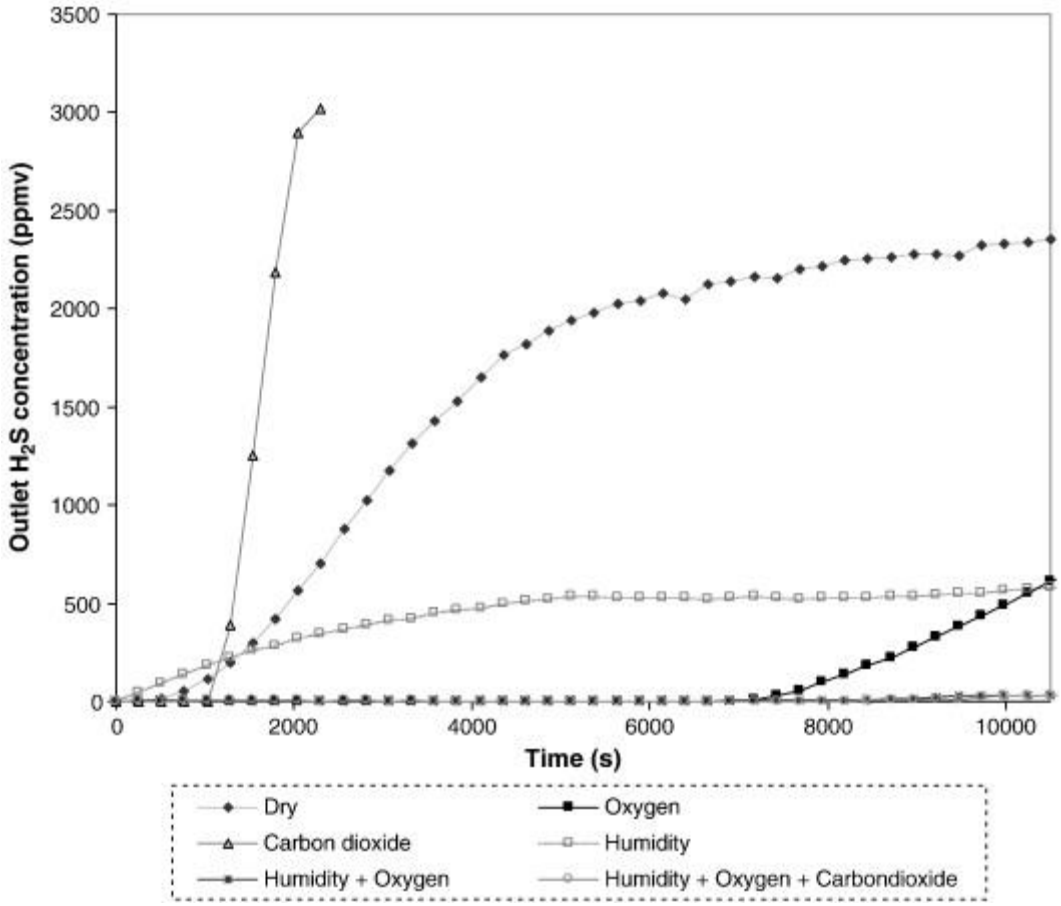

Figure 27. Breakthrough curves of H_2S on AC impregnated (Norit RGM1) with Cu and Cr salts; tests were performed using three different carrier gases (N_2, CO_2 and CH_4) and an inlet H_2S concentration of 1,000 ppm (reprinted with permission from Sitthikhankaew et al. [216]*).*

The reaction mechanism proposed by Sitthikhankaew et al. [216] is the following (H_2S adsorption and dissociation):

$$H_2S(ads) \rightarrow H_2S(ads - liq) \quad (35)$$

$$H_2S(ads - liq) \rightarrow HS^-(ads) + H^+ \quad (36)$$

$$H^+ + OH^- \rightarrow H_2O \quad (37)$$

The reactions involving oxygen are listed below:

$$O_2(g) \rightarrow O_2(ads) \quad (38)$$

$$O_2(ads) \rightarrow O_2(ads - liq) \quad (39)$$

$$O_2(ads - liq) \rightarrow 2O*(ads) \quad (40)$$

The adsorbed oxygen is dissociated and thus can react with HS^- ions to form one of the following sulfur species: S, SO_2 or H_2SO_4.

$$O*(ads) + HS^-(ads) \rightarrow S(ads) + OH^- \quad (41)$$

$$3O*(ads) + HS^-(ads) \rightarrow SO_2(ads) + OH^- \quad (42)$$

$$O*(ads) + SO_2(ads) + H_2O(ads) \rightarrow H_2SO_4(ads) \quad (43)$$

The more compact reaction mechanism for H_2S removal proposed by Bagreev and Bandosz [167], which is consistent with the previous set of reactions, is the following:

$$C_f + 1/2\,O_2 \rightarrow C(O) \quad (44)$$

$$C(O) + H_2S \rightarrow C_f + S + H_2O \quad (45)$$

$$S + xS \rightarrow S_{x+1} \quad (46)$$

$$S + O_2 \rightarrow SO_2 \quad (47)$$

C_f is an active site of the AC that is able to store atomic oxygen. It is worth noting that S might further react with O_2 to form SO_2 (which is an undesired emission).

The mechanism of H_2S removal on activated carbon in the presence of caustic impregnation is described further by Bagreev and Bandosz [167] as follows:

$$KOH + H_2S \rightarrow KHS + H_2O \quad (48)$$

$$2KOH + H_2S \rightarrow K_2S + 2H_2O \quad (49)$$

$$KHS + 1/2\,O_2 \rightarrow S + KOH \quad (50)$$

$$K_2S + 1/2\,O_2 + H_2O \rightarrow S + 2KOH \quad (51)$$

Hydrogen sulfide is oxidized on basic centers of alkali earth metal oxides and sulfur is formed [169]. The last two reactions show how KOH is regenerated with O_2 thus leaving elemental sulfur behind. Oxygen is thus fundamental to restore the catalytic activity of the impregnated AC. KOH can also react with H_2S to form potassium sulfate (see reaction below).

$$2KOH + H_2S + 2O_2 \rightarrow K_2SO_4 + 2H_2O \quad (52)$$

This is an undesired reaction as the catalytic site is consumed.

Discussion: guidelines for dealing with fuel contaminants

The presence of contaminants in the fuel feed, even at ppm or sub-ppm levels, can drastically reduce the performance and lifetime of the catalytic and electro-catalytic active surfaces encountered in solid oxide fuel cells. Alternative fuels different from natural gas, such as landfill and anaerobic digestion biogases, contain a wide variety of micro-contaminants found in different amounts depending on the specific biomass or biowaste from which the biogas has been produced.

Sulfur compounds (H_2S and organic sulfur compounds) and organic silicon compounds (siloxanes) are the most relevant and critical contaminants when dealing with biogas. Therefore, we have extensively reviewed the origin, typology and the amount of these contaminants in different biogases in this work. Sulfur is mostly present as H_2S in biogas and, despite high concentrations (i.e., thousands of ppm) can be found mainly in biogas from manure, food waste or diary waste effluents; the average concentration is often limited to a few tens of ppm in most of the cases (this is true especially for WWTP) thanks to in-situ abatement techniques that prevent the sulfur from reaching the gas phase.

Siloxanes are instead found almost exclusively in landfill and sewage biogas. Often D4 and D5 compounds make most of the overall silicon amount in biogas. Siloxanes derive from human-made products (such as detergents and cosmetics) that are discharged in the sewerage.

The critical point of biogas contaminants is that they can affect both the reformer of the fuel cell system (if present) and the fuel cell anode electrode. In both cases, the effect of sulfur is a relatively fast deactivation of the Ni active surface due sulfur coverage. Re-activation of the Ni surface is feasible at high temperature (800 °C), whereas at lower temperature a permanent degradation might be established. For what concerns siloxanes, a gradual accumulation of micro-silica deposits is instead observed, which is a non-reversible degradation process. Therefore, silicon contamination in the fuel feed is very detrimental for the operation of the fuel cell.

Tars and hydrocarbons (which are more abundant in bio-syngas from biomass gasification, but they can be also found to a lower extent into biogases) are generally dangerous since enhanced carbon deposition is triggered by carbon species having $C > 1$. Halogens are not really critical for the fuel cell electrode.

To provide a durable fuel cell system, a deep clean-up of the incoming biogas stream is required. Solid oxide fuel cell systems have been shown to be very sensitive to even trace amounts (ppb levels) of selected contaminants. Hence, a dedicated biogas clean-up upstream from the SOFC must be accounted for.

Adsorption processes based on impregnated activated carbons seem to be the most effective solution for biogas purification. Siloxanes are easily removed reaching loading rates above 10 wt. % on AC. Sulfur (H_2S) is effectively removed in the presence of some oxygen in the gas feed, which promotes its storage in the AC micropore volume. For biogas feeds with a very high inlet H_2S concentration, in-situ abatement techniques

(either biological or chemical routes) should be applied. Otherwise, iron oxide based sorbents or activated carbons can be also employed (however, the frequent bed replacement and its disposal might be critical from an economic point of view).

Since most of the high temperature fuel cell systems employ a either partial or full reforming of the inlet methane feed in order to provide the fuel cell stack with an anode feed rich in H_2 and CO, the reformer (which is often based on Ni catalyst) is the first component that will suffer from fuel contamination. Therefore, an early identification of the onset of deactivation of the reformer might be used as proxy to avoid a more severe and extended degradation of the fuel cell stacks (which are generally more delicate and expensive). By monitoring the online outlet composition of the reformer, early deactivation could be easily identified and correlated to a malfunctioning of the upstream clean-up system.

Conclusion

Biogas is a renewable fuel current exploitation of which lies well below the maximum potential. Biogas is available either as digester gas from the anaerobic digestion of putrescible organic matter – this is often wet bio-waste (e.g., urban and/or industrial sludge from wastewater treatment plants, manure, and food waste) or agricultural residues – or from landfill.

Hence, we first introduced the opportunities for biogas exploitation in advanced high-temperature fuel cell systems and the competitive advantages of fuel cells against conventional machines (e.g., ICEs) in terms of higher electrical conversion efficiency and reduced emissions of CO_2 and atmospheric pollutants. The appraisal of current biogas production trends and the potential for further production from different sources followed.

We have then extensively reviewed a range of topics connected with the use of biogas in solid oxide fuel cells. The focus was on the biogas contaminants, which can degrade the fuel cell reformer and state-of-the-art Ni anode. The origin, amount, and type of different contaminants that might be found in biogases have been widely reviewed showing how siloxanes are particularly relevant for sewage biogas. H_2S and other organic sulfur compounds are found instead at very high concentration in biogases from manure and food waste, while halogenated compounds (as well as siloxanes) are significant in landfill biogas.

Processes and techniques for the removal of biogas contaminants have been discussed in detail. Solid sorbents – especially impregnated activated carbons – seem to be the most effective and proven solution for the ultra-deep purification of biogas (polishing stage). Indeed, the SOFC requires a high-purity fuel stream and the co-removal of different contaminants entails complex physicochemical phenomena and thus an optimized surface chemistry of the adsorbent material. Further research work is encouraged in this area to identify cost-effective solutions for durable and reliable biogas clean-up from harmful contaminants.

Degradation on the fuel cell reformer and the Ni-anode showed to be extremely severe in the presence of siloxanes, thus remarking the crucial role of having an effective biogas clean-up system. Even trace amounts (tens of ppb) of siloxanes can cause a severe and irreversible damage on both the Ni-reformer and SOFC. The impact of H_2S is mild compared to siloxanes, and it is well understood. H_2S is certainly detrimental to the reformer and SOFC performance, however, more in the form of a temporary (catalyst or electro-catalyst) deactivation rather than as an irreversible degradation as in the case of siloxanes. Finally, HCl is the less critical contaminant of those investigated. The impact on the SOFC performance is almost negligible.

Acknowledgements

The research leading to these results has received funding from the European Union's Seventh Framework Program (FP7/2007-2013) for the Fuel Cells and Hydrogen Joint Technology Initiative under grant agreement number 278798 'SOFCOM'.

One of the authors, Davide Papurello, kindly acknowledges funding provided by the 'Fondazione Cassa di Risparmio di Trento e Rovereto' in the framework of the Biowaste for SOFCs (BWS) project.

References

[1] Trembly JP, Gemmen RS, Bayless DJ. The effect of coal syngas containing HCl on the performance of solid oxide fuel cells: Investigations into the effect of operational temperature and HCl concentration. J Power Sources 2007;169:347–54. doi:10.1016/j.jpowsour.2007.03.018.

[2] Madi H, Lanzini A, Papurello D, Diethelm S, Ludwig C, Santarelli M, et al. Solid oxide fuel cell anode degradation by the effect of hydrogen chloride in stack and single cell environments. J Power Sources 2016;326:349–56. doi:10.1016/j.jpowsour.2016.07.003.

[3] Kopetz H, Haara K. Biogas – an important renewable energy source. 2013.

[4] EurObserv'ER biogas barometer n.d. http://www.eurobserv-er.org/ (accessed August 16, 2016).

[5] Biogas Barometer – EUROBSERV'ER. 2014.

[6] EUROSTAT Database - Historical biogas production trends from 1990 to 2014 n.d. ec.europa.eu/eurostat/web/energy/data/database (accessed April 24, 2016).

[7] Aebiom. A Biogas Road Map for Europe. Brussels: 2009.

[8] Mininni G, Laera G, Bertanza G, Canato M, Sbrilli a. Mass and energy balances of sludge processing in reference and upgraded wastewater treatment plants. Environ Sci Pollut Res 2015;22:7203–15. doi:10.1007/s11356-014-4013-2.

[9] Biomasse Energie, Wirtschaftlichkeit Landwirtschaftlicher Biogasanlagen - Berechnungsintrument. n.d.

[10] Smil V. Biomass Energies. Boston, MA: Springer US; 1983. doi:10.1007/978-1-4613-3691-4.

[11] El-Mashad HM, Zhang R. Biogas production from co-digestion of dairy manure and food waste. Bioresour Technol 2010;101:4021–8. doi:10.1016/j.biortech.2010.01.027.

[12] Raposo F, De La Rubia MA, Fern??ndez-Cegr?? V, Borja R. Anaerobic digestion of solid organic substrates in batch mode: An overview relating to methane yields and experimental procedures. Renew Sustain Energy Rev 2012;16:861–77. doi:10.1016/j.rser.2011.09.008.

[13] US Environmental Protection Agency n.d.

[14] Food and Agricultural Organization of the United Nations (FAO) n.d. http://www.fao.org/save-food/resources/keyfindings/en/ (accessed August 17, 2016).

[15] Patrizio P, Leduc S, Chinese D, Dotzauer E, Kraxner F. Biomethane as transport fuel – A comparison with other biogas utilization pathways in northern Italy. Appl Energy 2015;157:25–34. doi:10.1016/j.apenergy.2015.07.074.

[16] Hardman S, Chandan A, Shiu E, Steinberger-Wilckens R. Consumer attitudes to fuel cell vehicles post trial in the United Kingdom. Int J Hydrogen Energy 2016;41:6171–9. doi:10.1016/j.ijhydene.2016.02.067.

[17] NEDO's Activities on Fuel Cell. 23rd IPHE SC Meet Wuhan, China 2015:1–20. http://www.iphe.net/docs/Meetings/SC23/Workshop/4_NEDO_Japan.pdf (accessed April 24, 2016).

[18] Ene.field project n.d. enefield.eu (accessed April 24, 2016).

[19] Li M, Rao AD, Brouwer J, Samuelsen GS. Design of highly efficient coal-based integrated gasification fuel cell power plants. J Power Sources 2010;195:5707–18. doi:10.1016/j.jpowsour.2010.03.045.

[20] Lanzini a., Kreutz TG, Martelli E, Santarelli M. Energy and economic performance of novel integrated gasifier fuel cell (IGFC) cycles with carbon capture. Int J Greenh Gas Control 2014;26:169–84. doi:10.1016/j.ijggc.2014.04.028.

[21] Kobayashi Y, Ando Y, Kabata T, Nishimura M, Tomida K, Matake N. Extremely High-efficiency

Thermal Power System-Solid Oxide Fuel Cell (SOFC) Triple Combined-cycle System. Mistubishi Heavy Ind Tech Rev 2011;48:9–15.

[22] Choi JH, Ahn JH, Kim TS. Performance of a triple power generation cycle combining gas/steam turbine combined cycle and solid oxide fuel cell and the influence of carbon capture. Appl Therm Eng 2014;71:301–9. doi:10.1016/j.applthermaleng.2014.07.001.

[23] Tjaden B, Gandiglio M, Lanzini a., Santarelli M, Järvinen M. Small-scale biogas-SOFC plant: Technical analysis and assessment of different fuel reforming options. Energy and Fuels 2014;28:4216–32. doi:10.1021/ef500212j.

[24] Ammermann H, Hoff P, Atanasiu M, Ayllor J, Kaufmann M, Tisler O. Advancing Europe's energy systems: Stationary fuel cells in distributed generation. 2015. doi:10.2843/088142.

[25] General Electric Power Generation n.d. https://powergen.gepower.com/products/reciprocating-engines (accessed August 17, 2016).

[26] AB Holding Spa n.d. http://www.gruppoab.it/it/biogas/ (accessed August 17, 2016).

[27] Lanzini a., Kreutz TG, Martelli E, Santarelli M. Energy and economic performance of novel integrated gasifier fuel cell (IGFC) cycles with carbon capture. Int J Greenh Gas Control 2014;26:169–84. doi:10.1016/j.ijggc.2014.04.028.

[28] Van herle J, Membrez Y, Bucheli O. Biogas as a fuel source for SOFC co-generators. J Power Sources 2004;127:300–12. doi:http://dx.doi.org/10.1016/j.jpowsour.2003.09.027.

[29] Van herle J, Maréchal F, Leuenberger S, Favrat D. Energy balance model of a SOFC cogenerator operated with biogas. J Power Sources 2003;118:375–83. doi:http://dx.doi.org/10.1016/S0378-7753(03)00103-4.

[30] Van herle J, Maréchal F, Leuenberger S, Membrez Y, Bucheli O, Favrat D. Process flow model of solid oxide fuel cell system supplied with sewage biogas. J Power Sources 2004;131:127–41. doi:10.1016/j.jpowsour.2004.01.013.

[31] Lanzini A, Leone P. Experimental investigation of direct internal reforming of biogas in solid oxide fuel cells. Int J Hydrogen Energy 2010;35:2463–76. doi:10.1016/j.ijhydene.2009.12.146.

[32] Leone P, Lanzini a., Santarelli M, Calì M, Sagnelli F, Boulanger A, et al. Methane-free biogas for direct feeding of solid oxide fuel cells. J Power Sources 2010;195:239–48. doi:10.1016/j.jpowsour.2009.06.108.

[33] Trendewicz a. a., Braun RJ. Techno-economic analysis of solid oxide fuel cell-based combined heat and power systems for biogas utilization at wastewater treatment facilities. J Power Sources 2013;233:380–93. doi:10.1016/j.jpowsour.2013.01.017.

[34] Self-generation Incentive Program (SGIP) n.d. https://www.pge.com/en_US/business/solar-and-vehicles/your-options/solar-programs/self-generation-incentive-program/self-generation-incentive-program.page (accessed August 17, 2016).

[35] Curletti F, Gandiglio M, Lanzini A, Santarelli M, Maréchal F. Large size biogas-fed Solid Oxide Fuel Cell power plants with carbon dioxide management: Technical and economic optimization. J Power Sources 2015;294:669–90. doi:10.1016/j.jpowsour.2015.06.091.

[36] Margalef P, Brown T, Brouwer J, Samuelsen S. Efficiency of poly-generating high temperature fuel cells. J Power Sources 2011;196:2055–60. doi:10.1016/j.jpowsour.2010.10.046.

[37] Rinaldi G, McLarty D, Brouwer J, Lanzini A, Santarelli M. Study of CO2 recovery in a carbonate fuel cell tri-generation plant. J Power Sources 2015;284:16–26. doi:10.1016/j.jpowsour.2015.02.147.

[38] SOFCOM Project - SOFC CCHP WITH POLY-FUEL OPERATION AND MAINTENANCE n.d. http://cordis.europa.eu/result/rcn/140630_en.html (accessed August 19, 2016).

[39] Gandiglio M, Lanzini A, Santarelli M, Leone P. ASME DC | Journal of Fuel Cell Science and Technology | Design and Balance-of-Plant of a Demonstration Plant With a Solid Oxide Fuel Cell Fed by Biogas From Waste-Water and Exhaust Carbon Recycling for Algae Growth. J Fuel Cell Sci Technol 2014;11:31003. doi:10.1115/1.4026088.

[40] Santarelli M, Lanzini A, Gandiglio M. SOFCOM Final Report. 2015.

[41] ATSDR - Landfill Gas Primer - An Overview for Environmental Health Professionals. 2001.

[42] Schweigkofler M, Niessner R. Removal of siloxanes in biogases. J Hazard Mater 2001;83:183–96. doi:10.1016/S0304-3894(00)00318-6.

[43] Haga K, Shiratori Y, Ito K, Sasaki K. Chlorine Poisoning of SOFC Ni-Cermet Anodes. J Electrochem Soc 2008;155:B1233–B1239. doi:10.1149/1.2980521.

[44] Jalali A, Motamedhashemi MMY, Egolfopoulos FN, Tsotsis T. Fate of Siloxane Impurities During the Combustion of Renewable Natural Gas. Combust Sci Technol 2013;185:953–74. doi:10.1080/00102202.2013.766606.

[45] Sánchez D, Monje B, Chacartegui R, Campanari S, Sa D. Potential of molten carbonate fuel cells to enhance the performance of CHP plants in sewage treatment facilities. Int J Hydrogen Energy 2013;38:394–405. doi:10.1016/j.ijhydene.2012.09.145.

[46] Papadias DD, Ahmed S, Kumar R. Fuel quality issues with biogas energy - An economic analysis for a stationary fuel cell system. Energy 2012;44:257–77. doi:10.1016/j.energy.2012.06.031.

[47] Fuel Cell Today, Matthey J. The Fuel Cell Industry Review. 2013. doi:10.1595/147106712X657535.

[48] Thijssen H. The Impact of Scale-Up and Production Volume on SOFC Manufacturing Cost. 2007.

[49] Argonne National Laboratory. GAS CLEAN-UP FOR FUEL CELL APPLICATIONS WORKSHOP. 2014.

[50] Gandiglio M, Lanzini A, Santarelli M, Leone P. ASME DC | Journal of Fuel Cell Science and Technology | Design and Balance-of-Plant of a Demonstration Plant With a Solid Oxide Fuel Cell Fed by Biogas From Waste-Water and Exhaust Carbon Recycling for Algae Growth. J Fuel Cell Sci Technol 2014;11:31003. doi:10.1115/1.4026088.

[51] Rasi S. Biogas Composition and upgrading to Biomethane. 2009.

[52] de Arespacochaga N, Valderrama C, Mesa C, Bouchy L, Cortina JLL. Biogas deep clean-up based on adsorption technologies for Solid Oxide Fuel Cell applications. Chem Eng J 2014;255:593–603. doi:10.1016/j.cej.2014.06.072.

[53] Papadias D. Biogas Impurities and Cleanup for Fuel Cells 2012.

[54] Rey MD, Font R, Aracil I. Biogas from MSW landfill: Composition and determination of chlorine content with the AOX (adsorbable organically bound halogens) technique. Energy 2013;63:161–7. doi:10.1016/j.energy.2013.09.017.

[55] Sevimoğlu O, Tansel B. Effect of persistent trace compounds in landfill gas on engine performance during energy recovery: A case study. Waste Manag 2013;33:74–80. doi:10.1016/j.wasman.2012.08.016.

[56] Piechota G, Igliński B, Buczkowski R. Development of measurement techniques for determination main and hazardous components in biogas utilised for energy purposes. Energy Convers Manag 2013;68:219–26. doi:10.1016/j.enconman.2013.01.011.

[57] Osorio F, Torres JC. Biogas purification from anaerobic digestion in a wastewater treatment plant for biofuel production. Renew Energy 2009;34:2164–71. doi:10.1016/j.renene.2009.02.023.

[58] Arnold M. Reduction and monitoring of biogas trace compounds. 2009.

[59] Saber DL, Manager SP, Cruz KMH, Scientist P. Pipeline quality biomethane: North American guidance document for introduction of dairy waste derived biomethane into existing natural gas networks: Task 2. 2009.

[60] Saber DL, Manager SP, Cruz KMH, Scientist P. Pipeline quality biomethane: North American guidance document for introduction of dairy waste derived biomethane into existing natural gas networks: Task 2. 2009.

[61] Gutierrez O, Park D, Sharma KR, Yuan Z. Iron salts dosage for sulfide control in sewers induces chemical phosphorus removal during wastewater treatment. Water Res 2010;44:3467–75. doi:10.1016/j.watres.2010.03.023.

[62] Surita SC, Tansel B. Emergence and fate of cyclic volatile polydimethylsiloxanes (D4, D5) in municipal waste streams: Release mechanisms, partitioning and persistence in air, water, soil and sediments. Sci Total Env 2013;468–469C:46–52. doi:10.1016/j.scitotenv.2013.08.006.

[63] Arespacochaga N De, Valderrama C, Raich-montiu J, Crest M. Understanding the effects of the origin , occurrence , monitoring , control , fate and removal of siloxanes on the energetic valorization of sewage biogas — A review. Renew Sustain Energy Rev 2015;52:366–81. doi:10.1016/j.rser.2015.07.106.

[64] Wang D-G, Aggarwal M, Tait T, Brimble S, Pacepavicius G, Kinsman L, et al. Fate of anthropogenic cyclic volatile methylsiloxanes in a wastewater treatment plant. Water Res 2015;72:209–17. doi:10.1016/j.watres.2014.10.007.

[65] Ohannessian A, Desjardin V, Chatain V, Germain P. Volatile organic silicon compounds: the most undesirable contaminants in biogases. Water Sci Technol 2008;58:1775–81. doi:10.2166/wst.2008.498.

[66] Madi H, Lanzini A, Diethelm S, Papurello D, Van herle J, Lualdi M, et al. Solid oxide fuel cell anode degradation by the effect of siloxanes. J Power Sources 2015;279:460–71. doi:10.1016/j.jpowsour.2015.01.053.

[67] Arnold M, Kajolinna T. Development of on-line measurement techniques for siloxanes and other trace compounds in biogas. Waste Manag 2010;30:1011–7. doi:10.1016/j.wasman.2009.11.030.

[68] Schweigkofler M, Niessner R. Determination of Siloxanes and VOC in Landfill Gas and Sewage Gas by Canister Sampling and GC-MS/AES Analysis. Environ Sci Technol 1999;33:3680–5. doi:10.1021/es9902569.

[69] Tower P. NEW TECHNOLOGY FOR REMOVAL OF SILOXANES IN DIGESTER GAS RESULTS IN LOWER MAINTENANCE COSTS AND AIR QUALITY BENEFITS IN POWER GENERATION EQUIPMENT. Proc. Water Environ. Fed. WEFTEC 2003 Sess. 31 through Sess. 40, pp. 440-447(8), Water Environment Federation; 2003, p. 440–447(8).

[70] Rasi S, Lehtinen J, Rintala J. Determination of organic silicon compounds in biogas from wastewater treatments plants, landfills, and co-digestion plants. Renew Energy 2010;35:2666–73. doi:10.1016/j.renene.2010.04.012.

[71] Papurello D, Soukoulis C, Schuhfried E, Cappellin L, Gasperi F, Silvestri S, et al. Monitoring of volatile compound emissions during dry anaerobic digestion of the Organic Fraction of Municipal Solid Waste by Proton Transfer Reaction Time-of-Flight Mass Spectrometry. Bioresour Technol 2012;126:254–65. doi:10.1016/j.biortech.2012.09.033.

[72] Lanzini a., Leone P, Guerra C, Smeacetto F, Brandon NPP, Santarelli M. Durability of anode supported Solid Oxides Fuel Cells (SOFC) under direct dry-reforming of methane. Chem Eng J 2013;220:254–63. doi:10.1016/j.cej.2013.01.003.

[73] Guerra C, Lanzini A, Leone P, Santarelli M, Brandon NP. Optimization of dry reforming of methane over Ni/YSZ anodes for solid oxide fuel cells. J Power Sources 2014;245:154–63.

doi:10.1016/j.jpowsour.2013.06.088.

[74] Lanzini A, Guerra C, Leone P, Santarelli M, Smeacetto F, Fiorilli S, et al. In fl uence of the microstructure on the catalytic properties of SOFC anodes under dry reforming of methane. Mater Lett 2016;164:312–5. doi:10.1016/j.matlet.2015.10.171.

[75] Janardhanan VM, Heuveline V, Deutschmann O. Performance analysis of a SOFC under direct internal reforming conditions. J Power Sources 2007;172:296–307. doi:10.1016/j.jpowsour.2007.07.008.

[76] Effendi A, Zhang ZG, Hellgardt K, Honda K, Yoshida T. Steam reforming of a clean model biogas over Ni/Al2O3 in fluidized- and fixed-bed reactors. Catal. Today, vol. 77, 2002, p. 181–9. doi:10.1016/S0920-5861(02)00244-4.

[77] Appari S, Janardhanan VM, Bauri R, Jayanti S. Deactivation and regeneration of Ni catalyst during steam reforming of model biogas: An experimental investigation. Int J Hydrogen Energy 2014;39:297–304. doi:10.1016/j.ijhydene.2013.10.056.

[78] Galvagno A, Chiodo V, Urbani F, Freni F. Biogas as hydrogen source for fuel cell applications. Int J Hydrogen Energy 2013;38:3913–20. doi:10.1016/j.ijhydene.2013.01.083.

[79] Chiodo V, Urbani F, Galvagno A, Mondello N, Freni S. Analysis of biogas reforming process for molten carbonate fuel cells. J Power Sources 2012;206:215–21. doi:10.1016/j.jpowsour.2012.01.114.

[80] Chiodo V, Galvagno A, Lanzini A, Papurello D, Urbani F, Santarelli M, et al. Biogas reforming process investigation for SOFC application. Energy Convers Manag 2015;98:252–8. doi:10.1016/j.enconman.2015.03.113.

[81] Kolbitsch P, Pfeifer C, Hofbauer H. Catalytic steam reforming of model biogas. Fuel 2008;87:701–6. doi:10.1016/j.fuel.2007.06.002.

[82] Benito M, García S, Ferreira-Aparicio P, Serrano LG. Development of biogas reforming Ni-La-Al catalysts for fuel cells. J Power Sources 2007;169:177–83. doi:10.1016/j.jpowsour.2007.01.046.

[83] Ashrafi M, Pröll T, Pfeifer C, Hofbauer H. Experimental Study of Model Biogas Catalytic Steam Reforming: 1. Thermodynamic Optimization. Energy & Fuels 2008;22:4182–9. doi:10.1021/ef800081j.

[84] Arbag H, Yasyerli S, Yasyerli N, Dogu G. Activity and stability enhancement of Ni-MCM-41 catalysts by Rh incorporation for hydrogen from dry reforming of methane. Int J Hydrogen Energy 2010;35:2296–304. doi:10.1016/j.ijhydene.2009.12.109.

[85] Ahmed S, Lee SHD, Ferrandon MS. Catalytic steam reforming of biogas – Effects of feed composition and operating conditions. Int J Hydrogen Energy 2015;40:1005–15. doi:10.1016/j.ijhydene.2014.11.009.

[86] Trimm DL. Catalyst design for reduced coking (review). Appl Catal 1983;5:263–90. doi:10.1016/0166-9834(83)80156-0.

[87] Sidjabat O, Trimm DL. Nickel-magnesia catalysts for the steam reforming of light hydrocarbons. Top Catal 2000;11–12:279–82. doi:10.1023/A:1027212301077.

[88] Angeli SD, Pilitsis FG, Lemonidou AA. Methane steam reforming at low temperature: Effect of light alkanes' presence on coke formation. Catal Today 2015:119–28. doi:10.1016/j.cattod.2014.05.043.

[89] Erekson EJ, Bartholomrw CH. Sulfur poisoning of nickel methanation catalysts. II. Effects of H2S concentration, CO and H2O partial pressures and temperature on reactivation rates. Appl Catal 1983;5:323–36. doi:10.1016/0166-9834(83)80160-2.

[90] Abild-Pedersen F, Lytken O, Engbæk J, Nielsen G, Chorkendorff I, Nørskov JK. Methane activation on Ni(1 1 1): Effects of poisons and step defects. Surf Sci 2005;590:127–37. doi:10.1016/j.susc.2005.05.057.

[91] Rostrup-Nielsen JR. Some principles relating to the regeneration of sulfur-poisoned nickel catalyst. J Catal 1971;21:171–8. doi:10.1016/0021-9517(71)90135-7.

[92] Alstrup I, Rostrup-Nielsen JR, Røen S. High temperature hydrogen sulfide chemisorption on nickel catalysts. Appl Catal 1 1981;1:303–14. doi:10.1016/0166-9834(81)80036-X.

[93] Bengaard H. Steam Reforming and Graphite Formation on Ni Catalysts. J Catal 2002;209:365–84. doi:10.1006/jcat.2002.3579.

[94] Ashrafi M, Pfeifer C, Pröll T, Hofbauer H. Experimental study of model biogas catalytic steam reforming: 2. Impact of sulfur on the deactivation and regeneration of Ni-based catalysts. Energy and Fuels 2008;22:4190–5. doi:10.1021/ef8000828.

[95] Hulteberg C. Sulphur-tolerant catalysts in small-scale hydrogen production, a review. Int J Hydrogen Energy 2012;37:3978–92. doi:10.1016/j.ijhydene.2011.12.001.

[96] Appari S, Janardhanan VM, Bauri R, Jayanti S, Deutschmann O. A detailed kinetic model for biogas steam reforming on Ni and catalyst deactivation due to sulfur poisoning. Appl Catal A Gen 2014;471:118–25. doi:10.1016/j.apcata.2013.12.002.

[97] Chattanathan SA, Adhikari S, McVey M, Fasina O. Hydrogen production from biogas reforming and the effect of H2S on CH4 conversion. Int J Hydrogen Energy 2014;39:19905–11. doi:10.1016/j.ijhydene.2014.09.162.

[98] Wang L, Murata K, Inaba M. Development of novel highly active and sulphur-tolerant catalysts for steam reforming of liquid hydrocarbons to produce hydrogen. Appl Catal A Gen 2004;257:43–7. doi:10.1016/S0926-860X(03)00590-8.

[99] Xie C, Chen Y, Li Y, Wang X, Song C. Sulfur poisoning of CeO2–Al2O3-supported mono- and bi-metallic Ni and Rh catalysts in steam reforming of liquid hydrocarbons at low and high temperatures. Appl Catal A Gen 2010;390:210–8. doi:10.1016/j.apcata.2010.10.012.

[100] Xie C, Chen Y, Li Y, Wang X, Song C. Influence of sulfur on the carbon deposition in steam reforming of liquid hydrocarbons over CeO2–Al2O3 supported Ni and Rh catalysts. Appl Catal A Gen 2011;394:32–40. doi:10.1016/j.apcata.2010.12.019.

[101] Lakhapatri SL, Abraham MA. Deactivation due to sulfur poisoning and carbon deposition on Rh-Ni/Al2O3 catalyst during steam reforming of sulfur-doped n-hexadecane. Appl Catal A Gen 2009;364:113–21. doi:10.1016/j.apcata.2009.05.035.

[102] Chiodo V, Meisano S, Zafarana G, Urbani F. Effect of pollutants on biogas steam reforming. Intenational J Hydrog Energy 2016;In press.

[103] Albertazzi S, Basile F, Brandin J, Einvall J, Fornasari G, Hulteberg C, et al. Effect of fly ash and H2S on a Ni-based catalyst for the upgrading of a biomass-generated gas. Biomass and Bioenergy 2008;32:345–53. doi:10.1016/j.biombioe.2007.10.002.

[104] Sehested J, Gelten JAP, Helveg S. Sintering of nickel catalysts: Effects of time, atmosphere, temperature, nickel-carrier interactions, and dopants. Appl Catal A Gen 2006;309:237–46. doi:10.1016/j.apcata.2006.05.017.

[105] Laosiripojana N, Charojrochkul S, Kim-Lohsoontorn P, Assabumrungrat S. Role and advantages of H2S in catalytic steam reforming over nanoscale CeO2-based catalysts. J Catal 2010;276:6–15. doi:10.1016/j.jcat.2010.08.015.

[106] Papadias DD, Ahmed S, Kumar R. Fuel quality issues with biogas energy - An economic analysis for a stationary fuel cell system. Energy 2012;44:257–77. doi:10.1016/j.energy.2012.06.031.

[107] Chiodo V, Maisano S, Zafarana G, Urbani F. Effect of pollutants on biogas steam reforming. Int J Hydrogen Energy 2016. doi:10.1016/j.ijhydene.2016.07.251.

[108] Sperle T, Chen D, Lødeng R, Holmen A. Pre-reforming of natural gas on a Ni catalyst: Criteria for carbon free operation. Appl Catal A Gen 2005;282:195–204. doi:10.1016/j.apcata.2004.12.011.

[109] Didenko LP, Savchenko VI, Arutyunov VS, Sementsova LA. Steam reforming of methane mixtures with ethylene over an industrial nickel catalyst. Pet Chem 2008;48:22–7. doi:10.1134/S0965544108010040.

[110] Laosiripojana N, Sangtongkitcharoen W, Assabumrungrat S. Catalytic steam reforming of ethane and propane over CeO2-doped Ni/Al2O3 at SOFC temperature: Improvement of resistance toward carbon formation by the redox property of doping CeO2. Fuel 2006;85:323–32. doi:10.1016/j.fuel.2005.06.013.

[111] Irvine JTS, Neagu D, Verbraeken MC, Chatzichristodoulou C, Graves C, Mogensen MB. Evolution of the electrochemical interface in high-temperature fuel cells and electrolysers. Nat Energy 2016;1:15014. doi:10.1038/nenergy.2015.14.

[112] Irvine JTS, Neagu D, Verbraeken MC, Chatzichristodoulou C, Graves C, Mogensen MB. Evolution of the electrochemical interface in high-temperature fuel cells and electrolysers. Nat Energy 2016;1:15014. doi:10.1038/nenergy.2015.14.

[113] Shiratori Y, Oshima T, Sasaki K. Feasibility of direct-biogas SOFC. Int J Hydrogen Energy 2008;33:6316–21. doi:10.1016/j.ijhydene.2008.07.101.

[114] Shiratori Y, Ijichi T, Oshima T, Sasaki K. Internal reforming SOFC running on biogas. Int J Hydrogen Energy 2010;35:7905–12. doi:10.1016/j.ijhydene.2010.05.064.

[115] Lanzini a., Leone P, Guerra C, Smeacetto F, Brandon NPP, Santarelli M. Durability of anode supported Solid Oxides Fuel Cells (SOFC) under direct dry-reforming of methane. Chem Eng J 2013;220:254–63. doi:10.1016/j.cej.2013.01.003.

[116] Hagen A, Rasmussen JFB, Thydén K. Durability of solid oxide fuel cells using sulfur containing fuels. J Power Sources 2011;196:7271–6. doi:10.1016/j.jpowsour.2011.02.053.

[117] Yokokawa H, Tu H, Iwanschitz B, Mai A. Fundamental mechanisms limiting solid oxide fuel cell durability. J Power Sources 2008;182:400–12. doi:10.1016/j.jpowsour.2008.02.016.

[118] Sasaki K, Yoshizumi T, Haga K, Yoshitomi H, Hosoi T, Shiratori Y, et al. Chemical Degradation of SOFCs: External Impurity Poisoning and Internal Diffusion-Related Phenomena. ECS Trans 2013;57:315–323. doi:10.1149/05701.0315ecst.

[119] Kromp A, Dierickx S, Leonide A, Weber A, Ivers-Tiffée E. Electrochemical Analysis of Sulphur-Poisoning in Anode-Supported SOFCs under Reformate Operation. ECS Trans 2012;41:161–169. doi:10.1149/1.3702423.

[120] Cheng Z, Wang J-H, Choi Y, Yang L, Lin MC, Liu M. From Ni-YSZ to sulfur-tolerant anode materials for SOFCs: electrochemical behavior, in situ characterization, modeling, and future perspectives. Energy Environ Sci 2011;4:4380. doi:10.1039/c1ee01758f.

[121] Papurello D, Lanzini A, Fiorilli S, Smeacetto F, Singh R, Santarelli M. Sulfur poisoning in Ni-anode solid oxide fuel cells (SOFCs): Deactivation in single cells and a stack. Chem Eng J 2016;283:1224–33. doi:10.1016/j.cej.2015.08.091.

[122] Weber a., Dierickx S, Kromp a., Ivers-Tiffée E. Sulfur Poisoning of Anode-Supported SOFCs under Reformate Operation. Fuel Cells 2013;13:487–93. doi:10.1002/fuce.201200180.

[123] Hauch A, Hagen A, Hjelm J, Ramos T. Sulfur Poisoning of SOFC Anodes: Effect of Overpotential on Long-Term Degradation. J Electrochem Soc 2014;161:F734–43. doi:10.1149/2.080406jes.

[124] Hagen A. Sulfur Poisoning of the Water Gas Shift Reaction on Anode Supported Solid Oxide Fuel Cells. J Electrochem Soc 2013;160:F111–F118. doi:10.1149/2.060302jes.

[125] Nagel FP, Schildhauer TJ, Sfeir J, Schuler A, Biollaz SMA. The impact of sulfur on the performance of a solid oxide fuel cell (SOFC) system operated with hydrocarboneous fuel gas. J Power Sources 2009;189:1127–31. doi:10.1016/j.jpowsour.2008.12.092.

[126] Sasaki K, Haga K, Yoshizumi T, Minematsu D, Yuki E, Liu R, et al. Chemical durability of Solid Oxide Fuel Cells: Influence of impurities on long-term performance. J Power Sources 2011;196:9130–9140. doi:10.1016/j.jpowsour.2010.09.122.

[127] Zha S, Cheng Z, Liu M. Sulfur Poisoning and Regeneration of Ni-Based Anodes in Solid Oxide Fuel Cells. J Electrochem Soc 2007;154:B201–6. doi:10.1149/1.2404779.

[128] Cheng Z, Liu M. Characterization of sulfur poisoning of Ni–YSZ anodes for solid oxide fuel cells using in situ Raman microspectroscopy. Solid State Ionics 2007;178:925–35. doi:10.1016/j.ssi.2007.04.004.

[129] Li TS, Wang WG, Chen T, Miao H, Xu C. Hydrogen sulfide poisoning in solid oxide fuel cells under accelerated testing conditions. J Power Sources 2010;195:7025–32. doi:10.1016/j.jpowsour.2010.05.009.

[130] Cheng Z, Zha S, Liu M. Influence of cell voltage and current on sulfur poisoning behavior of solid oxide fuel cells. J Power Sources 2007;172:688–93. doi:10.1016/j.jpowsour.2007.07.052.

[131] Hansen JB. Correlating Sulfur Poisoning of SOFC Nickel Anodes by a Temkin Isotherm. Electrochem Solid-State Lett 2008;11:B178. doi:10.1149/1.2960521.

[132] Mogensen M, Høgh J, Hansen K V, Jacobsen T. A critical review of models of the H2/H2O/Ni/SZ electrode kinetics. ECS Trans 2007;7:1329–38. doi:10.1149/1.2729236.

[133] Sasaki K, Susuki K, Iyoshi A, Uchimura M, Imamura N, Kusaba H, et al. H2S poisoning of solid oxide fuel cells. J Electrochem Soc 2006;153:A2023–9. doi:10.1149/1.2336075.

[134] Perdereau M, Oudar J. Structure, mécanisme de formation et stabilité de la couche d'adsorption du soufre sur le nickel. Surf Sci 1970;20:80–98. doi:10.1016/0039-6028(70)90207-4.

[135] McCarty JG, Sancier KM, Wise H. Thermodynamics of sulfur chemisorption on metals. IV. Alumina-supported platinum. J Catal 1983;82:92–7. doi:10.1016/0021-9517(83)90120-3.

[136] Mougin J, Petitjean M, Castelli P, Sommacal B. Evaluation of the Performance and Degradation of an SOFC Fed with Biosyngas. Proc. 8th Eur. SOFC Forum, Lucerne, Switz., 2008.

[137] Lanzini A, Leone P, Asinari P. Microstructural characterization of solid oxide fuel cell electrodes by image analysis technique. J Power Sources 2009;194:408–22.

[138] Faes A, Jeangros Q, Wagner JB, Hansen TW, Van Herle J, Brisse A, et al. In situ Reduction and Oxidation of Nickel from Solid Oxide Fuel Cells in a Transmission Electron Microscope. ECS Trans 2009;25:1985–92. doi:10.1149/1.3205743.

[139] Ivey DG, Brightman E, Brandon N. Structural modifications to nickel cermet anodes in fuel cell environments. J Power Sources 2010;195:6301–11. doi:10.1016/j.jpowsour.2010.04.059.

[140] Li TS, Xu C, Chen T, Miao H, Wang WG. Chlorine contaminants poisoning of solid oxide fuel cells. J Solid State Electrochem 2010;15:1077–1085. doi:10.1007/s10008-010-1166-x.

[141] Trembly JP, Gemmen RS, Bayless DJ. The effect of coal syngas containing HCl on the performance of solid oxide fuel cells: Investigations into the effect of operational temperature and HCl concentration. J Power Sources 2007;169:347–54. doi:10.1016/j.jpowsour.2007.03.018.

[142] Xu C, Gong M, Zondlo JW, Liu X, Finklea HO. The effect of HCl in syngas on Ni-YSZ anode-supported solid oxide fuel cells. J Power Sources 2010;195:2149–58. doi:10.1016/j.jpowsour.2009.09.079.

[143] Haga K, Shiratori Y, Ito K, Sasaki K. Chemical Degradation and Poisoning Mechanism of Cermet Anodes in Solid Oxide Fuel Cells. ECS Trans 2009;25:2031–2038. doi:10.1149/1.3205748.

[144] Madi H, Diethelm S, Poitel S, Ludwig C, Van herle J. Damage of Siloxanes on Ni-YSZ Anode Supported SOFC Operated on Hydrogen and Bio-Syngas. Fuel Cells 2015;15:718–27. doi:10.1002/fuce.201400185.

[145] Madi H. Investigations into the Effects of Biofuel Contaminants on Solid Oxide Fuel Cells. École polytechnique fédérale de Lausanne EPFL, 2016. doi:10.5075/epfl-thesis-7161.

[146] Ishikura A, Sakuno S, Komiyama N, Sasatsu H, Masuyama N, Itoh H, et al. Influence of H2S Poisoning on Anode Layer of SOFC. ECS Trans 2007;7:845–50. doi:10.1149/1.2729174.

[147] Grgicak CM, Green RG, Giorgi JB. SOFC anodes for direct oxidation of hydrogen and methane fuels containing H2S. J Power Sources 2008;179:317–28. doi:10.1016/j.jpowsour.2007.12.082.

[148] Zhang L, Jiang SP, He HQ, Chen X, Ma J, Song XC. A comparative study of H2S poisoning on electrode behavior of Ni/YSZ and Ni/GDC anodes of solid oxide fuel cells. Int J Hydrogen Energy 2010;35:12359–68. doi:10.1016/j.ijhydene.2010.08.067.

[149] Brightman E, Ivey DG, Brett DJL, Brandon NP. The effect of current density on H2S-poisoning of nickel-based solid oxide fuel cell anodes. J Power Sources 2011;196:7182–7. doi:10.1016/j.jpowsour.2010.09.089.

[150] Trembly JP, Marquez AI, Ohrn TR, Bayless DJ. Effects of coal syngas and H2S on the performance of solid oxide fuel cells: Single-cell tests. J Power Sources 2006;158:263–73. doi:10.1016/j.jpowsour.2005.09.055.

[151] Haga K, Adachi S, Shiratori Y, Itoh K, Sasaki K. Poisoning of SOFC anodes by various fuel impurities. Solid State Ionics 2008;179:1427–31. doi:10.1016/j.ssi.2008.02.062.

[152] Bao J, Krishnan GN, Jayaweera P, Perez-Mariano J, Sanjurjo A. Effect of various coal contaminants on the performance of solid oxide fuel cells: Part I. Accelerated testing. J Power Sources 2009;193:607–16. doi:10.1016/j.jpowsour.2009.04.034.

[153] Papurello D, Lanzini A, Tognana L, Silvestri S, Santarelli M. Waste to energy: Exploitation of biogas from organic waste in a 500 Wel solid oxide fuel cell (SOFC) stack. Energy 2015;85:145–58. doi:10.1016/j.energy.2015.03.093.

[154] Papurello D, Borchiellini R, Bareschino P, Chiodo V, Freni S, Lanzini A, et al. Performance of a Solid Oxide Fuel Cell short-stack with biogas feeding. Appl Energy 2014;125:254–63.

[155] Hagen A, Rasmussen JFB, Thydén K. Durability of solid oxide fuel cells using sulfur containing fuels. J Power Sources 2011;196:7271–6. doi:10.1016/j.jpowsour.2011.02.053.

[156] Rasmussen JFB, Hagen A. The effect of H2S on the performance of Ni-YSZ anodes in solid oxide fuel cells. J Power Sources 2009;191:534–41. doi:10.1016/j.jpowsour.2009.02.001.

[157] Abatzoglou N, Boivin S. A review of biogas purification processes. Biofuels, Bioprod Biorefining 2009;6:42–71. doi:10.1002/bbb.

[158] Aravind P V., De Jong W. Evaluation of high temperature gas cleaning options for biomass gasification product gas for Solid Oxide Fuel Cells. Prog Energy Combust Sci 2012;38:737–64. doi:10.1016/j.pecs.2012.03.006.

[159] Papurello D, Lanzini A, Leone P, Santarelli M. The effect of heavy tars (toluene and naphthalene) on the electrochemical performance of an anode-supported SOFC running on. Renew Energy 2016;99:747–53. doi:10.1016/j.renene.2016.07.029.

[160] Díaz I, Ramos I, Fdz-Polanco M. Economic analysis of microaerobic removal of H 2 S from biogas in full-scale sludge digesters. Bioresour Technol 2015;192:280–6. doi:10.1016/j.biortech.2015.05.048.

[161] Horikawa MS, Rossi F, Gimenes ML, Costa CMM, Silva MGC da. Chemical absorption of H2S for biogas purification. Brazilian J Chem Eng 2004;21:415–22. doi:10.1590/S0104-66322004000300006.

[162] Cherosky P, Li Y. Hydrogen sulfide removal from biogas by bio-based iron sponge. Biosyst Eng 2013;114:55–9. doi:10.1016/j.biosystemseng.2012.10.010.

[163] Steven McKinsey Zicari. Removal of hydrogen sulfide from biogas using cow manure compost. Cornell University, 203AD.

[164] Truong LVA, Abatzoglou N. A H2S reactive adsorption process for the purification of biogas prior to its use as a bioenergy vector. Biomass and Bioenergy 2005;29:142–51. doi:10.1016/j.biombioe.2005.03.001.

[165] Xiao Y, Wang S, Wu D, Yuan Q. Experimental and simulation study of hydrogen sulfide adsorption on impregnated activated carbon under anaerobic conditions. J Hazard Mater 2008;153:1193–200. doi:10.1016/j.jhazmat.2007.09.081.

[166] Xiao Y, Wang S, Wu D, Yuan Q. Catalytic oxidation of hydrogen sulfide over unmodified and impregnated activated carbon. Sep Purif Technol 2008;59:326–32. doi:10.1016/j.seppur.2007.07.042.

[167] Bagreev A, Bandosz TJ. On the Mechanism of Hydrogen Sulfide Removal from Moist Air on Catalytic Carbonaceous Adsorbents. Ind Eng Chem Res 2005;44:530–8. doi:10.1021/ie049277o.

[168] Yan R, Chin T, Ng YL, Duan H, Liang DT, Tay JH. Influence of Surface Properties on the Mechanism of H 2 S Removal by Alkaline Activated Carbons. Environ Sci Technol 2004;38:316–23. doi:10.1021/es0303992.

[169] Seredych M, Bandosz TJ. Desulfurization of Digester Gas on Catalytic Carbonaceous Adsorbents: Complexity of Interactions between the Surface and Components of the Gaseous Mixture. Ind Eng Chem Res 2006;45:3658–65. doi:10.1021/ie051388f.

[170] Gutiérrez Ortiz FJ, Aguilera PG, Ollero P. Biogas desulfurization by adsorption on thermally treated sewage-sludge. Sep Purif Technol 2014;123:200–13. doi:10.1016/j.seppur.2013.12.025.

[171] Papurello D, Schuhfried E, Lanzini A, Romano A, Cappellin L, Märk TD, et al. Influence of co-vapors on biogas filtration for fuel cells monitored with PTR-MS (Proton Transfer Reaction-Mass Spectrometry). Fuel Process Technol 2014;118:133–40. doi:10.1016/j.fuproc.2013.08.011.

[172] Papurello D, Soukoulis C, Schuhfried E, Cappellin L, Gasperi F, Silvestri S, et al. Monitoring of volatile compound emissions during dry anaerobic digestion of the Organic Fraction of Municipal Solid Waste by Proton Transfer Reaction Time-of-Flight Mass Spectrometry. Bioresour Technol 2012;126:254–65. doi:10.1016/j.biortech.2012.09.033.

[173] Yang RT. Gas Separation by Adsorption Processes. vol. 2. Butterworths; 1988. doi:10.1016/0950-4214(88)80042-2.

[174] Cabrera-Codony A, Montes-Moran MA, Sanchez-Polo M, Martin MJ, Gonzalez-Olmos R. Biogas upgrading: Optimal activated carbon properties for siloxane removal. Environ Sci Technol 2014;48:7187–95. doi:10.1021/es501274a.

[175] Matsui T, Imamura S. Removal of siloxane from digestion gas of sewage sludge. Bioresour Technol 2010;101:S29–32. doi:10.1016/j.biortech.2009.05.037.

[176] Ajhar M, Travesset M, Yüce S, Melin T. Siloxane removal from landfill and digester gas – A technology overview. Bioresour Technol 2010;101:2913–23. doi:10.1016/j.biortech.2009.12.018.

[177] Wheless E, Pierce J. Siloxanes in Landfill and Digester Gas Update. SWANA 27th Landfill Gas Conf., 2004.

[178] Ricaurte Ortega D, Subrenat a. Siloxane treatment by adsorption into porous materials. Environ Technol 2009;30:1073–83. doi:10.1080/09593330903057540.

[179] Papurello D, Soukoulis C, Schuhfried E, Cappellin L, Gasperi F, Silvestri S, et al. Monitoring of volatile compound emissions during dry anaerobic digestion of the Organic Fraction of Municipal Solid Waste

by Proton Transfer Reaction Time-of-Flight Mass Spectrometry. Bioresour. Technol., vol. 126, 2012, p. 254–65.

[180] Hernández SP, Scarpa F, Fino D, Conti R. Biogas purification for MCFC application. Int J Hydrogen Energy 2011;36:8112–8. doi:10.1016/j.ijhydene.2011.01.055.

[181] Hernández S, Solarino L, Orsello G, Russo N, Fino D, Saracco G, et al. Desulfurization processes for fuel cells systems. Int J Hydrogen Energy 2008;33:3209–14. doi:10.1016/j.ijhydene.2008.01.047.

[182] Sisani E, Cinti G, Discepoli G, Penchini D, Desideri U, Marmottini F. Adsorptive removal of H2S in biogas conditions for high temperature fuel cell systems. Int J Hydrogen Energy 2014;39:21753–66. doi:10.1016/j.ijhydene.2014.07.173.

[183] Biasioli F, Yeretzian C, Märk TD, Dewulf J, Van Langenhove H. Direct-injection mass spectrometry adds the time dimension to (B)VOC analysis. TrAC - Trends Anal Chem 2011;30:1003–17. doi:10.1016/j.trac.2011.04.005.

[184] Hansen MJ, Liu D, Guldberg LB, Feilberg A. Application of Proton-Transfer-Reaction Mass Spectrometry to the Assessment of Odorant Removal in a Biological Air Cleaner for Pig Production 2012:3–10.

[185] Papurello D, Schuhfried E, Lanzini A, Romano A, Cappellin L, Märk TD, et al. Influence of co-vapors on biogas filtration for fuel cells monitored with PTR-MS (Proton Transfer Reaction-Mass Spectrometry). Fuel Process Technol 2014;118:133–40. doi:10.1016/j.fuproc.2013.08.011.

[186] Papurello D, Tognana L, Lanzini A, Smeacetto F, Santarelli M, Belcari I, et al. Proton transfer reaction mass spectrometry technique for the monitoring of volatile sulfur compounds in a fuel cell quality clean-up system. Fuel Process Technol 2015;130:136–46. doi:10.1016/j.fuproc.2014.09.041.

[187] Pei J, Zhang JS. On the performance and mechanisms of formaldehyde removal by chemi-sorbents. Chem Eng J 2011;167:59–66. doi:10.1016/j.cej.2010.11.106.

[188] Yuan B, Hu WW, Shao M, Wang M, Chen WT, Lu SH, et al. VOC emissions, evolutions and contributions to SOA formation at a receptor site in eastern China. Atmos Chem Phys 2013;13:8815–32. doi:10.5194/acp-13-8815-2013.

[189] Papurello D, Tomasi L, Silvestri S, Santarelli M. Evaluation of the Wheeler-Jonas parameters for biogas trace compounds removal with activated carbons. Fuel Process Technol 2016;152:93–101. doi:10.1016/j.fuproc.2016.06.006.

[190] Blondeau P, Tiffonnet AL, Allard F, Haghighat F. Physically Based Modelling of the Material and Gaseous Contaminant Interactions in Buildings: Models, Experimental Data and Future Developments. Adv Build Energy Res 2008;2:57–93. doi:10.3763/aber.2008.0203.

[191] Das D, Gaur V, Verma N. Removal of volatile organic compound by activated carbon fiber. Carbon N Y 2004;42:2949–62. doi:10.1016/j.carbon.2004.07.008.

[192] Brunauer S, Emmett PH. Chemisorptions of Gases on Iron Synthetic Ammonia Catalysts '. Carbon N Y 1938;62:1732–46.

[193] Ng C, Losso JN, Marshall WE, Rao RM. Freundlich adsorption isotherms of agricultural by-product-based powdered activated carbons in a geosmin-water system. Bioresour Technol 2002;85:131–5. doi:10.1016/S0960-8524(02)00093-7.

[194] Schindler BJ, Buettner LC, Douglas LeVan M. Transition to Henry's law in ultra-low concentration adsorption equilibrium for n-pentane on BPL activated carbon. Carbon N Y 2008;46:1285–93. doi:10.1016/j.carbon.2008.05.001.

[195] Chakraborty A, Sun B. An adsorption isotherm equation for multi-types adsorption with thermodynamic correctness. Appl Therm Eng 2014;72:190–9. doi:10.1016/j.applthermaleng.2014.04.024.

[196] Rosen JB. Kinetics of a Fixed Bed System for Solid Diffusion into Spherical Particles. J Chem Phys 1952;20:387. doi:10.1063/1.1700431.

[197] Rasmuson A. Exact solution of a model for diffusion and transient adsorption in particles and longitudinal dispersion in packed beds. AIChE J 1981;27:1032–5. doi:10.1002/aic.690270625.

[198] Wakao N, Funazkri T. Effect of fluid dispersion coefficients on particle-to-fluid mass transfer coefficients in packed beds. Chem Eng Sci 1978;33:1375–84. doi:10.1016/0009-2509(78)85120-3.

[199] Khazraei Vizhemehr A, Haghighat F, Lee C-S. Predicting gas-phase air-cleaning system efficiency at low concentration using high concentration results: Development of a framework. Build Environ 2013;68:12–21. doi:10.1016/j.buildenv.2013.05.023.

[200] Markham EC, Benton AF. THE ADSORPTION OF GAS MIXTURES BY SILICA. J Am Chem Soc 1931;53:497–507. doi:10.1021/ja01353a013.

[201] Broughton D. Adsorption Isotherms for Binary Gas Mixtures. Ind Eng Chem 1948;40:1506–8. doi:Doi 10.1021/Ie50464a036.

[202] Kapoor A, Ritter JA, Yang RT. An extended Langmuir model for adsorption of gas mixtures on heterogeneous surfaces. Langmuir 1990;6:660–4. doi:10.1021/la00093a022.

[203] Myers AL, Prausnitz JM. Thermodynamics of mixed-gas adsorption. AIChE J 1965;11:121–7. doi:10.1002/aic.690110125.

[204] Simon CM, Smit B, Haranczyk M. PyIAST: Ideal adsorbed solution theory (IAST) Python package. Comput Phys Commun 2016;200:364–80. doi:10.1016/j.cpc.2015.11.016.

[205] Guiochon G, Shiraza S, Katti A. Fundamentals of preparative and nonlinear chromatography. Academic Press; 2005.

[206] Hutchins RA. Designing Granular Activated Carbon Systems for Maximum Performance. Proc. Annu. WWEMA Ind. Pollut. Conf. WWEMA, Atlanta, GA: 1977, p. 491–512.

[207] Narbaitz RM, Benedek A. Least Cost Process Design for Granular Activated Carbon Adsorbers. J Water Pollut Control Fed 1983:1244–1251.

[208] Rasi S, Veijanen A, Rintala J. Trace compounds of biogas from different biogas production plants. Energy 2007;32:1375–80. doi:10.1016/j.energy.2006.10.018.

[209] Papurello D, Lanzini A, Drago D, Leone P, Santarelli M. Limiting factors for planar solid oxide fuel cells under different trace compound concentrations. Energy 2016;95:67–78. doi:10.1016/j.energy.2015.11.070.

[210] Papurello D, Lanzini A, Smeacetto F, Santarelli M. SORBENT MATERIALS FOR THE CLEANING OF SEWAGE BIOGAS IN HIGH TEMPERATURE FUEL CELL PLANTS. Environ Eng Manag J 2013;12:73–6.

[211] Papurello D, Tomasi L, Silvestri S, Santarelli M. Evaluation of the Wheeler-Jonas parameters for biogas trace compounds removal with activated carbons. Fuel Process Technol 2016;152:93–101. doi:10.1016/j.fuproc.2016.06.006.

[212] Papurello D, Schuhfried E, Lanzini A, Romano A, Cappellin L, Märk TD, et al. Proton transfer reaction-mass spectrometry as a rapid inline tool for filter efficiency of activated charcoal in support of the development of Solid Oxide Fuel Cells fueled with biogas. Fuel Process Technol 2015;130:78–86. doi:10.1016/j.fuproc.2014.09.042.

[213] Wood GO. A review of the effects of covapors on adsorption rate coefficients of organic vapors adsorbed onto activated carbon from flowing gases. Carbon N Y 2002;40:685–94. doi:10.1016/S0008-6223(01)00185-3.

[214] Balachia M. A dynamic model used to predict competitive adsorption of biogas contaminants with

experimental validations. Politecnico di Torino, 2015.

[215] Papurello D, Tomasi L, Silvestri S, Belcari I, Santarelli M, Smeacetto F, et al. Biogas trace compound removal with ashes using proton transfer reaction time-of-flight mass spectrometry as innovative detection tool. Fuel Process Technol 2016;145:62–75. doi:10.1016/j.fuproc.2016.01.028.

[216] Sitthikhankaew R, Chadwick D, Assabumrungrat S, Laosiripojana N. Effects of humidity, O2, and CO2 on H2S adsorption onto upgraded and KOH impregnated activated carbons. Fuel Process Technol 2014;124:249–57. doi:10.1016/j.fuproc.2014.03.010.